University of Alberta

Experimental and Theoretical Study of Chalcogenide Glasses for Erbium-Doped Waveguide Amplifiers

by

Trevor Warren Allen 

A thesis submitted to the Faculty of Graduate Studies and Research in partial fulfillment of the requirements for the degree of **Master of Science**.

Department of Electrical and Computer Engineering

Edmonton, Alberta

Spring, 2004

Your file Votre référence
ISBN: 0-612-96441-8
Our file Notre référence
ISBN: 0-612-96441-8

Abstract

The main purpose of this thesis was to determine the suitability of chalcogenide glass as a host material for erbium-doped waveguide amplifiers. These glasses have often been identified as potentially good hosts, although to date, no in-depth studies have been performed to confirm this hypothesis.

GaGeSe was chosen as a test material from several chalcogenide alloys due to its performance in photoluminescence lifetime measurements. Using measured absorption data, the McCumber and Judd-Ofelt theories were used to calculate absorption and emission cross-sections and energy state lifetimes - necessary parameters for simulation.

Simulations of the most common erbium-doped amplifier pumping schemes were performed using the transfer matrix and Newton-Raphson methods. The results showed that 980-nm pumping is infeasible, due to the low probability of a key transition caused by the low maximum phonon energy in chalcogenide glasses. Due to the values of the absorption and emission cross-sections of erbium in the chalcogenide glasses studied, there are also severe drawbacks associated with 1480-nm pumping.

To my parents

Chessy and William

Acknowledgements

So now that my thesis is finally done, the feeling of euphoria that comes with the completion of a document of this magnitude (in terms of page count, at least) is tempered by the inevitable realization that it couldn't have been finished without the help of certain stellar individuals and organizations. They are listed below, in no particular order.

Thanks to my supervisors, Dr. Ray DeCorby and Dr. Chris Haugen, for their excellent guidance, and for not kicking me out of their offices whenever I asked my typically inane questions.

Thanks to Dave Clegg for his indispensable advice in the lab, and for not noticing those lasers I hid in the back of the cabinet for some reason or other.

Thanks to Garth Hanson, for helping me out in the lab, and for finally answering that age-old question, "Are my LEDs here yet?"

Thanks to Dr. Safa Kasap, Dancho Tochev, Cyril Koughia, Martin Munzar, and the rest of the research group at the University of Saskatchewan for their incomparable work on the materials end of this project.

Thanks to Matthew Hawkeye for his help with measurements and good ideas.

Thanks to TRLabs, NSERC and iCORE for their much-appreciated financial assistance.

Thanks to the staff at TRLabs for making my tenure as an M.Sc. student enjoyable and somewhat less than maddening.

And last but not least, thanks to my family for their continuing support and encouragement in all things I do.

Table of Contents

List of Tables

List of Figures

List of Symbols and Abbreviations

Symbols

A, A_{ji}	Probability per unit time (spontaneous emission) [s^{-1}]
A_{eff}	Effective modal area of light in waveguide [m^2]
c	Speed of light (3×10^8 m s^{-1})
C_{ij}	Cross-relaxation coefficient [m^3 s^{-1}]
Cup_i	Cooperative upconversion coefficient [m^3 s^{-1}]
d	Thickness of layer [m]
e	Electron charge (1.602×10^{-19} C)
E	Energy [eV], [cm^{-1}], Electric field [V m^{-1}]
f	Oscillator strength of transition
g	Degeneracy of ion level
G	Gain [dB]
$g(\upsilon)$	Lineshape function [s]
h	Planck's constant (6.626×10^{26} J s)
$\hbar$	Planck's constant / 2π (1.055×10^{-34} J s)
I	Intensity [W m^{-2}]
J	Orbital momentum of atomic state
k	Boltzmann's constant (1.308×10^{-23} J K^{-1})
L	Length [m], Angular momentum of atomic state
$\hat{L}+2\hat{S}$	Magnetic dipole operator
m	Mass of electron (9.1039×10^{-31} kg)
M	Structure transfer matrix
n	Refractive index

N_i	Ion population [m^{-3}]
N, n_i	Complex refractive index
$n(T)$	Bose-Einstein occupation number
p	Number of phonons
$P(E)$	Probability of ion existing at energy E (Boltzmann statistics)
r	Ion separation [m], Reflection coefficient
R_{ij}	Pump-induced probability rate (absorption) [s^{-1}]
R_{ji}	Pump-induced probability rate (stimulated emission) [s^{-1}]
R	Reflectance
S	Spin of atomic state
s_{ed}	Electric dipole oscillator line strength
sl	Scattering loss [m^{-1}]
s_{md}	Magnetic dipole oscillator line strength
t	Transmission coefficient
T	Temperature [K], Transmittance
U^t	Reduced matrix elements of unit tensors
W_{ij}	Signal-induced probability rate (absorption) [s^{-1}]
W_{ji}	Signal-induced probability rate (stimulated emission) [s^{-1}]
α	Absorption coefficient [m^{-1}]
$\Delta\lambda^{eff}$	Effective widths of transition cross-sections [m]
ε	Temperature-dependant excitation energy [eV]
ε_o	Permittivity of free space (8.854×10^{-12} F m^{-1})
ϕ	Photon flux density [m^{-2} s^{-1}]
Γ	Core confinement factor

κ	Extinction coefficient
λ	Wavelength [m]
ρ	Concentration of erbium [m^{-3}]
σ_e, σ_{ji}	Emission cross-section [m^2]
σ_a, σ_{ij}	Absorption cross-section [m^2]
τ, τ_{ji}	Lifetime of energy state [s]
υ	Frequency [Hz]
Ω_t	Judd-Ofelt parameter [m^2]

Abbreviations

EDFA	Erbium-Doped Fibre Amplifier
EDWA	Erbium-Doped Waveguide Amplifier
FL	Füchtbauer-Ladenburg theory
LED	Light Emitting Diode
PL	Photoluminescence
PLE	Photoluminescence Excitation

1. Introduction

For the past several years, the benefits of optical technologies have led to the replacement of electronics by optics in communications systems. These advantages play a large part in increasing the speed and quality of data transfer, and include large available bandwidth, low dispersion, and low cross-talk between optical fibres. However, not all signal processing functions (such as amplification, modulation and splitting of light) can be performed in one integrated circuit, and as such losses are incurred as signals are transferred between different devices. The field of integrated optics, first postulated in the late 1960s [1], is aimed at counteracting this problem. The goal of this field is to implement multiple optical devices in a single material system, analogous to integrated chips in the electronic domain. The subsequent miniaturization of optical systems would lead to an increase in efficiency and performance, and an ability to mass-produce these systems through cost-effective means.

The key problem in realizing integrated optics is finding a material that can be used for the many types of functions needed in optical signal processing, since each device's functionality requires a unique set of host properties for efficient operation. As two examples, high refractive index helps to confine light to the core of waveguides, and high nonlinearities enable active switching devices such as electro-optic modulators. One group of materials that show promise for the implementation of many optical functions is the chalcogenide glasses, so named because they contain one or more of the chalcogen elements, S, Se, and Te. As studies on chalcogenides have progressed over the years, the useful optical properties of these glasses have become more and more apparent, including high transparency in the infrared range and ability to undergo structural changes during illumination [2]. The properties of these glasses will be discussed in more detail in Chapter 2.

Optical amplifiers are one of the basic building blocks of any optical transmission network, and are used to compensate for power losses that can be incurred in a communications signal at various stages in the signal transmission process. One method of amplifying optical signals is to convert the signal into the electrical domain for amplification, and then back again to the optical domain for further transmission.

However, this procedure has its own drawbacks such as limiting the bandwidth of the system. A more common solution is the erbium-doped fibre amplifier (EDFA), which was first introduced for amplification of signals at 1550 nm in 1987 [3]. Among the benefits of EDFAs are their low noise, linear gain response, and temperature and polarization insensitivity. The availability of EDFAs has had a significant impact on the development of optical networks as we know them today, and the first erbium absorption line has set the telecommunications wavelength standard at 1550 nm [3]. If integrated optics is to be viable, an amplifying device similar to the EDFA is needed. For this purpose, the erbium-doped waveguide amplifier (EDWA) has also been developed recently, and working devices have been demonstrated in various glass systems [4-10].

The basic principle of an erbium-doped amplifier is as follows: a pump beam of wavelength shorter than 1550 nm (usually 980 nm or 1480 nm) is used to excite erbium ions doped into the host material and create a population inversion available for stimulated emission, which amplifies the longer wavelength signal. The amount of erbium ions needed in a host material to get a certain amount of gain is inversely proportional to the amount of material present. Hence, in an EDFA, with lengths on the order of 50 m, low doping concentrations can still produce high amounts of gain, but in an EDWA, with lengths in the range of 5-10 cm, high doping concentrations on the order of 10^{26} ions/m^3 are needed. This high doping concentration makes several materials inefficient hosts for EDWAs [4]. A material that has good solubility for erbium ions and properties that assist amplification is needed for efficient and compact EDWAs to be realized.

Although they are commonly used for fibre amplifiers, silica and silicate glasses tend to exhibit clustering of rare earth dopant ions at the high concentrations necessary for waveguide amplifiers (for doping concentrations greater than 10^{24} ions/m^3) [4]. This clustering greatly reduces the gain produced by amplifiers in these materials. Silicate glasses also suffer from a relatively low refractive index, which leads to poor confinement of the pump and signal beams [4].

Phosphate glass EDWAs have shown better performance than those fabricated in silicate glasses, and have been manufactured as commercial devices, although these

devices tend to exhibit poor chemical durability [8]. Clustering is less of a problem in phosphate glass, reducing the probability of ion-ion interactions that decrease amplifier performance [9].

Al_2O_3 glass shows potential as an EDWA host material for several reasons. First, waveguide fabrication technology is well developed for this material system. Al_2O_3 also has a relatively high refractive index that helps with light confinement and allows for small waveguide bending radii. In addition, Al_2O_3 exhibits a similar valence and crystal structure to Er_2O_3, and therefore allows for higher concentrations of erbium without inducing serious clustering effects [4].

Another potential material undergoing research is silicon rich oxide (SRO). In this material system, silicon nanocrystals are used as the erbium excitation path rather than direct light absorption by erbium. These nanocrystals can be formed in erbium-doped silicon oxide glasses with excess silicon by rapidly annealing them until nanocrystals precipitate. The nanocrystals enable a very efficient excitation over a wide range of wavelengths, potentially allowing the use of a broadband excitation source such as LEDs [10].

Table 1.1: Comparison of key parameters of EDWA host glasses.

Glass	Silicate [3]	Phosphate [9]	Al_2O_3 [3]	SRO [10]	Chalcogenide
Refractive index (n) (typical)	1.5	1.52	1.64	1.46 [(1)]	2.32
Emission cross-section (σ_e) [m^2]	5×10^{-25}	9×10^{-25}	6×10^{-25}	6×10^{-23}	1.58×10^{-24}
Gain per cm [dB cm^{-1}]	1	4.2	1.33	7 [(2)]	15.5 [(3)]
Corresponding erbium doping concentration [m^{-3}]	1.4×10^{26}	1.5×10^{26}	2.7×10^{26}	2.1×10^{25} [(4)]	2.26×10^{26}

[(1)] Depends on concentration of Si nanocrystals [(2)] Calculated theoretical maximum gain [10]

[(3)] Calculated theoretical maximum gain (see Section 4.6) [(4)] Estimated from 0.03 at.% [10]

Many references in the literature point to chalcogenide glasses as being good candidates for erbium-doped waveguide amplifiers [11-17], due to their low phonon energies (~ 0.05 eV, compared to ~ 0.12 eV in SiO_2), high stimulated emission cross-sections for rare-earth ions, high refractive index, and relatively high solubility for

erbium ions. Table 1.1 summarizes some of the key parameters of various glasses that have been studied as EDWA hosts.

Emission cross-section is a host-dependent parameter of the erbium ions that impacts the maximum gain of the amplifier, and will be further explained later in the thesis. High refractive index and emission cross-section make chalcogenide glass an attractive alternative to traditional glasses. However, to our knowledge, no formal, detailed studies have been performed on EDWAs implemented in chalcogenide glass. Hence, the goals of this thesis are to study chalcogenide glass, and then simulate waveguide amplifiers to confirm or refute the potential of chalcogenide as an EDWA host material. An outline of the thesis follows.

Chapter 2 gives background information necessary for the understanding of waveguide amplifiers. The operating mechanism behind erbium-doped amplifiers is explained, including the two common pumping schemes at 980 nm and 1480 nm. Important ion transitions that affect amplifier performance are discussed, along with the parameters that determine the magnitude of their effect, such as absorption and emission cross-sections and photoluminescence lifetimes. Also, adverse effects that hinder erbium-doped waveguide amplifiers are discussed. Finally, some information on chalcogenide glasses is given, including their properties and some specific reasons for choosing the alloys studied in this thesis.

Chapter 3 details the spectroscopic techniques used to calculate parameters of the erbium ions in the glass. These techniques are the McCumber theory, used to calculate absorption and emission cross-sections, and the Judd-Ofelt theory, used to find luminescence lifetimes. Some brief details on the fabrication of bulk samples of erbium-doped chalcogenide alloys are given. Next, the measurements that were performed on these alloys are detailed, including the measurement of lifetimes, which were used to select the most promising glass alloy that would be used for subsequent experiments. Measurements of the absorption spectra are shown, along with the results of McCumber and Judd-Ofelt calculations that used this data.

In Chapter 4, the results obtained from the work in Chapter 3 were used to simulate chalcogenide erbium-doped waveguide amplifiers. First, a detailed explanation

of the transfer matrix method used to simulate the waveguide amplifiers is given, followed by explanations of the two models used to simulate 980-nm and 1480-nm pumping, along with definitions of the rate equations used to mathematically describe these models. Next, the simulation procedure is explained using a step-by-step approach. The remainder of the chapter details the results obtained from both the 980-nm and 1480-nm pumping simulations, showing the problems that arise in erbium-doped waveguide amplifiers in this glass system. The sources of these problems are investigated and discussed.

Finally, conclusions are drawn in Chapter 5, along with a brief discussion of potential future work and solutions to the difficulties observed in Chapter 4. In addition, three appendices are attached, dealing with the values of the reduced-matrix elements used in Judd-Ofelt calculations, a summary of the luminescence measurements performed in the course of research, and the Newton-Raphson method for solving non-linear systems of equations.

2. Background Theory

2.1. The waveguide amplifier

In optical communication systems, amplification is necessary in order to ensure that signals can be transmitted over long distances and to compensate for losses incurred in propagation through fibres and other components. Waveguide amplifiers are one way of accomplishing this task.

When a waveguide is doped with a rare earth element such as erbium or neodymium, it has the potential to be an amplifying medium for certain wavelengths of light, depending on the absorption and emission lines of the rare earth ion used. Erbium emits light at 1550 nm, a wavelength commonly used in telecommunications applications since 1550 nm corresponds to a low absorption operating point in silica fibre. A simple view of the energy levels of an Er^{3+} ion in a glass is shown in Figure 2.1:

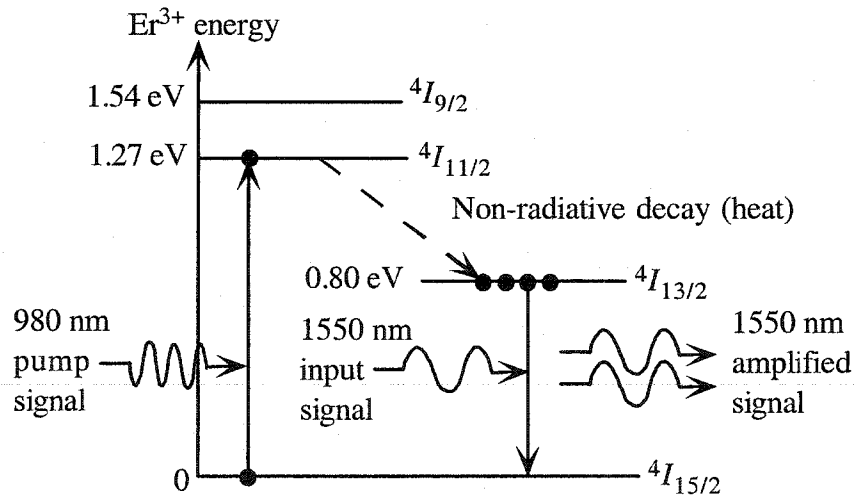

Figure 2.1: Energy of erbium ion in a glass medium with illustration of 980-nm pumping scheme and light amplification by stimulated emission [18].

The $^4I_{15/2}$ labels are a standard naming convention that gives the *SLJ* values (see Section 3.1.2) of the atomic state through the form $^{2S+1}L_J$, where $L = 0, 1, 2, 3, 4\ldots$ is denoted by a letter: *S*, *P*, *D*, *F*, *G*... [21]. These labels will be used throughout the thesis.

$^4I_{15/2}$ corresponds to the lowest energy possible for the ion (ground state). The two energy levels labelled $^4I_{11/2}$ and $^4I_{9/2}$ are suitable for pumping the erbium, and correspond to pumping wavelengths of 980 nm and 800 nm, respectively. 980 nm is the

more commonly used pumping wavelength as it results in the best gain and efficiency [19].

When a 980-nm photon enters the glass, it can be absorbed by an erbium ion, which will then become excited to the energy state $^4I_{11/2}$. From here, the ion decays non-radiatively through phonon (heat) emissions to level $^4I_{13/2}$, creating a population inversion between $^4I_{13/2}$ and $^4I_{15/2}$. $^4I_{13/2}$ is a metastable state, meaning that the time an ion will remain excited in that state is relatively long (typical lifetimes are on the order of 10 ms [18] and depend on the host material, distribution of ions, and other factors). Once the ions are at $^4I_{13/2}$, they can go through one of a number of different possible transitions that will bring them back to the ground state $^4I_{15/2}$.

In stimulated emission, a photon of energy equal to that of the gap between $^4I_{13/2}$ and $^4I_{15/2}$ (i.e., $E_{photon} = h\upsilon = E_2 - E_1$, where h is Planck's constant and υ is the photon frequency) travelling through the glass causes an ion to lose its energy and return to the ground state while releasing another photon. This new photon has the same frequency, phase, polarization and direction of propagation as the first – essentially an exact copy. Thus, the signal is amplified as it passes through the device. The probability of stimulated emission is given by $W_{21} = \phi_s \sigma_e(\lambda_s)$ [s^{-1}], where ϕ_s [m^{-2} s^{-1}] is the photon flux density of the incoming signal and $\sigma_e(\lambda_s)$ [m^2] is the emission cross-section of the erbium ions at the signal wavelength. If a population of ions N_2 [m^{-3}] is present in the excited state, the rate of stimulated emission will be given by $N_2 W_{21}$ [m^{-3} s^{-1}].

Another way for the ion to return to ground state is by spontaneous emission, where the ion relaxes on its own, releasing a photon of energy equal to $E_2 - E_1$. Since there is no signal causing this decay, the emitted photon is random in phase, polarization and direction, and as such light emitted by this process into the signal mode becomes noise. The probability per unit time of spontaneous emission is defined as $A_{21} = 1/\tau_{21}$ [s^{-1}] where τ_{21} [s] is the lifetime of the excited state. The rate of spontaneous emission is then $N_2 A_{21}$ [m^{-3} s^{-1}].

A second common method to create a population inversion in EDWAs is to use a 1480-nm pump beam. This process is illustrated schematically in Figure 2.2. Due to a phenomenon known as Stark splitting, an ion's energy levels (sharp and clearly defined

in free space) become split into a series of energy sublevels when the ion is in a solid. This spreading of energy states allows a pump beam of higher energy (lower wavelength) to excite ions to energies within the $^4I_{13/2}$ energy band above the energy corresponding to 1550 nm, thereby creating a population inversion. A requirement of 1480-nm pumping is that the absorption cross-section be larger than the emission cross-section for the pumping wavelength, which is true in all glasses for the lower wavelengths of the 1550-nm energy band.

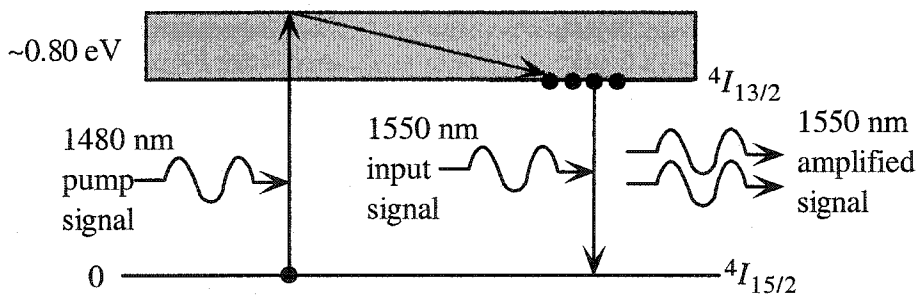

Figure 2.2: Basic principle of 1480-nm pumping.

Fibre amplifiers with 1480-nm pumps have come into widespread use for two main reasons. First, the absorption cross-section values (explained in the coming paragraphs) around 1480 nm are typically comparable to the values around 980 nm, and the broad absorption band removes the need to carefully tune the pump beam wavelength, and allows the use of highly multimode pumps. Secondly, high-power 1480-nm lasers are commercially available [19]. However, 1480-nm pumped amplifiers are much more susceptible to adverse effects such as excited state absorption, due to the presence of a ladder of energy levels in erbium with gaps that correspond to wavelengths in the range of 1550 nm. Also, the close proximity of the pump and signal wavelengths can lead to a degradation of the noise factor.

It is important to note that while the incoming signal photons can cause ions to return from $^4I_{13/2}$ to the ground state through stimulated emission, they can also be absorbed by ions in the ground state, which are then excited to $^4I_{13/2}$. This absorption causes attenuation in the signal rather than gain, and its probability rate is described as $W_{12} = \phi_s \sigma_a(\lambda_s)$ [s^{-1}], where $\sigma_a(\lambda_s)$ [m^2] is the absorption cross-section at the signal wavelength. The corresponding transition rate is $N_1 W_{12}$ [m^{-3} s^{-1}]. Boltzmann statistics

states that the probability P of an ion being at a certain energy E in a system in thermal equilibrium is given by:

$$P(E) \propto \exp\left(-\frac{E}{kT}\right) \tag{2.1}$$

where k is Boltzmann's constant and T is the temperature. From this relation, the population of ions in the lower energy state will be much greater than that of higher energy levels, and as such absorption will always exceed stimulated emission at thermal equilibrium, causing a decrease in the signal.

To ensure that stimulated emission exceeds absorption, a population inversion is needed, that is, more erbium ions need to be at the excited state $^4I_{13/2}$ than at the ground state $^4I_{15/2}$. When this condition is met, the probability that an incoming photon will cause stimulated emission will be much greater than the probability of it being absorbed by an ion in the ground state. This inversion can be accomplished by applying a pump signal of sufficient intensity to the gain medium. The pumping probability density is denoted by $R_{13} = \phi_p \sigma_a(\lambda_p)$ [s^{-1}], where ϕ_p [m^{-2} s^{-1}] is the photon flux density of the pump and $\sigma_a(\lambda_p)$ [m^2] is the absorption cross-section at the pump wavelength, and the corresponding rate of pumping is given as $N_1 R_{13}$ [m^{-3} s^{-1}].

The net optical gain of the amplifier can be expressed as:

$$G = \frac{I_{out}}{I_{in}} = \exp\left(L\left(\sigma_e N_2 - \sigma_a N_1\right)\right) \tag{2.2}$$

where I_{out} and I_{in} are the signal intensities exiting and entering the device, σ_e and σ_a are the stimulated emission and absorption cross-sections of the erbium ions, L is the length of the device, N_2 is the population of ions in the excited state and N_1 is the population of ions in the ground state.

The stimulated emission cross-section and its counterpart, the absorption cross-section, are parameters that are interpreted as an equivalent cross-sectional area of an atom or ion in a medium as seen by the signal photon flux in the material. They determine the probability that a photon will induce stimulated emission or be absorbed (in qualitative terms, a photon that enters the cross-sectional area around an atom defined

by these parameters can interact with that ion). The emission cross-section is given by the following equation [20]:

$$\sigma_e(\upsilon) = \frac{c^2 g(\upsilon)}{8\pi n^2 \upsilon^2 \tau_{rad}} \tag{2.3}$$

where c is the speed of light in vacuum (3×10^8 m/s), $g(\upsilon)$ is the line shape function of the transition (this function defines the strength of emission caused by radiation that causes excited ions to relax to a lower energy state), υ is the frequency in question, and τ_{rad} is the radiative lifetime of ions in the excited state. The derivation of this equation assumes that the spectral width of the signal energy density is small compared to the line shape function $g(\upsilon)$, or in other words, all signal photons are of one wavelength. An alternate form of the equation is also useful:

$$\frac{1}{\tau_{rad}} = \frac{8\pi n^2}{c^2} \int \upsilon^2 \sigma_e(\upsilon) d\upsilon \tag{2.4}$$

Actual calculation of the emission cross-section can be a complicated task. Later on in the thesis, Equation (2.4) will be used in the calculation of the emission cross-sections.

Absorption cross-sections (σ_a) are much simpler to obtain by direct measurement using the following expression and absorption data:

$$\sigma_a(\upsilon) = \frac{1}{NL} \ln\left(\frac{I_o(\upsilon)}{I(\upsilon)}\right) \tag{2.5}$$

where N is the total number of erbium ions in the material and I_o and I are the intensities of light entering and exiting the sample, respectively (taking Fresnel reflection at the sample's surfaces into account) [20].

Another important factor in amplifiers is the lifetime of ions in their excited states, i.e., the length of time an ion remains excited before an internal mechanism like spontaneous emission or phonon (vibration) emission causes the ion to lose its energy and relax to a lower state. The lifetime of excited ions can have a beneficial or detrimental effect on the performance of the amplifier, depending on the energy level and wavelengths involved. For instance, if the lifetime of energy level $^4I_{13/2}$, as shown in

Figure 2.1, is too low, excited ions in that state will return to ground state by spontaneous emission quickly, thereby producing noise and depleting the population of ions available to amplify the input signal. On the other hand, if the lifetime of ions is too long in the $^4I_{11/2}$ state, they are much more difficult to get to the $^4I_{13/2}$ state where they are needed for amplification. It is also important to note that a short lifetime can indicate the presence of adverse affects that will hinder the performance of the amplifier.

Since both radiative and non-radiative transitions may depopulate a given state, the overall lifetime (τ) of a state is defined as:

$$\frac{1}{\tau} = \frac{1}{\tau_{rad}} + \frac{1}{\tau_{nr}} \tag{2.6}$$

It should be noted that the overall lifetime of a transition is typically dominated by radiative or non-radiative decay, depending on the energy state. Also, depending on the state involved, there may be several different radiative and non-radiative transitions that make up the components in Equation (2.6). They are combined similarly to give the separate components of the overall lifetime:

$$\frac{1}{\tau_{rad}} = \frac{1}{\tau_{rad1}} + \frac{1}{\tau_{rad2}} + \cdots \tag{2.7}$$

$$\frac{1}{\tau_{nr}} = \frac{1}{\tau_{nr1}} + \frac{1}{\tau_{nr2}} + \cdots \tag{2.8}$$

2.2. Limiting factors of erbium-doped waveguide amplifiers

2.2.1. Cooperative upconversion and cross-relaxation

To obtain high gain in erbium-doped amplifiers, a large number of erbium ions is needed. In a fibre amplifier, the erbium ions can be spread over the length of the fibre, since there is a long length of host material to work with. However, in erbium-doped waveguide amplifiers, the goal is to achieve high gain in a short length that will be compatible with integrated optics. Thus, high erbium concentrations must be doped into a small amount of host material in order to get high gain per unit length. As an example, to obtain gain of 10 dB in a fibre amplifier with emission cross-section 10^{-21} cm^{-2} and length 2000 cm, an erbium concentration of approximately 1.2×10^{18} cm^{-3} is needed. In a

waveguide amplifier with the same emission cross-section and length 2 cm, approximately 6×10^{20} cm^{-3} of erbium is needed, approximately 600 times that of the fibre amplifier. When the concentration of erbium is this high, the erbium ions are very closely spaced, and the odds that they will interact with each other to cause effects adverse to amplification become very high (the probability of ion-ion interaction is proportional to r^{-6}, where r is the ion separation) [21]. This interaction is called cooperative upconversion or cross-realxation.

There are many possible cases of upconversion and cross-relaxation, depending on the energy levels occupied by the interacting ions and the energy levels available for them to go to. The main difference between the two processes is that cooperative upconversion involves two ions at the same energy level, while cross-relaxation involves two ions at different energies. In both cases, one ion transfers some or all of its energy to another, pushing the other to a higher energy state while the first relaxes to a lower state.

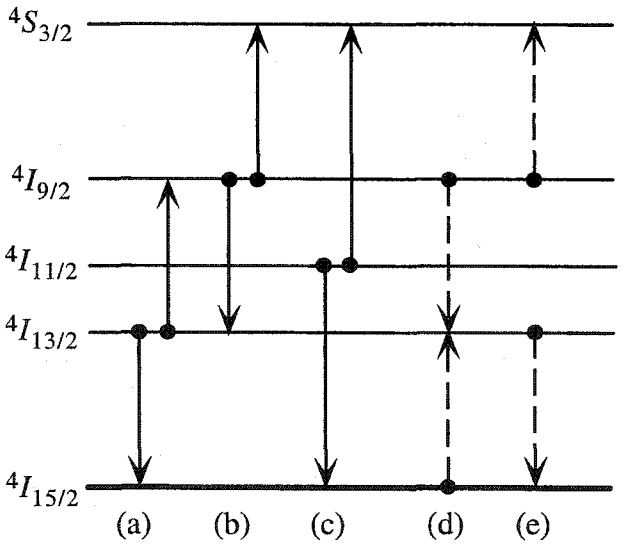

Figure 2.3: Examples of cooperative upconversion and cross-relaxation. Cooperative upconversion transitions are denoted by solid lines, and cross-relaxations are denoted by dashed lines.

At worst, cooperative upconversion can deplete two ions from the $^4I_{13/2}$ energy state, as seen in Figure 2.3 (a), thereby reducing the number of ions available for amplification. At best, it will add one ion to the $^4I_{13/2}$ excited state (Figure 2.3 (b)), but this case is not as common due to the generally high population of $^4I_{13/2}$ relative to other

energy states. Upconversion originating in the $^4I_{11/2}$ state (Figure 2.3 (c)) can usually be seen as 540-nm light as the ions excited into the upper states relax through spontaneous emission. Cross-relaxation transitions have an opposite range of effects; at best they can repopulate two ions into $^4I_{13/2}$ (Figure 2.3 (d)), and at worst they can depopulate one (Figure 2.3 (e)).

The depletion of excited erbium ions and subsequent loss in gain caused by upconversion and cross-relaxation can be offset by an increase in the pump beam power. However, more pump photons can lead to excited state absorption, another problem that will be discussed further on. In order to decrease upconversion effects while maintaining maximum pumping efficiency, the best course of action is to choose a host material that allows for an even distribution of erbium ions to minimize clustering and the probability of ion-ion interactions.

2.2.2. Excited state absorption

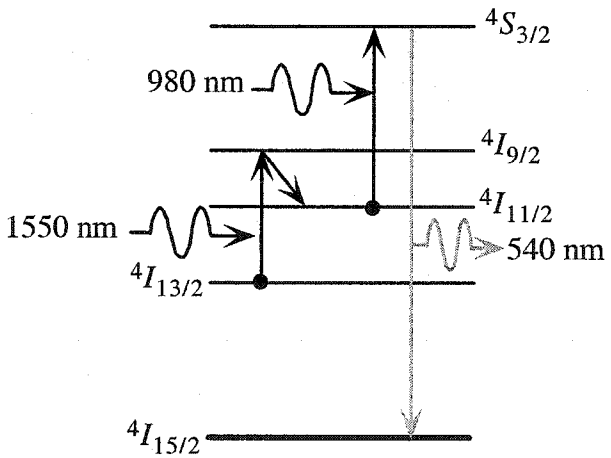

Figure 2.4: Two possible forms of excited state absorption. On the left, the ion starts at $^4I_{13/2}$ and eventually decays non-radiatively back to $^4I_{13/2}$. On the right, the ion starts at $^4I_{11/2}$, and decays to ground by emitting green light.

Excited state absorption is another phenomenon that affects the efficiency of erbium-doped waveguide amplifiers. In this transition, light is absorbed by already excited ions, causing them to move to a higher state. Two examples that are of particular concern to erbium-doped amplifiers are shown in Figure 2.4. If the ion is excited from the metastable state $^4I_{13/2}$, it will decay non-radiatively to $^4I_{11/2}$, and subsequently back to

$^4I_{13/2}$ again, as shown in the left portion of Figure 2.4. The second transition, shown in the right portion of Figure 2.4, occurs when ions in the energy level $^4I_{11/2}$ are excited to a higher energy state by the pump beam in the short time before they relax to $^4I_{13/2}$. From here they decay to the ground state by releasing green light. Excited state absorption depends on the power of the pump and the lifetime of the excited ions, as a higher power (which corresponds to more photons) or a longer lifetime will increase the likelihood that this effect will occur. Eventually, excited state absorption will limit the amount of pump power that can be converted into useful signal amplification.

2.2.3. Amplified spontaneous emission

As mentioned previously, spontaneous emission of erbium ions in the excited metastable state leads to the addition of noise to the signal. The photons released through spontaneous emission propagate in random directions in the waveguide and can also cause other excited ions to undergo stimulated emission, which amplifies the spontaneous emission. Amplified spontaneous emission (ASE) has a broad spectral range due to the Stark effect. Thus, a spectrum of wavelengths will be released that scales with the emission cross-section of the erbium ions (since the spectral shape of the spontaneously emitted light is proportional to the emission cross-section band) [4]. Increasing the power of the input 1550-nm signal can decrease amplified spontaneous emission, as a higher power input signal will increase the probability that excited ions will be used for stimulated emission.

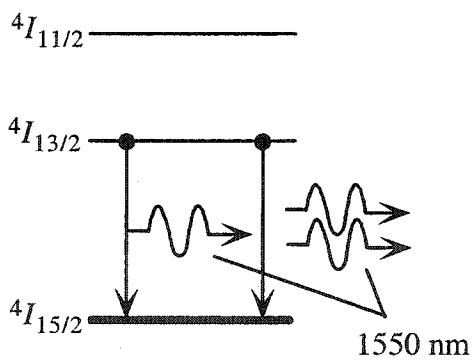

Figure 2.5: Amplified spontaneous emission. An excited ion spontaneously emits, inducing stimulated emission in another excited ion.

2.2.4. Energy migration

The efficiency of erbium-doped waveguide amplifiers can also be affected by energy migration and quenching, an effect that is present in bulk glasses [3]. Energy can migrate through the material by transferring between erbium ions through resonant interactions.

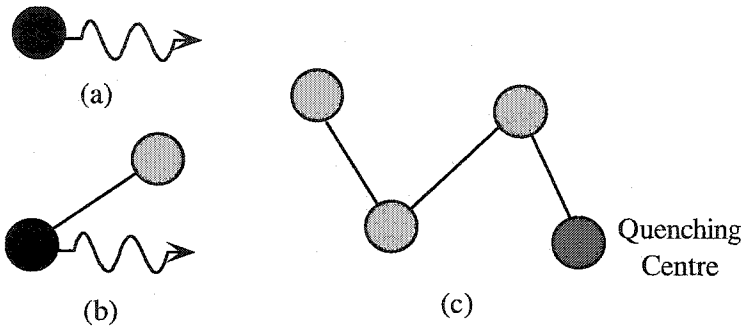

Figure 2.6: Three possible energy transitions: (a) Excited erbium ion emits a photon. (b) Energy migrates between excited erbium ions before emission. (c) Energy migrates between excited erbium ions until it is absorbed by quenching centre, and no photon is emitted.

This migration will continue until the energy is emitted as a photon, or is absorbed by a quenching centre, which is a defect in the glass such as an OH impurity. This absorption of the energy results in a decrease in the lifetime of the excited ions, but the decrease will only occur if the glass contains impurities that have the ability to couple to the erbium ions.

2.3. Chalcogenide glass

Chalcogenide glasses - amorphous semiconductors containing one of the chalcogen elements, tellurium, selenium or sulphur - have many properties that make them a promising material system for integrated optics, and for waveguide amplifiers in particular. A high refractive index (in the range of 2.0 to 3.0 [17,22]) allows for the creation of highly confining waveguides (a higher refractive index in the core will decrease the amount of light that leaks out of the waveguide by radiation), and improves the efficiency of transmission of light. Higher light confinement also allows smaller waveguide bend radii, aiding the development of high-density optical circuits. The high index of refraction also increases the emission and absorption cross-sections of the erbium ions [11], two important factors in increasing pump efficiency and gain.

Chalcogenide glasses also have low maximum phonon energy, which inhibits excited erbium ions from decaying through non-radiative recombinations. Rare earth ions such as erbium are highly soluble in chalcogenide glasses, allowing ions to distribute evenly and thereby minimize the amount of detrimental effects caused by clustering. This solubility allows higher doping concentrations than what would be possible in most other glass systems. Another advantage is the high transparency range of chalcogenide glasses, from approximately 800 nm to 16000 nm, depending on the alloy [22], which makes them ideal for transmitting many different signal wavelengths. Chalcogenide glasses also have relatively large third-order nonlinear effects, and are promising for all-optical signal processing. When exposed to light near the bandgap energy, chalcogenide glasses experience a change in refractive index. This phenomenon is known as the photodarkening effect [11], and can be used to pattern various device structures such as waveguides or gratings, simply by applying light to the glass [2].

Chalcogenide glasses also exhibit an interesting property when doped with erbium or other rare earth ions, in that the glass itself provides another path for erbium ions to become excited, i.e., wavelengths other than those at the absorption lines of the erbium ions can be used as pump sources. An example of this effect is illustrated in Figure 2.7.

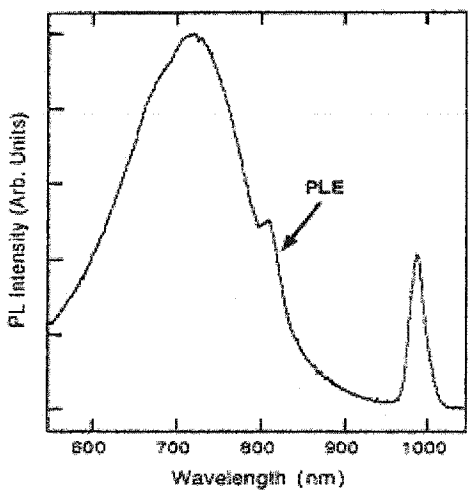

Figure 2.7: PLE spectra of erbium-doped chalcogenide glass taken at 300 K. The expected erbium excitation peaks can be seen at 810 nm and 980 nm, along with a broad excitation band [12].

The plot shows the photoluminescence excitation (PLE) spectrum, which is defined as the measured output intensity (in this case at 1550 nm) as a function of pump wavelength. The two expected peaks in the PLE spectrum at the pump wavelengths of 980 nm and 810 nm can be seen, corresponding to $^4I_{11/2}$ and $^4I_{9/2}$ in Figure 2.1. However, there is a wide range of other wavelengths that also produce 1550-nm emission. It is believed that defects in the glass that would normally cause the glass to photoluminesce interact with the erbium ions, which absorb the energy captured by the defects and become excited. The intensity of the light emitted by this process has been observed to increase in intensity as the concentration of erbium ions increases [11], which makes sense intuitively, as doping more erbium ions into the system would decrease the average distance between the ions and the glass defects, and increase the probability of interaction. The data shown in Figure 2.8 illustrates this behaviour.

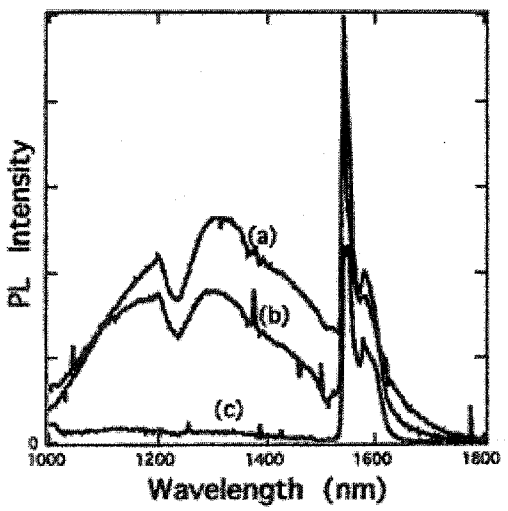

Figure 2.8: PL spectrum taken at 5 K and excited at 550 nm [11]. (a) 200 ppm erbium concentration. (b) 1100 ppm. (c) 7400 ppm.

The photoluminescence spectrum is plotted for three different erbium concentrations. For the lower concentrations, there is a peak at 1550 nm corresponding to the emission of the excited erbium ions, and a smaller band of output wavelengths that correspond to the defects causing the glass to undergo photoluminescence. As the erbium concentration increases, the photoluminescence band of the glass decreases, and the erbium emission line increases in intensity. These results qualitatively show the extra erbium ions taking energy away from the glass photoluminescence processes.

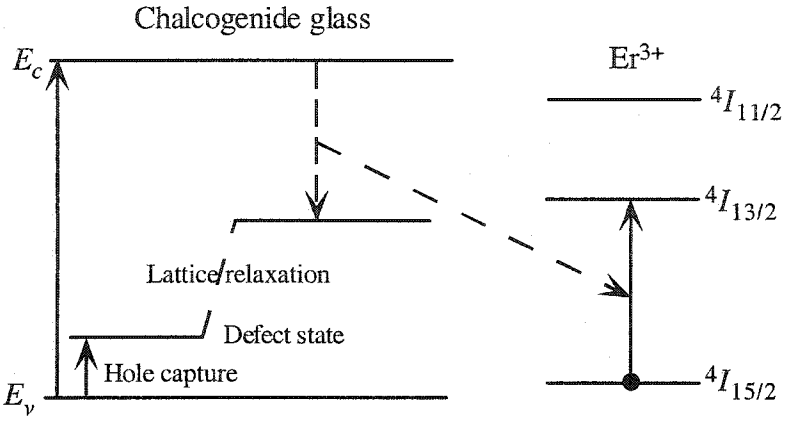

Figure 2.9: Mott Davis Street model of broadband excitation [11].

The Mott Davis Street model, illustrated in Figure 2.9, is typically used to explain this broadband excitation effect. If a photon of the correct energy enters the glass, it will create an electron-hole pair. The created hole is then captured by a defect state in the glass, and this change in charge in the defect state causes it to change energies and move to a higher energy in the bandgap through a lattice relaxation. Normally, at this point the electron-hole pair would recombine and release energy as a photon or phonons. However, when the glass is doped with a rare earth ion such as erbium, the energy can instead transfer to the erbium ions, and we obtain an alternative method of exciting the erbium at different pump wavelengths.

2.4. Chalcogenide alloy properties

Designing chalcogenide alloys for waveguide amplifier applications involves choosing component elements that will aid the fabrication and performance of these devices. Several materials with promising properties were examined.

Arsenic-based glasses tend to exhibit large photoinduced effects, which can potentially be used to directly pattern waveguides and gratings [14]. Adding arsenic is also known to generally improve the glass-forming ability of the alloy. Previous studies have reported that adding Ga to traditional Ge/As/S/Se chalcogenide glasses is essential in enabling uniform distribution of rare-earth dopants. For this reason, GaGeS and GaGeSe are among the most promising chalcogenide alloys for this purpose [15-16,23-24]. With these properties in mind, three different alloys were studied: GaGeS and GaGeSe because they are good hosts for erbium ions, and GaGeAsSe because it

combines the possibility of being a good rare-earth host with the possibility of exhibiting photoinduced effects.

In addition to the different alloys of glass, Er doping sources are also available in different chemical compounds. Two different doping sources were tested: Er_2S_3, due to previously reported successes [14] and the ability of S to fit in with the glass structure, and $ErCl_3$, due to its lower melting temperature, which could potentially ease glass preparation.

Measurements detailed in the next chapter were used to determine which glass system would be used as the amplifier medium for simulations.

3. Spectroscopic Theory

3.1. Calculation of parameters for simulation

In order to model erbium-doped waveguide amplifiers, it is necessary to determine parameters of the erbium ions within the host material. This section details the methods used to find several of these values.

3.1.1. Determination of Er cross-sections

The absorption cross-sections can be easily obtained from absorption measurements on the doped glass, but determining the emission cross-sections directly through experimental means is much more difficult. A common method that avoids complicated experiments is to first measure the absorption cross-section as a function of λ ($\sigma_a(\lambda)$), and then calculate the emission cross-sections ($\sigma_e(\lambda)$) using a theory that relates the two. For many ions, the Füchtbauer-Ladenburg (FL) theory is used, which takes the form:

$$\sigma_a(\lambda) = \frac{g_2}{g_1}\frac{\Delta\lambda_e^{eff}}{\Delta\lambda_a^{eff}}\sigma_e(\lambda) \tag{3.1}$$

where g_1 and g_2 are the degeneracies of the ion energy levels for the transition in question, and $\Delta\lambda_e^{eff}$ and $\Delta\lambda_a^{eff}$ are the effective widths of the transition cross-sections. However, in order for this equation to be rigorously accurate, the populations of all the Stark-split sublevels of the energy level in question must be equally distributed. This condition can be met only when the total Stark splitting energy is less than kT, which is not true in the case of erbium, whose Stark splitting is close to $2kT$ [21]. Therefore, a different method must be used.

In 1991, Miniscalco and Quimby [25] applied the more general McCumber theory to calculate cross-sections of erbium. The only condition that this theory imposes is that the time required for thermal distribution to be established within a manifold must be short in relation to the lifetime of that manifold, which is true in erbium. The absorption and emission cross-sections are then related by:

$$\sigma_e(\upsilon) = \sigma_a(\upsilon)\exp\left[\frac{\varepsilon - h\upsilon}{kT}\right] \tag{3.2}$$

where h is Planck's constant, υ is the frequency, and ε is the temperature-dependent excitation energy for the erbium transition being studied. The absorption cross-section data can be obtained from intensity measurements using the following equation:

$$\sigma_a(\upsilon) = \frac{1}{NL}\ln\left(\frac{I_o(\upsilon)}{I(\upsilon)}\right) \tag{3.3}$$

where N is the concentration of erbium ions, L is the path length of the sample, and I_o and I are the intensities of light incident on and exiting the sample, respectively. The excitation energy ε must now be calculated so that the emission cross-sections can then be obtained. However, this is no simple task, as knowledge of the electronic structure of the erbium ions is necessary. This problem can be avoided by making a simple substitution using the following equation that relates emission cross-section to the radiative lifetime, τ, of the state [25]:

$$\frac{1}{\tau} = \frac{8\pi n^2}{c^2}\int \upsilon^2 \sigma_e(\upsilon) d\upsilon \tag{3.4}$$

where n is the refractive index of the glass and c is the speed of light in vacuum. By substituting Equation (3.2) for $\sigma_e(\upsilon)$ in Equation (3.4), an equation for ε in terms of easily measured values is obtained [26]:

$$\varepsilon = kT\left[\frac{c^2}{8\pi n^2 \tau \int \upsilon^2 \sigma_a(\upsilon)\exp\left(\frac{-h\upsilon}{k_B T}\right)d\upsilon}\right] \tag{3.5}$$

Once ε is known, $\sigma_e(\upsilon)$ follows from Equation (3.2).

3.1.2. Determination of lifetimes

The radiative lifetime of the transition being studied can be either measured or calculated using the Judd-Ofelt theory. In this theory, the probability of spontaneous

emission A corresponding to the electric dipole transition between the initial state SLJ and the final state $S'L'J'$ is given as:

$$A^{ed}(SLJ,S'L'J') = \frac{64\pi^4\bar{\upsilon}^3}{3(2J+1)hc^3}\frac{n(n^2+2)^2}{9}s_{ed}(SLJ,S'L'J') \tag{3.6}$$

where $\bar{\upsilon}$ is the average frequency of the transition, n is the refractive index, and S, L and J are the spin, angular momentum and orbital momentum, respectively, of the initial state, used in Russell-Saunders coupling [21]. The factor $(n^2+2)^2/9$ is a local field correction factor, and s_{ed} is the electric dipole line strength, given by:

$$s_{ed}(SLJ,S'L'J') = e^2\sum_{t=2,4,6}\Omega_t\left(\left\langle f^N\gamma SLJ\left|U^{(t)}\right|f^N\gamma S'L'J'\right\rangle\right)^2 \tag{3.7}$$

where $\Omega_{t=2,4,6}$ are the three Judd-Ofelt phenomenological parameters and $U^{(t=2,4,6)}$ are the reduced matrix elements of the unit tensors, which are almost insensitive to the host material and can be found in many references [27-29] (see Appendix A).

There is also a component of spontaneous emission corresponding to the magnetic dipole transition:

$$A^{md}(SLJ,S'L'J') = \frac{64\pi\bar{\upsilon}}{3(2J+1)c}n^3 s_{md}(SLJ,S'L'J') \tag{3.8}$$

where n^3 is a local field correction factor for the magnetic dipole and s_{md} is the magnetic dipole oscillator line strength, given by:

$$s_{md} = \frac{e\hbar}{2mc}\left|\left\langle f^N\gamma SLJ\left|\left(\hat{L}+2\hat{S}\right)\right|f^N\gamma S'L'J'\right\rangle\right|^2 \tag{3.9}$$

where $\hbar = h/2\pi$, m is the mass of the electron and $\hat{L}+2\hat{S}$ is the magnetic dipole operator. The magnetic dipole is normally much smaller than the electric dipole, and as such it is usually ignored [21]. However, in the case of erbium, the transition from the $^4I_{15/2}$ (ground) state to the $^4I_{13/2}$ state has a significant magnetic dipole component, which must be taken into account [13].

The Judd-Ofelt parameters can be calculated using values for the oscillator strength of the absorption transitions, $f(SLJ, S'L'J')$, which are obtained through the equation:

$$f(SLJ,S'L'J') = \frac{mc^2}{\pi e^2 Nl}\int \ln\left(\frac{I_o(\upsilon)}{I(\upsilon)}\right)d\upsilon \tag{3.10}$$

where I_o and I are as defined in Section 3.1.1. After the oscillator strength values are calculated, they can be related to the electric dipole line strengths by:

$$f(SLJ,S'L'J') = \frac{8\pi^2 m\bar{\upsilon}}{3h(2J+1)e^2}\frac{\left(n^2+2\right)^2}{9n}s_{ed}(SLJ,S'L'J') \tag{3.11}$$

By substituting Equation (3.7) into Equation (3.11) and using the calculated values of $f(SLJ, S'L'J')$, the Judd-Ofelt parameters can then be calculated using a linear least-squares-fitting method. It is important to note that since there are three unknown parameters to be obtained, this method requires at least three absorption line spectra to obtain the independent variables (oscillator strength f, mean frequency $\bar{\upsilon}$, and reduced matrix elements $U^{(t)}$). After the parameters are found, the probability of spontaneous emission and lifetime ($\tau = 1/A$) of the excited state can be found. It is important to note that the values for the reduced matrix elements $U^{(t)}$ for a given transition are slightly different for emission than they are for absorption. As such, when we are calculating the Judd-Ofelt parameters using absorption spectral data, the absorption values for $U^{(t)}$ are used, and when the spontaneous emission probability A is calculated, the emission values are used.

3.2. Experimental Work

Measurements were taken on bulk glass samples with two purposes in mind. The first goal was to get a general idea of which glass alloy would be the best suited to use as a host for waveguide amplifiers. The second goal was to obtain the absorption characteristics needed to calculate theoretical lifetimes and cross-sections for simulations.

3.2.1. Bulk sample fabrication

Dr. Safa Kasap's materials research group at the University of Saskatchewan designed and fabricated the bulk glass samples to be used in erbium-doped waveguide amplifier research. The appropriate combinations of components (As, Se, Ge, Ga, S, Er_2S_3 or $ErCl_3$) were placed in evacuated, fused silica ampoules, which were then placed in a rocking furnace for approximately 20 hours at 1000 °C. The finished samples were quenched in water and cut into small pieces for measurement. The approximate concentrations of elements in the alloys were as follows:

GaGeAsSe – $Ga_3Ge_5(As_2Se_3)_{92}$

GaGeS – $(Ga_2S_3)_{20}(GeS_2)_{80}$

GaGeSe – $Ga_{6\text{-}9}Ge_{27}Se_{61\text{-}65}$

3.2.2. Photoluminescence lifetimes measurement

The photoluminescence lifetimes of the erbium ions within the various chalcogenide glass samples were measured using the experimental setup shown in Figure 3.1.

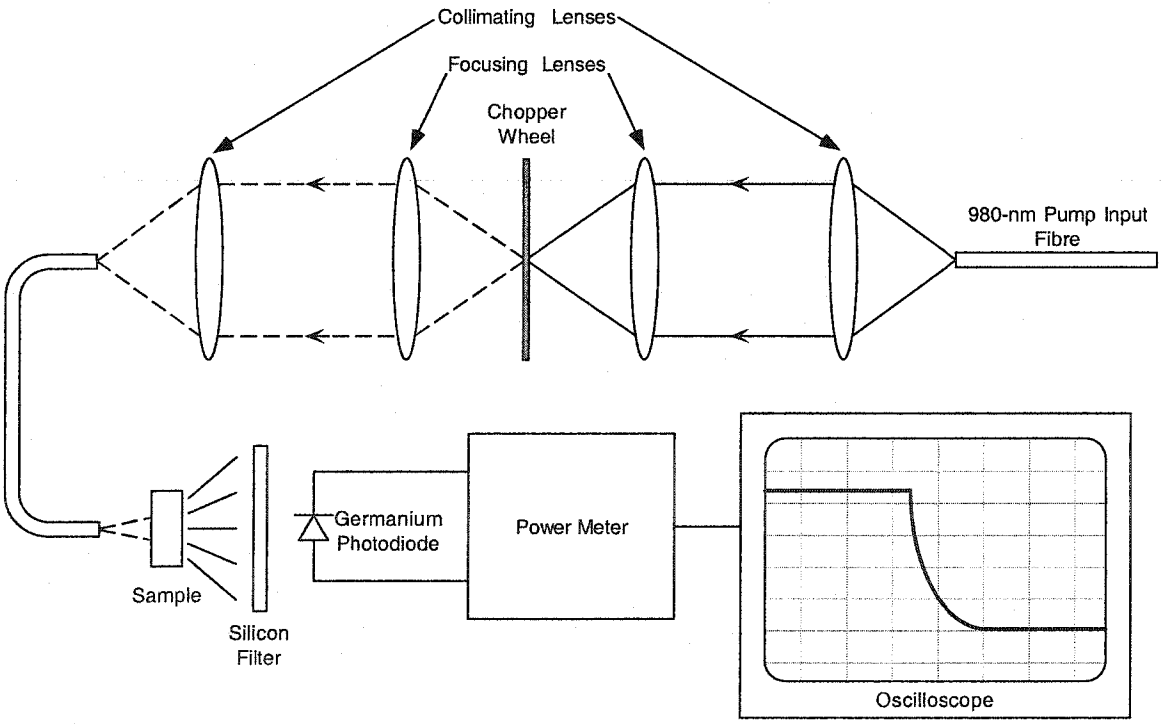

Figure 3.1: Experimental set-up for measurement of PL lifetimes.

The 980-nm pump beam is collimated and then focused to a diffraction-limited spot, where the chopper wheel modulates it into an 8-Hz square wave. This modulated beam is used to pump the erbium ions in the sample being measured, producing 1550-nm emission. This signal is then passed through a silicon filter to remove any residual pump, and picked up by a germanium detector. Finally, the signal from the detector is displayed on an oscilloscope and saved.

The exponential decay of the light signal seen after the chopper shuts off the pump beam provides the lifetime of the erbium ions in the excited state. This decay can be easily curve-fitted to a basic exponential function (i.e.: $I = I_o \exp(-t/\tau)$, where I_o is the initial intensity and τ is the lifetime of the erbium ions) using graphic analysis software. This method will also indicate if adverse effects such as cooperative upconversion or quenching are present in the glass sample, although it will not differentiate between them. Since these effects cause the erbium ions to decay from their excited states at an accelerated rate, they are seen on the plot as a sharp drop in luminescence, followed by the expected exponential decay, as illustrated in Figure 3.2 (b).

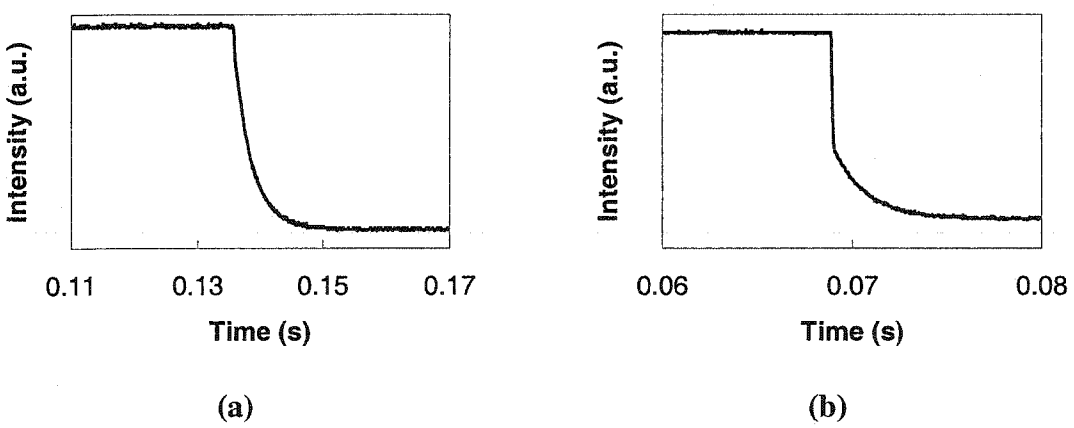

Figure 3.2: Example decay curve plots. (a) shows a curve without any apparent deleterious effects, and (b) shows a curve with a sharp initial drop in luminescence, indicating the presence of some quenching effect.

The differences in these two cases can be seen more clearly by plotting the log of the intensities versus time, as shown in Figure 3.3.

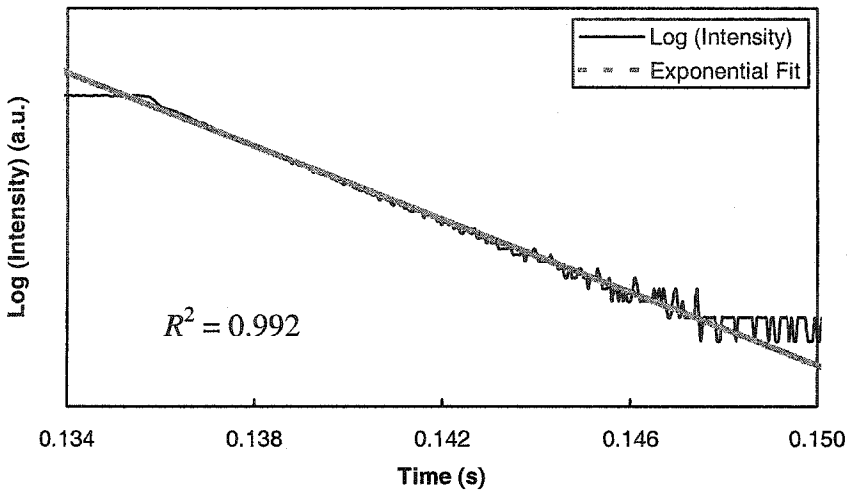

(a)

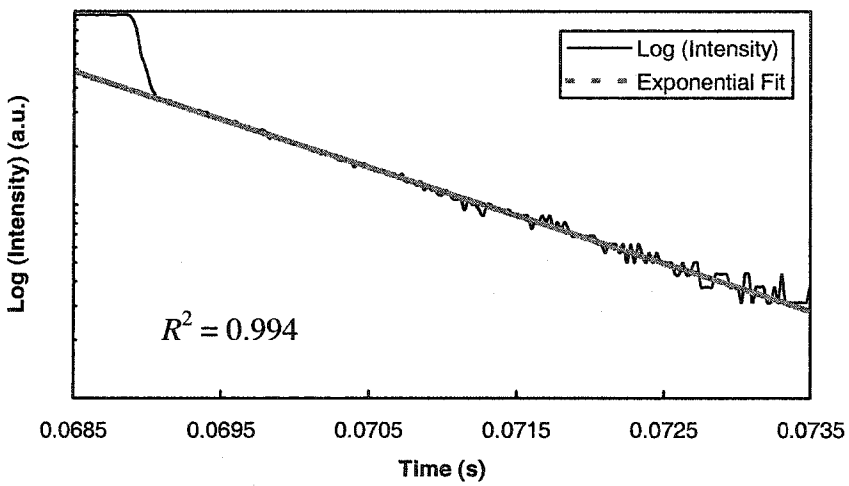

(b)

Figure 3.3: Semilog plots of the example decay curves showing exponential fits. (a) shows the curve with no major adverse effects and (b) shows the curve experiencing some quenching effect. The R^2 values are the regression coefficients indicating the quality of the curve fit to the 1550-nm decay.

The curve with no deleterious effects shows a good fit to a single exponential function, as expected, with a small discrepancy that corresponds to the pump beam that leaks through the silicon filter. The second curve shows a much more pronounced initial exponential decay that corresponds to the heavy quenching present in the glass, followed by the expected luminescence decay, which does fit to the expected single exponential.

There are two main sources of error inherent in this experimental apparatus. The photodetector has an associated falltime, which will skew the resulting lifetime a small amount. The largest error comes from the chopper wheel. Since the beam has a finite width at the focus point, it takes a measurable amount of time for the chopper to completely stop the beam. This error was measured by observing the decay time of the 980-nm pump beam, which was found to range from 130 μs to 200 μs, depending on how well the lenses were aligned. Since typical lifetimes of good samples are in the range of 1-4 ms, this experimental setup gives values with an acceptable level of error.

The photoluminescence lifetimes were needed in order to determine which alloy of glass was most suitable to be used as an amplification medium, and also to be used later for simulation of waveguide amplifiers. The effects of other factors were also observed through the measurement of lifetimes. These factors included the doping concentration of erbium and the source of the erbium (i.e., Er_2S_3 or $ErCl_3$). See Section 2.1 for a discussion of the importance of photoluminescence lifetimes.

3.2.3. Photoluminescence lifetimes results

As different glass alloys were fabricated and the glass-forming procedures were perfected, the lifetimes of the produced samples were measured. Early samples showed inconsistent lifetimes until the final procedures were settled on (a summary of all lifetime measurements is presented in Appendix B). When measuring the PL lifetime of the samples, it was found that the alloys using $ErCl_3$ as a dopant source had virtually no lifetime that could be differentiated from the error produced by the chopper wheel, while the Er_2S_3-doped samples exhibited lifetimes in the 1-4 ms range. Of the three Er_2S_3-doped alloys investigated, GaGeAsSe had the lowest lifetimes, in the range of 1-1.5 ms. The GaGeSe and GaGeS samples showed the most promise for optical amplifier applications, showing lifetimes in the range of 2-4 ms.

The behaviour of the 1550 luminescence was examined with respect to increasing Er^{3+} concentration for the two more promising alloys. In GaGeS, the PL lifetime was constant at approximately 2.75 ms until it began to decrease at the higher erbium concentrations, as seen in Figure 3.4. GaGeSe showed a similar trend as the lifetime reached a peak and then decreased slightly at higher concentrations. The shorter lifetimes

observed at the lower Er^{3+} concentrations are possibly due to the difficulty in measuring and analyzing the weaker 1550 luminescence signal produced by those samples, since a weaker luminescence signal was much more susceptible to corruption from noise and leak-through from the pump beam.

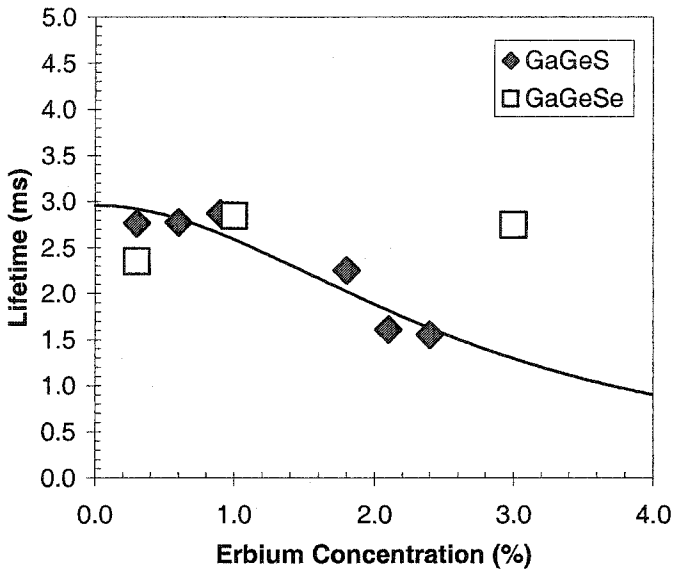

Figure 3.4: Dependence of PL lifetime on erbium concentration. The line is the curve-fit found using Equation (3.12) for the GaGeS samples.

3.2.4. Discussion on photoluminescence lifetimes

The lack of a discernable lifetime observed in the $ErCl_3$-doped samples indicates that $ErCl_3$ is not a good source for doping the chalcogenide alloys studied. The presence of Cl in the glass acts as quenching centre, and causes instability in the glass structure [30]. Arsenic also causes a decrease in the lifetime, as we saw when we compared the lifetime of GaGeAsSe (~1.5 ms) to that of GaGeSe (~2.9 ms). It is known that rare earth ions have limited solubility in As-S-Se glasses [17], suggesting that Er clustering may be increased by the addition of As. Clustering of Er ions is known to lead to increases in upconversion processes, which will reduce the lifetime of the metastable state [21].

Concentration quenching of the luminescence lifetime is commonly described by the empirical relation [31]:

$$\tau(\rho) = \frac{\tau_0}{1+\left(\rho / \rho_q\right)^2} \tag{3.12}$$

where $\tau(\rho)$ is the observed lifetime, τ_0 is the lifetime at zero Er concentration (interpolated from the lifetime versus Er concentration plot), ρ is the concentration of Er, and ρ_q is the concentration at which the lifetime becomes half of τ_0. The behaviour described by this plot is similar to that observed in the GaGeS samples. Although we have a small set of points, a curve-fit using this expression gives values of $\tau_0 = 2.96$ ms and $\rho_q = 10.5 \times 10^{26}$ m^{-3}. These values compare well to silicate and phosphate glasses [19], which typically have ρ_q values in the 3-8 $\times 10^{26}$ m^{-3} range.

It is also interesting to note that the lifetime versus erbium concentration behaviour of the two glasses decreases after reaching a peak at 1 at. %. To further investigate this trend, measurements were performed on luminescence intensity produced by the glass samples. Relative luminescent intensities were obtained by exciting the samples with a 980-nm pump and measuring the total luminescence over the 1550-nm band with a germanium photodetector. Care was taken to ensure that the pump beam intensity was approximately uniform over the entire cross-section of the samples, to ensure that relative comparisons could be made. Each sample was then weighed, and the weights were used to scale the total intensity measurements. These measurements allowed a weight-relative comparison of the luminescence intensity of samples of different Er concentration and size.

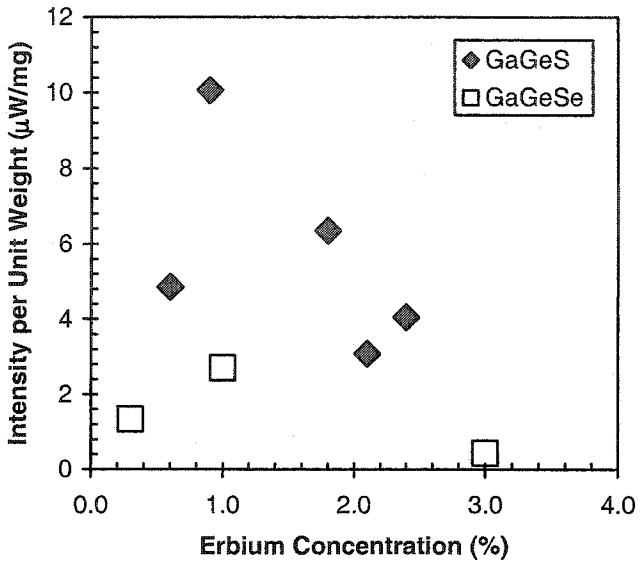

Figure 3.5: Dependence of relative PL intensity on erbium concentration.

Figure 3.5 illustrates the effect of erbium concentration on the relative photoluminescence emitted by the sample. In the case of both GaGeS and GaGeSe, the luminescence intensity reaches a peak value at about 1 at. % Er^{3+} and then decreases as the concentration is increased. These results suggest that approximately 1 at. % Er^{3+} may be an optimum value for these glass compositions [45].

3.2.5. Absorption spectra measurement

Absorption spectra of a $Ga_{8.17}Ge_{21.06}Se_{68.88}S_{1.25}Er_{0.65}$ bulk sample were measured by our collaborators at the University of Saskatchewan, using a spectrophotometer [32]. The results obtained can be seen in Figure 3.6 and Figure 3.7.

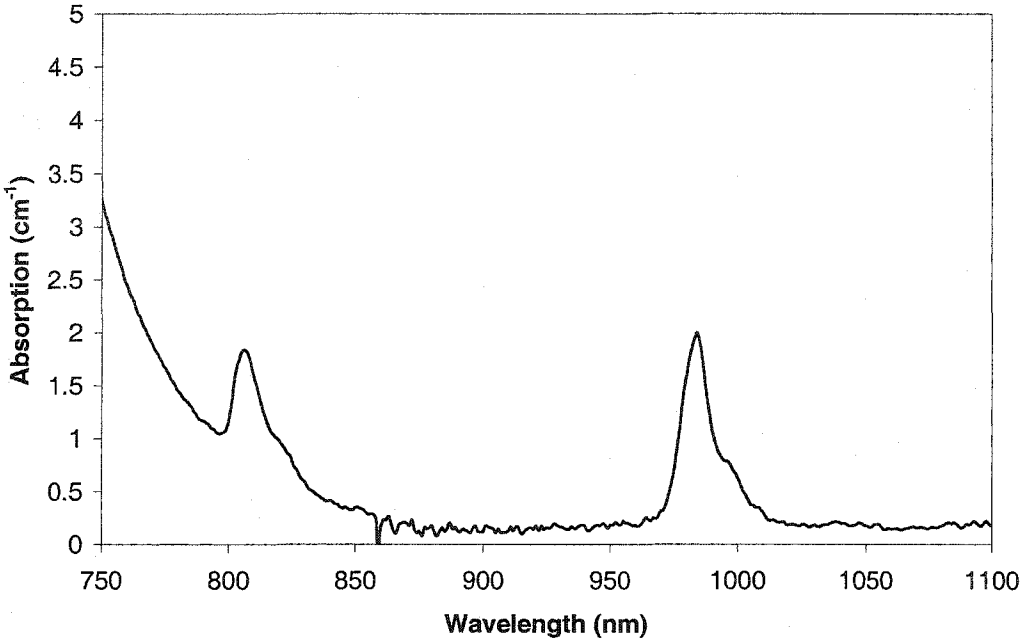

Figure 3.6: Absorption spectra for $Ga_{8.17}Ge_{21.06}Se_{68.88}S_{1.25}Er_{0.65}$ sample [32]. This figure shows the erbium 800-nm and 980-nm bands, along with the glass absorption below 850 nm.

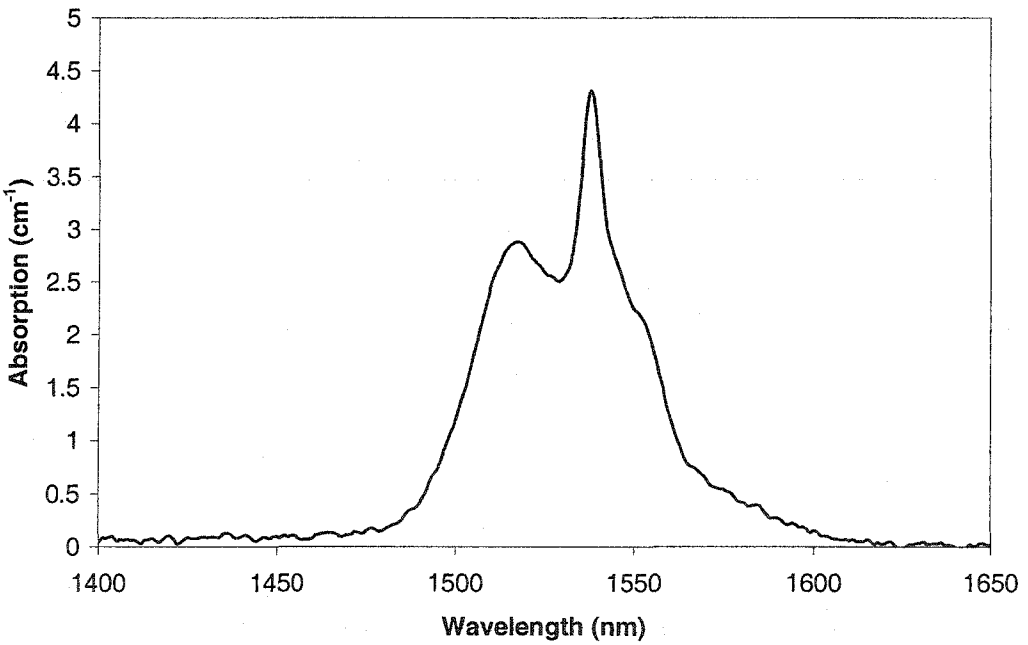

Figure 3.7: Absorption spectra for $Ga_{8.17}Ge_{21.06}Se_{68.88}S_{1.25}Er_{0.65}$ sample [32]. This figure shows the 1550-nm erbium band.

These absorption results were used to determine the lifetimes using the Judd-Ofelt theory, and the absorption and emission cross-sections of the erbium ions in the glass using the McCumber theory.

3.3. Lifetime calculations

The lifetimes to be used in simulations were taken from calculations performed for the paper in reference [32]. Through Judd-Ofelt theory, the Judd-Ofelt parameters were found to be $\Omega_2 = 16\times10^{-26}$ m^2, $\Omega_4 = 4.2\times10^{-26}$ m^2 and $\Omega_6 = 1.2\times10^{-26}$ m^2. From these, the probabilities of relevant transitions were calculated.

These values, listed in Table 3.1, are reasonably close to those obtained for similar glasses by other researchers [31, 33]. As can be seen, the 3 to 2 transition has a low probability, which may hinder the performance of the amplifier as discussed in Section 2.1. The calculated lifetime of the metastable level ($^4I_{13/2}$) is 1.39 ms, which is significantly lower than the values of about 2.9 ms measured previously on bulk samples (see Section 3.2.3). This discrepancy is unaccounted for, but it is possible that the lifetimes are different because the samples were from two different batches.

Table 3.1: Transition probabilities obtained through Judd-Ofelt theory.

Transition	Probability (s^{-1})	Lifetime (ms)
$^4I_{13/2}$ to $^4I_{15/2}$	719	1.39
$^4I_{11/2}$ to $^4I_{15/2}$	960	1.04
$^4I_{11/2}$ to $^4I_{13/2}$	117	8.54
$^4I_{9/2}$ to $^4I_{15/2}$	1563	0.64
$^4I_{9/2}$ to $^4I_{13/2}$	182	5.49
$^4I_{9/2}$ to $^4I_{11/2}$	4	250

Since Judd-Ofelt theory only calculates probabilities for radiative transitions, it is necessary to calculate the non-radiative probability in order to get the overall lifetime for transitions that have a significant non-radiative component. The following equation is commonly used to calculate the non-radiative lifetime [13]:

$$A_{nr} = C\left[n(T)+1\right]^p \exp\left(-\alpha\Delta E\right) \tag{3.13}$$

where C and α are host-dependent constants, $n(T)$ is the Bose-Einstein occupation number, and p is the number of phonons necessary to satisfy the energy gap ΔE between the states in question. Given a maximum phonon energy of 425 cm^{-1} or 0.05 eV [13], the minimum number of phonons was determined to be 9. The values for C and α were set as 10^6 s^{-1} and 2.9×10^{-3} cm, respectively, from data on a similar glass system [13]. $n(T)$ was calculated to be 0.124 using the following equation [21]:

$$n(T) = \frac{1}{\exp\left(\frac{hc}{\lambda kT}\right) - 1} \tag{3.14}$$

These values gave a non-radiative decay rate of 53.88 s^{-1}. Using Equation (2.6), the total transition rate from $^4I_{11/2}$ to $^4I_{13/2}$ was found to be 170 s^{-1}, with a corresponding lifetime of 5.86 ms. The $^4I_{9/2}$ to $^4I_{11/2}$ transition also has a strong non-radiative component of 4044.3 s^{-1}, giving an overall lifetime of 0.25 ms. These values are significantly lower than that for the purely radiative lifetime, showing that phonon emission is an integral part of these transitions.

3.4. Cross-section calculations

Using the measured absorption data and the lifetimes calculated through the Judd-Ofelt theory, the absorption and emission cross-sections of the 980-nm and 1550-nm states were calculated using the McCumber theory as detailed in Section 3.1.1. The results are displayed in Figure 3.8 and Figure 3.9.

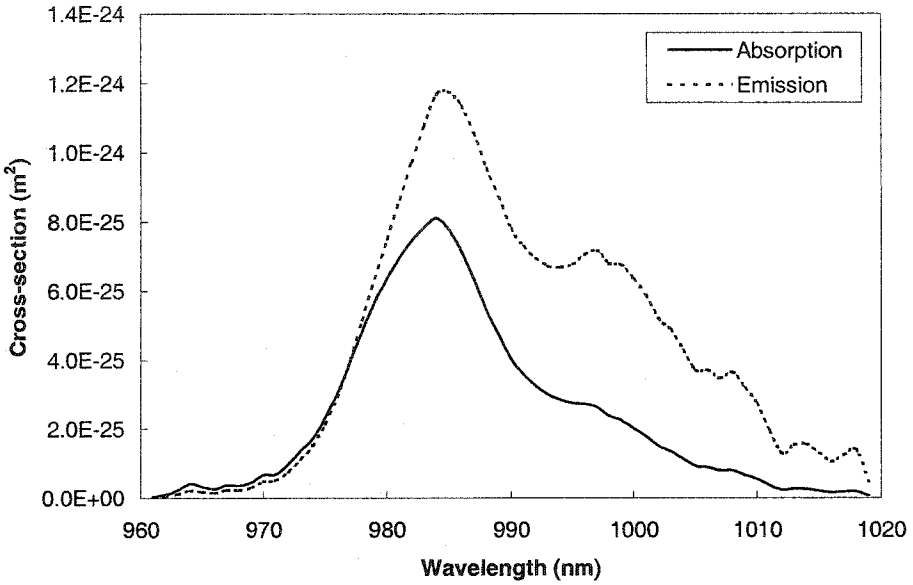

Figure 3.8: 980-nm band absorption and emission cross-sections.

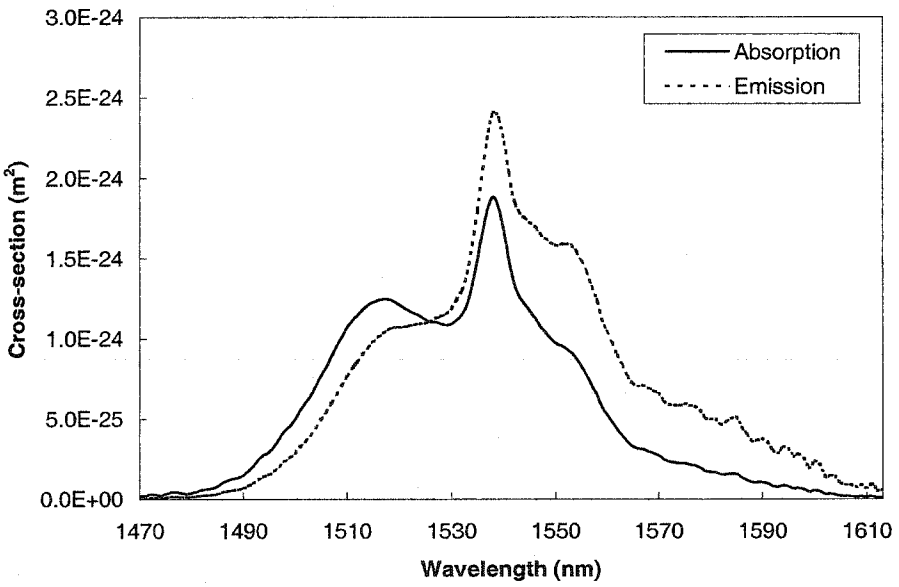

Figure 3.9: 1550-nm band absorption and emission cross-sections.

The 1550-nm cross-sections show expected behaviour, with peak values being of the same order of magnitude. It can also be seen that the emission cross-section is lower than the absorption cross-section for wavelengths lower than about 1530 nm, which is necessary if the $^4I_{13/2}$ band is to be used for both pumping and amplification (this fact enables pumping of erbium-doped fibre amplifiers at 1480 nm). It should also be noted

that the cross-sections for erbium are larger in the chalcogenide glasses studied than in other glasses (such as phosphate or SiO_2), which are typically in the order of 10^{-25} m^2 [5-6,19,34]. Higher emission cross-sections typically indicate more gain, as was seen in Equation (2.2), but at the same time, higher absorption cross-sections can lead to increased signal absorption.

What will potentially cause problems is the non-negligible emission cross-section in the 980-nm band. Normally, stimulated emission of 980-nm pump photons is ignored in waveguide amplifier simulations, due to the high probability of the non-radiative transition from $^4I_{11/2}$ to $^4I_{13/2}$ [1,4,19] in phosphate or silicate glasses. There is not enough time for ions in the $^4I_{11/2}$ state to enter thermal equilibrium, and the McCumber theory cannot be used (see Section 3.1.1). However, in chalcogenide glasses, the probability of this mostly non-radiative transition is actually quite low (~170 s^{-1}, while in other glasses typically used for EDWAs, this number is in the range of 10^6 s^{-1}), and the McCumber theory applies, producing a finite emission cross-section. The low probability of the $^4I_{11/2}$ to $^4I_{13/2}$ non-radiative transition coupled with the high probability of the level $^4I_{11/2}$ to ground stimulated emission transition hinders the realization of the necessary population inversion. This problem is discussed fully in Chapter 4.

4. Simulation

4.1. Transfer matrix method

The transfer matrix method is commonly used to find the magnitudes of electric and magnetic fields in layered media. It is an easy technique to implement and gives exact numerical solutions. A general example of this type of problem is illustrated in Figure 4.1:

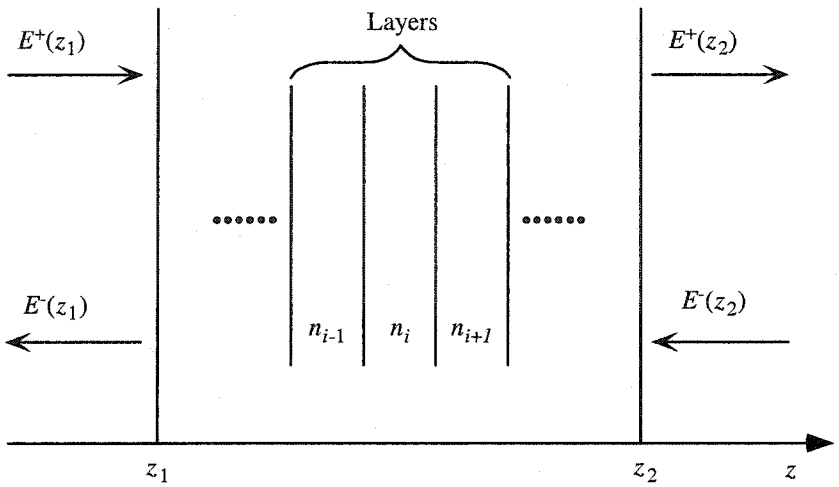

Figure 4.1: General multi-layer structure.

$E^+(z)$ and $E^-(z)$ are the electric field complex amplitudes travelling in the forward and backward directions, respectively, at a given point along the direction of propagation. n_i denotes the complex refractive index of a given layer within the structure. The fields at the two points z_1 and z_2 can be related as follows:

$$\begin{bmatrix} E^+(z_1) \\ E^-(z_1) \end{bmatrix} = \begin{bmatrix} M_{11} & M_{12} \\ M_{21} & M_{22} \end{bmatrix} \begin{bmatrix} E^+(z_2) \\ E^-(z_2) \end{bmatrix} \tag{4.1}$$

where M_{11}, M_{12}, M_{21} and M_{22} are the coefficients of the structure's overall transfer matrix. To determine the overall matrix of the device, the matrices of the individual sections of the structure are multiplied together in order from left to right. There are two basic matrices for a dielectric structure such as the one seen in Figure 4.1, one that describes the interface between two layers, and another that describes the bulk of a layer. The matrix for an interface is given by:

$$M_{in} = \frac{1}{2n_i}\begin{bmatrix} n_i + n_{i+1} & n_i - n_{i+1} \\ n_i - n_{i+1} & n_i + n_{i+1} \end{bmatrix} \tag{4.2}$$

and the matrix for a layer is as follows:

$$M_{lay} = \begin{bmatrix} \exp(jk_o n_i d_i) & 0 \\ 0 & \exp(-jk_o n_i d_i) \end{bmatrix} \tag{4.3}$$

where $k_o = 2\pi/\lambda$ is the wavenumber in vacuum, and d_i is the thickness of the layer. The overall matrix of a structure is then given by:

$$M = M_{in1} \times M_{lay1} \times M_{in2} \times M_{lay2} \times M_{in3} \times \cdots \tag{4.4}$$

This method can be applied to waveguide devices by treating them as a dielectric structure, where effective modal indices are used instead of material indices [35]. Since the transfer matrix can be determined by stepping through the separate layers, the behaviour of the pump and signal beams can be observed as they travel through the waveguide, and the length d of the layers can be decreased or increased depending on the desired accuracy of results [36]. The layer structure also has an added element of flexibility in that a grating structure can be added to the waveguide model, in the event that a wavelength selective device is being studied.

In addition to finding the values of the electric field amplitude throughout the waveguide, the overall matrix can be used to calculate the reflectance and transmittance of the signals travelling through the structure. The reflection and transmission coefficients (r and t) at an incident plane are given by:

$$r = \left.\frac{E^-(z_1)}{E^+(z_1)}\right|_{E^-(z_2)=0} = \frac{M_{21}}{M_{11}} \tag{4.5}$$

$$t = \left.\frac{E^+(z_1)}{E^+(z_1)}\right|_{E^-(z_2)=0} = \frac{1}{M_{11}} \tag{4.6}$$

The reflectance R is found by simply squaring Equation (4.5), and the transmittance T is found by squaring Equation (4.6) and including the possibility of the incident and transmitted waves being in media of different refractive indices.

$$R = \left| \frac{M_{21}}{M_{11}} \right|^2 \tag{4.7}$$

$$T = \frac{n_L}{n_o} \left| \frac{1}{M_{11}} \right|^2 \tag{4.8}$$

where n_o and n_L are the refractive indices of the materials surrounding the structure [37].

If we assume there is no wave travelling in the reverse direction (i.e., $E^-(L) = 0$, where L is the length of the waveguide), the matrix equation relating the input and output fields can be simplified to:

$$E^+(L) = \frac{1}{M_{11}} E^+(0) \tag{4.9}$$

$$E^-(0) = \frac{M_{21}}{M_{11}} E^+(0) \tag{4.10}$$

These two equations are used in order to relate the field at any point in the guide to the input field, $E^+(0)$. The electric fields at an arbitrary point z_p in the guide are defined with a new transfer matrix M_p that extends from the plane at z_p to the exit plane at L:

$$\begin{bmatrix} E^+(z_p) \\ E^-(z_p) \end{bmatrix} = \begin{bmatrix} M_{p11} & M_{p12} \\ M_{p21} & M_{p22} \end{bmatrix} \begin{bmatrix} E^+(L) \\ E^-(L) \end{bmatrix} \tag{4.11}$$

By substituting in $E^-(L) = 0$ and equations (4.9) and (4.10), the electric fields at z_p are obtained in terms of the input field:

$$E^+(z_p) = M_{p11} \frac{1}{M_{11}} E^+(0) \tag{4.12}$$

$$E^-(z_p) = M_{p21} \frac{1}{M_{11}} E^+(0) \tag{4.13}$$

The total intensity $I(z_p)$ is then found:

$$I(z_p) = \frac{1}{2} c \varepsilon_o n(z_p) \left[\left| E^-(z_p) \right|^2 + \left| E^+(z_p) \right|^2 \right] \tag{4.14}$$

where ε_o is the permittivity of free space [36].

It should be noted that this method only gives the intensity profile of a signal in the direction of propagation, and not in the plane of the waveguide cross-section. The transverse properties of the guided signal and pump modes are reduced to overlap factors (as seen in Section 4.3). These factors reduce the three-dimensional waveguide propagation problem to one dimension. This approach was previously verified for accuracy by Giles and Desurvire [38]. For the present work, a previously developed transfer matrix model for phosphate glass EDWAs, provided by Dr. R. G. Decorby [35], was modified to simulate chalcogenide EDWAs.

4.2. The rate equations

Simulating amplifier systems requires knowledge of the populations of the various energy states of the rare-earth ions in order to determine the gain or absorption that the signal and pump beams experience as they travel through the waveguide. These populations can be solved for using rate equations, which describe how the populations of the energy levels change with time. Two separate models were used in order to simulate the performance of chalcogenide amplifiers under two different pumping conditions: 980-nm pumping and 1480-nm pumping.

4.2.1. 980-nm pump model

The following 5-level model was used to simulate chalcogenide waveguides under a 980-nm pump beam:

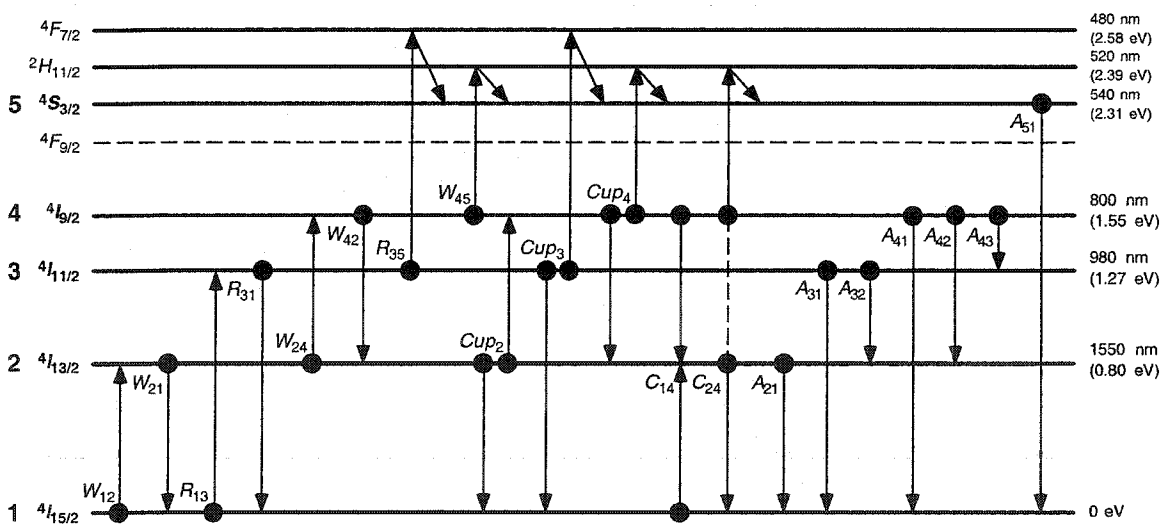

Figure 4.2: 5-level model for 980-nm pump simulations.

The states used in the model are numbered 1-5 for simplification, and each level's transition energy and wavelength relative to the ground state are given for reference. Also, the ions that reach the $^4F_{7/2}$ and $^2H_{11/2}$ state are assumed to decay instantaneously and non-radiatively to $^4S_{3/2}$. The $^4F_{9/2}$ state is not used in the model but is shown as a dashed line for reference. Table 4.1 summarizes the transition parameters used in this model.

Table 4.1: Description of 980-nm pump model parameters.

Parameter	Description
$R_{13} = \phi_p \sigma_{13}$	980-nm pumping to populate state 3.
$R_{31} = \phi_p \sigma_{31}$	980-nm stimulated emission from state 3.
$W_{21} = \phi_s \sigma_{21}$	1550-nm stimulated emission from state 2.
$W_{12} = \phi_s \sigma_{12}$	1550-nm signal absorption from state 1 to 2.
$A_{21} = 1/\tau_{21}$	Spontaneous emission from state 2 to 1.
$A_{31} = 1/\tau_{31}$	Spontaneous emission from state 3 to 1.
$A_{32} = 1/\tau_{32}$	Non-radiative relaxation from state 3 to 2.
$A_{41} = 1/\tau_{41}$	Spontaneous emission from state 4 to 1.
$A_{42} = 1/\tau_{42}$	Spontaneous emission from state 4 to 2.
$A_{43} = 1/\tau_{43}$	Non-radiative relaxation from state 4 to 3.
$A_{51} = 1/\tau_{51}$	Spontaneous emission from state 5 to 1.
$W_{24} = \phi_s \sigma_{24}$	Excited state absorption of signal (state 2 to 4).
$W_{42} = \phi_s \sigma_{42}$	1550-nm stimulated emission from state 4 to 2.
$R_{35} = \phi_p \sigma_{35}$	Excited state absorption of pump (state 3 to 5).
$W_{45} = \phi_s \sigma_{45}$	Excited state absorption of signal (state 4 to 5).
Cup_2	Cooperative upconversion coefficient for ions at state 2.
Cup_3	Cooperative upconversion coefficient for ions at state 3.
Cup_4	Cooperative upconversion coefficient for ions at state 4.
C_{14}	Cross-relaxation coefficient for ions at states 1 and 4.
C_{24}	Cross-relaxation coefficient for ions at states 2 and 4.

For the sake of simplicity, any stimulated emission or absorption transition, including excited state absorption, is denoted by R or W if it is induced by the pump or signal beam, respectively.

In this chalcogenide EDWA model, several transitions that are typically ignored in models for erbium in phosphosilicate glass hosts [4,7,38,39] need to be taken into account. Since the spontaneous emission probability A_{32} is so low, other transitions from the ${}^4I_{11/2}$ state have a greater effect, and as such the spontaneous emission A_{31} and stimulated emission W_{31} caused by the pump are added to the model. Also, many other models ignore several of the excited state absorption and cooperative upconversion processes that cannot be ignored here.

The rate equations are formulated using these parameters and the 5-level model of the system.

$$\frac{dN_1}{dt} = -(W_{12}+R_{13})N_1 + (W_{21}+A_{21})N_2 + (R_{31}+A_{31})N_3 + A_{41}N_4 + A_{51}N_5 - C_{14}N_1N_4 + C_{24}N_2N_4 + Cup_2N_2^2 + Cup_3N_3^2 \tag{4.15}$$

$$\frac{dN_2}{dt} = W_{12}N_1 - (W_{21}+W_{24}+A_{21})N_2 + A_{32}N_3 + (W_{42}+A_{42})N_4 + 2C_{14}N_1N_4 - C_{24}N_2N_4 - 2Cup_2N_2^2 + Cup_4N_4^2 \tag{4.16}$$

$$\frac{dN_3}{dt} = R_{13}N_1 - (R_{31}+R_{35}+A_{31}+A_{32})N_3 + A_{43}N_4 - 2Cup_3N_3^2 \tag{4.17}$$

$$\frac{dN_4}{dt} = W_{24}N_2 - (W_{45}+W_{42}+A_{43}+A_{42}+A_{41})N_4 - C_{14}N_1N_4 - C_{24}N_2N_4 + Cup_2N_2^2 - 2Cup_4N_4^2 \tag{4.18}$$

$$\frac{dN_5}{dt} = R_{35}N_3 + W_{45}N_4 - A_{51}N_5 + C_{24}N_2N_4 + Cup_3N_3^2 + Cup_4N_4^2 \tag{4.19}$$

$$N_t = N_1 + N_2 + N_3 + N_4 + N_5 \tag{4.20}$$

N_t is the total concentration of erbium ions in the device, and N_1, N_2, N_3, N_4 and N_5 denote the ion populations of their respective energy levels. The population changes caused by cooperative upconversion and cross-relaxation are multiplied by two in

Equations (4.16), (4.17) and (4.18) since two ions are lost or gained in these processes at the second and third levels. To avoid a transient analysis, the system is assumed to be at steady state, i.e., $dN_1/dt = dN_2/dt = dN_3/dt = dN_4/dt = dN_5/dt = 0$. This substitution leaves a system of non-linear equations that can be solved numerically using the Newton-Raphson method (detailed in Appendix C).

4.2.2. 1480-nm pump model

The use of 1480-nm pumping brings additional complexity to the rate equations due to the similar wavelengths of the pump and signal beams. The model used for simulations is shown in Figure 4.3:

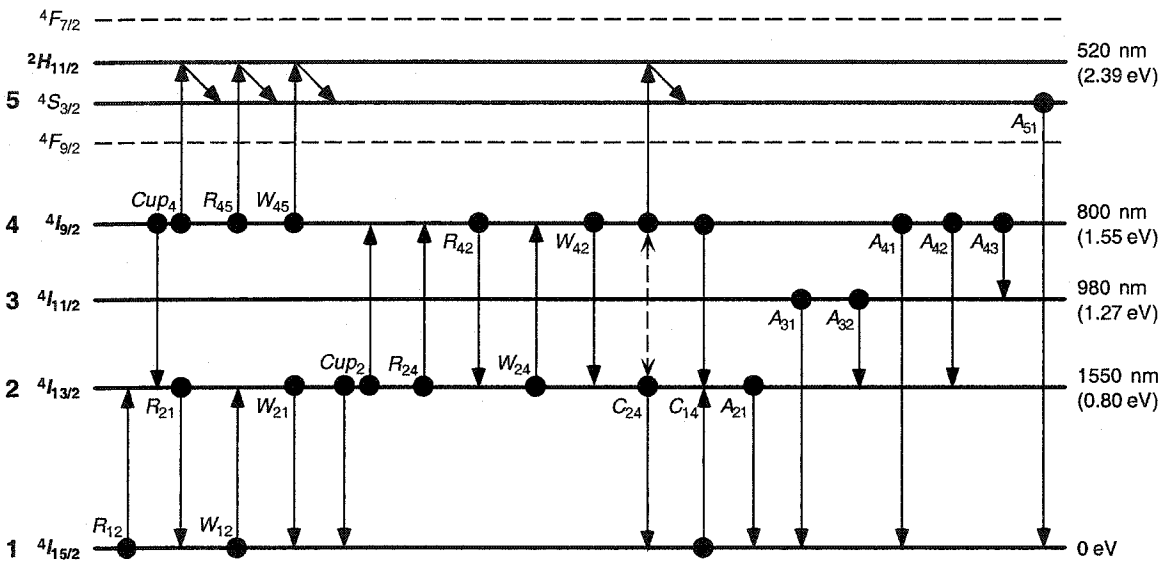

Figure 4.3: 5-level model for 1480-nm pump simulations.

Again, ions that reach $^2H_{11/2}$ are assumed to decay instantaneously and non-radiatively to $^4S_{3/2}$ for simplicity and consistency. The terms in the model are summarized in Table 4.2:

Table 4.2: Description of 1480-nm pump model parameters.

Parameter	Description
$R_{12} = \phi_p \sigma_{12p}$	1480-nm pump absorption from state 1 to 2.
$R_{21} = \phi_p \sigma_{21p}$	1480-nm stimulated emission from state 2.
$W_{12} = \phi_s \sigma_{12s}$	1550-nm signal absorption from state 1 to 2.
$W_{21} = \phi_s \sigma_{21s}$	1550-nm stimulated emission from state 2.
$R_{24} = \phi_p \sigma_{24p}$	1480-nm pump absorption from state 2 to 4 (excited state absorption).
$R_{42} = \phi_p \sigma_{42p}$	1480-nm stimulated emission from state 4 to 2.
$W_{24} = \phi_s \sigma_{24s}$	1550-nm signal absorption from state 2 to 4 (excited state absorption).
$W_{42} = \phi_s \sigma_{42s}$	1550-nm stimulated emission from state 4 to 2.
$R_{45} = \phi_p \sigma_{45p}$	1480-nm pump absorption from state 4 to 5 (excited state absorption).
$W_{45} = \phi_s \sigma_{45s}$	1550-nm signal absorption from state 4 to 5 (excited state absorption).
$A_{21} = 1/\tau_{21}$	Spontaneous emission from state 2 to 1.
$A_{31} = 1/\tau_{31}$	Spontaneous emission from state 3 to 1.
$A_{32} = 1/\tau_{32}$	Non-radiative relaxation from state 3 to 2.
$A_{41} = 1/\tau_{41}$	Spontaneous emission from state 4 to 1.
$A_{42} = 1/\tau_{42}$	Spontaneous emission from state 4 to 2.
$A_{43} = 1/\tau_{43}$	Non-radiative relaxation from state 4 to 3.
$A_{51} = 1/\tau_{51}$	Spontaneous emission from state 5 to 1.
Cup_2	Cooperative upconversion coefficient for ions at state 2.
Cup_4	Cooperative upconversion coefficient for ions at state 4.
C_{14}	Cross-relaxation coefficient for ions at states 1 and 4.
C_{24}	Cross-relaxation coefficient for ions at states 2 and 4.

The cross-sections in Table 4.2 contain a p or s in the subscript to denote whether they correspond to the pump or signal wavelength. The rate equations are formulated similarly to the 980-nm model:

$$\frac{dN_1}{dt} = -(W_{12} + R_{12})N_1 + (W_{21} + R_{21} + A_{21})N_2 + A_{31}N_3 + A_{41}N_4 + A_{51}N_5 + C_{24}N_2N_4 + Cup_2N_2^2 - C_{14}N_1N_4 \quad (4.21)$$

$$\frac{dN_2}{dt} = (W_{12} + R_{12})N_1 - (W_{21} + R_{21} + A_{21} + W_{24} + R_{24})N_2 + A_{32}N_3 + (W_{42} + R_{42} + A_{42})N_4 - C_{24}N_2N_4 - 2Cup_2N_2^2 + 2C_{14}N_1N_4 + Cup_4N_4^2 \quad (4.22)$$

$$\frac{dN_3}{dt} = -(A_{31} + A_{32})N_3 + A_{43}N_4 \quad (4.23)$$

$$\frac{dN_4}{dt} = (W_{24} + R_{24})N_2 - (W_{42} + R_{42} + W_{45} + R_{45} + A_{43} + A_{42} + A_{41})N_4 - C_{24}N_2N_4 + Cup_2N_2^2 - C_{14}N_1N_4 - 2Cup_4N_4^2 \quad (4.24)$$

$$\frac{dN_5}{dt} = (W_{45} + R_{45})N_4 - A_{51}N_5 + C_{24}N_2N_4 + Cup_4N_4^2 \quad (4.25)$$

$$N_t = N_1 + N_2 + N_3 + N_4 + N_5 \quad (4.26)$$

4.3. Model procedure

The model used for simulations goes through seven basic steps, and outputs the magnitude of signal and pump intensity through the waveguide, signal gain, and pump depletion.

(1) The signal and pump fields $E_{s,p}$ are calculated from the initial input signal and pump powers $P_{s,p}$ using

$$E_{s,p} = \sqrt{\frac{2P_{s,p}}{c\varepsilon_o n A_{eff}}} \quad (4.27)$$

where A_{eff} is the effective modal area of the light in the guide.

(2) Initial values for the pump absorption and signal gain coefficients, $\alpha_{p,s}$, are calculated using initial guesses for the populations of the appropriate energy levels. The pump absorption for 980-nm pumping is given by:

$$\alpha_{p980} = \Gamma_p (N_1\sigma_{13} - N_3\sigma_{31} + N_3\sigma_{35}) + sl_p \quad (4.28)$$

where Γ_p is a core confinement factor used to account for the partial overlap of the pump beam with the doped core of the waveguide [21], N_1 and N_3 are the population densities of the ground and third energy states, and sl_p is the scattering

loss of the pump. The signal absorption coefficient for 980-nm pumping is calculated by:

$$\alpha_{s980} = \Gamma_s \left(N_1\sigma_{12} - N_2\sigma_{21} + N_2\sigma_{24} - N_4\sigma_{42} + N_4\sigma_{45} \right) + sl_s \tag{4.29}$$

The pump and signal absorption coefficients for 1480-nm pumping are given by:

$$\alpha_{p1480} = \Gamma_p \left(N_1\sigma_{12p} + N_2\sigma_{24p} + N_4\sigma_{45p} - N_2\sigma_{21p} - N_4\sigma_{42p} \right) + sl_p \tag{4.30}$$

$$\alpha_{s1480} = \Gamma_s \left(N_1\sigma_{12s} + N_2\sigma_{24s} + N_4\sigma_{45s} - N_2\sigma_{21s} - N_4\sigma_{42s} \right) + sl_s \tag{4.31}$$

These absorption coefficients allow the calculation of the extinction coefficient κ, and subsequently the complex refractive index N of the device at the point in question, necessary for the transfer matrix formulation.

$$N_{s,p} = n - i\kappa_{s,p} = n - i\left(\frac{\alpha_{s,p}\lambda_{s,p}}{4\pi} \right) \tag{4.32}$$

(3) The transfer matrices describing the propagation of the pump and signal fields are then calculated for every point along the length of the waveguide, as detailed in Section 4.1. Using equations (4.12) to (4.14), new values for the pump and signal field intensities are found for each point in the waveguide.

(4) From the new signal and pump intensities, values for the absorption, stimulated emission and pumping probability densities are found (since they depend on the flux of the signal or pump), taking into account the core confinement factors.

$$W_{12} = \Gamma_s \phi_s \sigma_{12} = \frac{\Gamma_s I_s \lambda_s \sigma_{12}}{hc} \tag{4.33}$$

Similar equations apply for W_{21}, W_{31}, R_{13}, R_{24} and R_{35}, and all other probability rates with the appropriate parameters substituted in. With these new values, the rate equations are then solved using the Newton-Raphson method to obtain a new estimate of the energy level populations.

(5) The new populations are used to calculate a new set of absorption coefficients, and steps (2) to (4) are repeated until the difference between successive calculated

populations of the excited level (N_2) is less than a specified threshold value. The signal gain and pump depletion are calculated, along with the final intensity profiles of the pump and signal. Gain and depletion are found as follows:

$$signal\ gain\,(\mathrm{dB}) = 10\log_{10}\left(\frac{I_s(Z)}{I_s(0)}\right) \tag{4.34}$$

$$pump\ depletion\,(\mathrm{dB}) = 10\log_{10}\left(\frac{I_p(Z)}{I_p(0)}\right) \tag{4.35}$$

where $I_{s,p}(Z)$ and $I_{s,p}(0)$ are the signal and pump intensities at the end and beginning of the waveguide, respectively.

4.4. Model confirmation

To confirm that the model was valid, results produced by the 980-nm simulator were compared to previously published experimental results for a phosphate EDWA on silicon [39]. The parameters of the waveguide are listed in Table 4.3.

Table 4.3: Parameters of phosphate EDWA. All values are from [39] unless otherwise noted.

Parameter	Value
L	1 cm
σ_{12}	5.4×10^{-25} m^2
σ_{21}	5.4×10^{-25} m^2
σ_{13}	2.2×10^{-25} m^2
τ_{21}	4.0×10^{-3} s
τ_{32}	2.7×10^{-6} s (estimated from similar glass [8])
τ_{43}	2.4×10^{-6} s
Cup_2	$(2.0\pm0.5)\times10^{-24}$ m^3 s^{-1}
n	1.5
N_t	5.3×10^{26} m^{-3}
A_{eff}	4×10^{-12} m^2
Γ_s	0.76 (calculated from numerical mode solver [35])
Γ_p	0.85 (calculated from numerical mode solver [35])
$sl_p = sl_s$	20.7 m^{-1}

All other parameters were set to near-zero values. Cup_2 was varied within the given 0.5×10^{-24} m^3 s^{-1} error until a good fit to the experimental results was obtained, as shown in Figure 4.4.

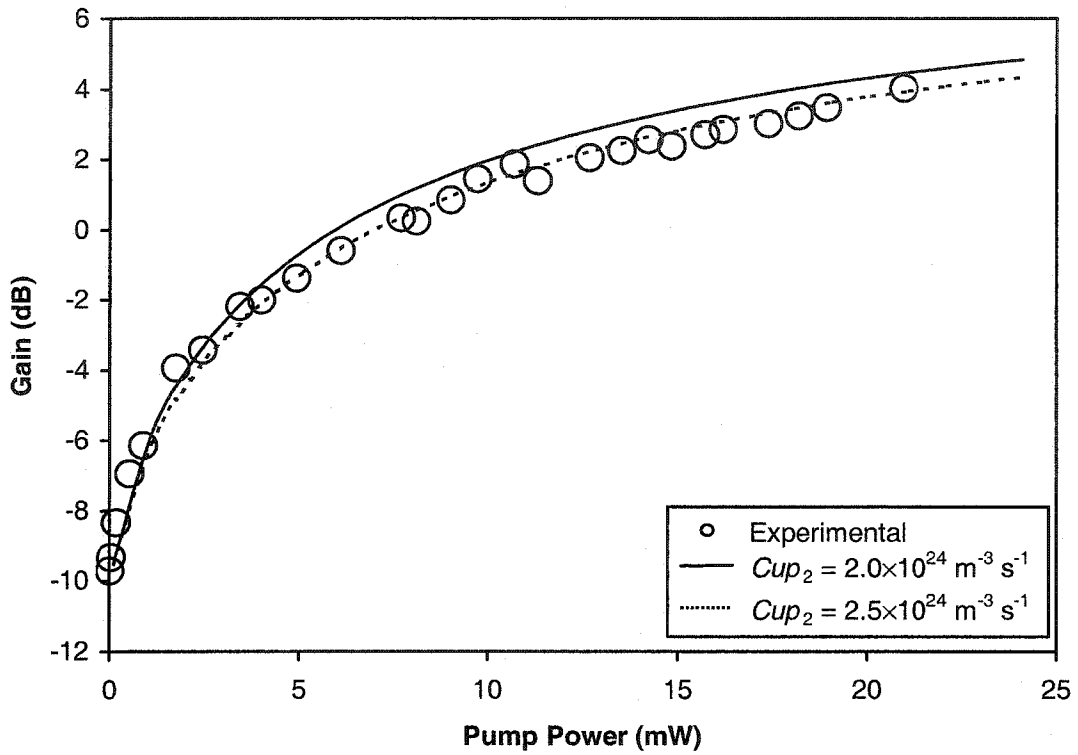

Figure 4.4: Comparison of experimental [39] and simulated results for phosphate EDWA. λ_s = 1534 nm, λ_p = 980 nm.

4.5. Simulation parameters

Since not all the necessary glass parameters could be measured in a reasonable time frame, some had to be estimated from data on similar glasses in other sources. Table 4.4 summarizes the values used for simulations, and where those values were obtained. A signal wavelength of 1535 nm is assumed in all cases, and all parameters are taken to be constant with changing erbium concentration.

Table 4.4: Summary of parameter values and sources.

Parameter	Value	Model	Source
$\sigma_{12} = \sigma_{12s}$	1.34×10^{-24} m^2	980, 1480	McCumber calculations in Section 3.4
$\sigma_{21} = \sigma_{21s}$	1.58×10^{-24} m^2	980, 1480	McCumber calculations in Section 3.4
σ_{12p}	3.88×10^{-26} m^2	1480	McCumber calculations in Section 3.4
σ_{21p}	1.46×10^{-26} m^2	1480	McCumber calculations in Section 3.4
σ_{13}	6.36×10^{-25} m^2	980	McCumber calculations in Section 3.4
σ_{31}	7.51×10^{-25} m^2	980	McCumber calculations in Section 3.4
$\sigma_{24} = \sigma_{24s}$	0.25×10^{-25} m^2	980, 1480	[40], Al_2O_3 glass
$\sigma_{42} = \sigma_{42s}$	0.5×10^{-25} m^2	980, 1480	Estimated based on values of σ_{24} from [5], [40], Al_2O_3 glass
σ_{24p}	0.25×10^{-25} m^2	1480	[40], Al_2O_3 glass
σ_{42p}	0.5×10^{-25} m^2	1480	Estimated based on values of σ_{24} from [5], [40], Al_2O_3 glass
σ_{35}	7×10^{-25} m^2	980	[41], Te glass
$\sigma_{45} = \sigma_{45p}$	1×10^{-25} m^2	980, 1480	Estimated based on values of σ_{24} from [5], [40], Al_2O_3 glass
Cup_2	6×10^{-24} m^3/s	980, 1480	[42], $Ge_{24}Ga_{10}S_{66}$ glass
Cup_3	8×10^{-24} m^3/s	980	[42], $Ge_{24}Ga_{10}S_{66}$ glass
Cup_4	6×10^{-24} m^3/s	980, 1480	Assumed to be same as Cup_2
C_{14}	6×10^{-24} m^3/s	980, 1480	Assumed to be same as Cup_2
C_{24}	6×10^{-24} m^3/s	980, 1480	Assumed to be same as Cup_2
$\tau_{21} = 1/A_{21}$	1.39×10^{-3} s	980, 1480	Judd-Ofelt calculations [32]
$\tau_{31} = 1/A_{31}$	1.04×10^{-3} s	980, 1480	Judd-Ofelt calculations [32]
$\tau_{32} = 1/A_{32}$	5.86×10^{-3} s	980, 1480	Judd-Ofelt calculations [32]
$\tau_{41} = 1/A_{41}$	0.64×10^{-3} s	980, 1480	Judd-Ofelt calculations [32]
$\tau_{42} = 1/A_{42}$	5.49×10^{-3} s	980, 1480	Judd-Ofelt calculations [32]
$\tau_{43} = 1/A_{43}$	0.25×10^{-3} s	980, 1480	Judd-Ofelt calculations [32]
$\tau_{51} = 1/A_{51}$	0.081×10^{-3} s	980, 1480	[31], $60GaS_{3/2}10GeS_2 27LaS_{3/2}ErS_{3/2}$ glass

In addition, the refractive index used was 2.32 (from measurements). Rather than designing a new waveguide amplifier structure, some numbers for the phosphate EDWA simulations were used for simplicity. These numbers included the effective cross-sectional area of the signal and pump beams ($A_{eff} = 4\times10^{-12}$ m^2), the signal and pump core confinement factors ($\Gamma_s = 0.76$ and $\Gamma_p = 0.85$), and the signal and pump scattering losses ($sl_s = sl_p = 20.7$ m^{-1}).

Other values such as the length of the waveguide, the concentration of erbium ions and the pump and signal powers were varied to assess their impacts on the waveguide amplifier.

4.6. 980-nm pump simulations

If an amplifier has perfect population inversion (i.e., $N_1 = 0$ and $N_2 = N_t$), the amplifier's corresponding gain will be at the fundamental limit of the amplifier. This limit is given by

$$G_L = \exp(\sigma_e L N_2) \tag{4.36}$$

which is Equation (2.2) with $N_1 = 0$. For a waveguide amplifier in chalcogenide glass of length 1 cm, $N_2 = N_t = 2.26\times10^{26}$ m^{-3}, and σ_e as listed above in Table 4.4, the fundamental limit is 15.5 dB. This number is very high compared to other glasses (a glass with $\sigma_e = 5\times10^{-25}$ m^2 would have a gain limit of approximately 4.9 dB), and illustrates why chalcogenide glass is considered a good potential host for EDWAs.

An initial simulation was performed using the 980-nm pump model with all upconversion, excited state absorption and cross-relaxation coefficients set to near-zero values. This simulation was intended to determine the best-case operation of the amplifier given the basic cross-section values, which are known. The gain and pump depletion (defined in Section 4.3) were monitored as the pump power was increased from zero to 50 mW. The results are plotted in Figure 4.5.

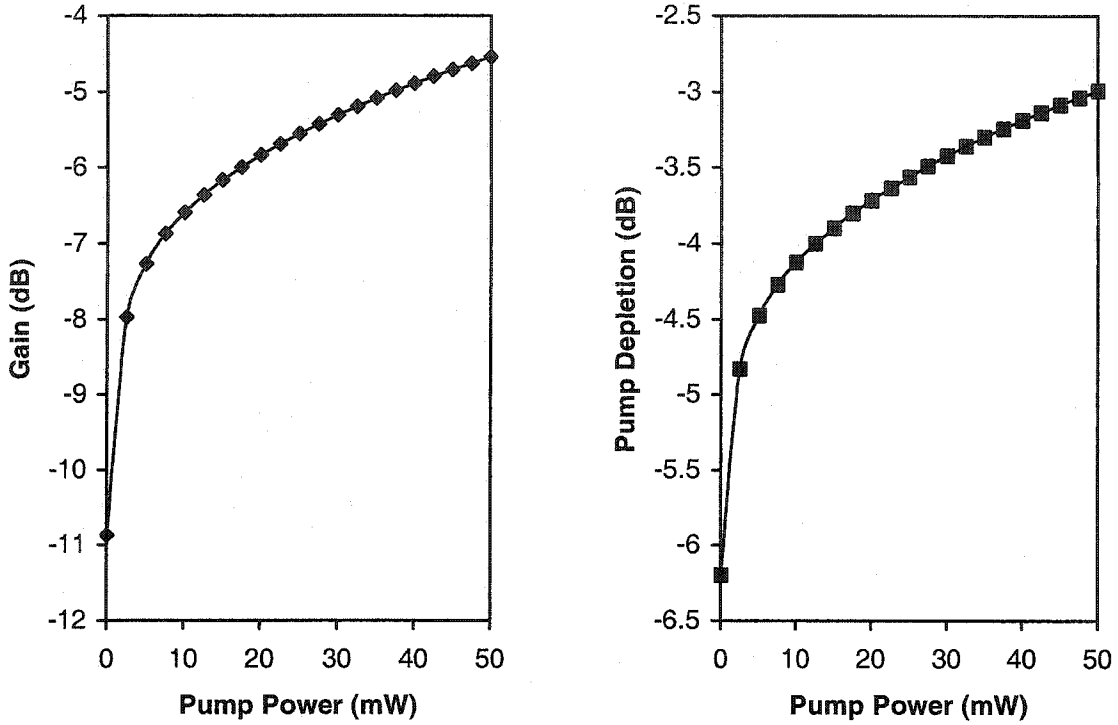

Figure 4.5: Gain and pump depletion behaviour for 980-nm pumping in chalcogenide EDWA with no adverse effects. Input signal power = -30 dBm, N_t = 2.26×10^{26} m^{-3}, total length = 1 cm, λ_s = 1534 nm, λ_p = 980 nm.

Although this is the best-case scenario, negative values are obtained for the signal gain even at high powers and small pump depletion. Since the normal adverse effects are not present in the model, this behaviour indicates that some other internal process is preventing ions from reaching the $^4I_{13/2}$ state. As mentioned previously, there are several parameters of the erbium ions in chalcogenide glass that may cause problems not seen in other glasses, namely the high stimulated emission cross-section at 980 nm (σ_{31}) and the lower probability of an ion decaying from the $^4I_{11/2}$ to $^4I_{13/2}$ state (A_{32}). A quick look at the rates of the transitions originating from the $^4I_{11/2}$ state gives a general idea of what is happening. The rates seen in Figure 4.6 are monitored at a position halfway through the waveguide.

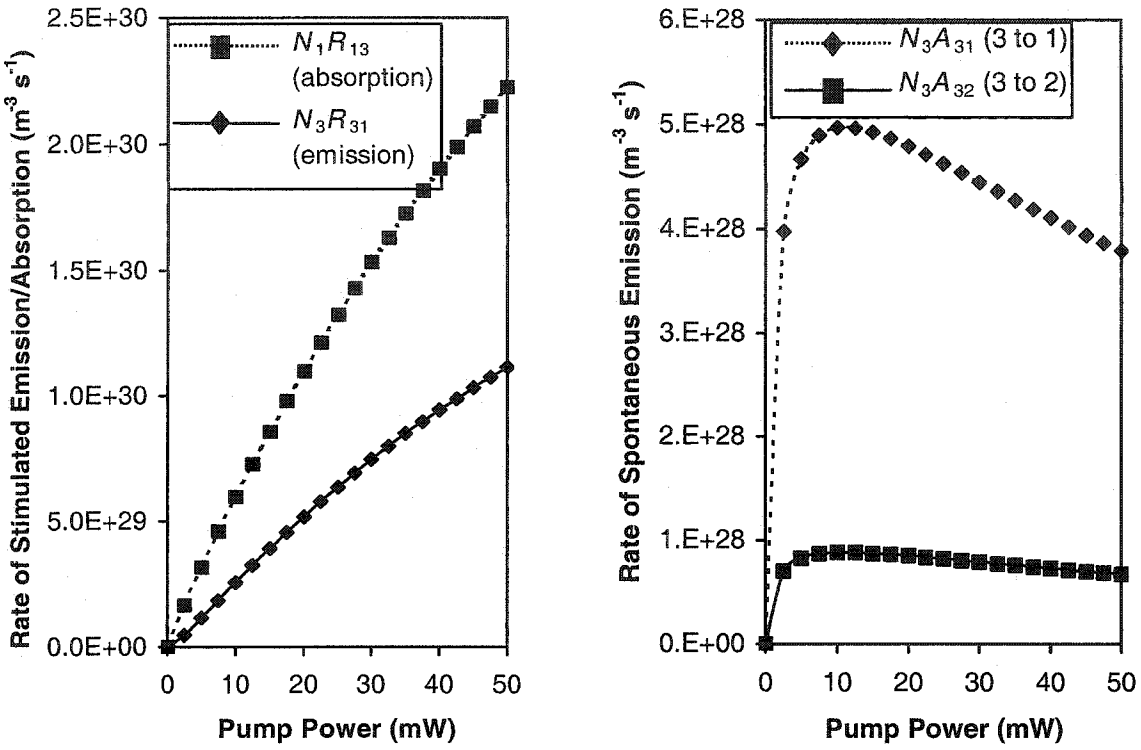

Figure 4.6: Main rates affecting the population of N_3. Input signal power = -30 dBm, $N_t = 2.26\times10^{26}$ m^{-3}, total length = 1 cm, λ_s = 1534 nm, λ_p = 980 nm. These rates are monitored at 0.5 cm.

As can be seen, the rate of pump absorption is closely followed by the rate of stimulated emission due to the comparable values of their cross-sections. The depletion of the $^4I_{11/2}$ level by stimulated emission is accentuated by the low probability of the $^4I_{11/2}$ to $^4I_{13/2}$ state. This factor is a major bottleneck that severely affects the performance of the amplifier. As seen in Figure 4.6 (b), the populating of the 1550-nm state is greatly exceeded by spontaneous emission to ground, a process that is normally ignored in silicate glass systems. Two more simulations were performed to see how varying the emission cross-section σ_{31} and the probability rate A_{32} would change the gain of the amplifier. The pump power was held constant at 50 mW. The results are shown in Figure 4.7 and Figure 4.8.

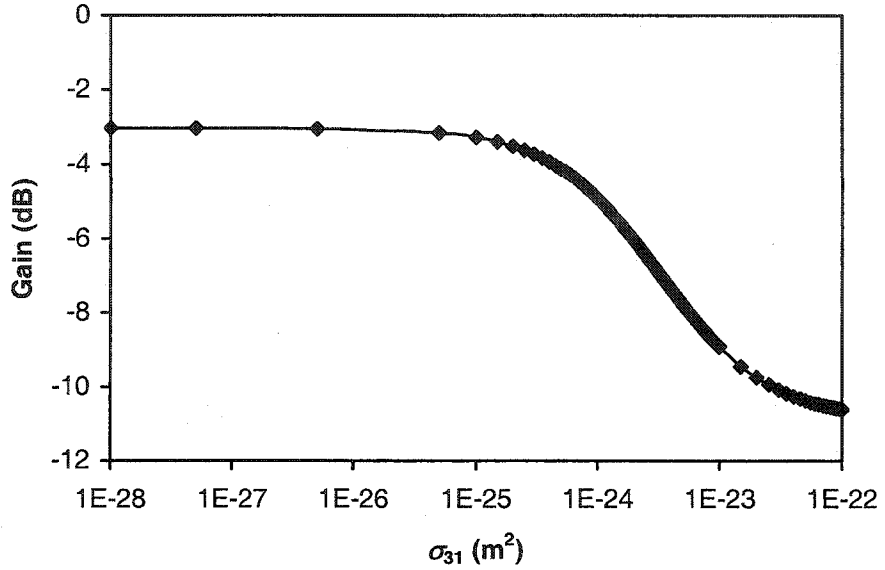

Figure 4.7: Gain as a function of stimulated emission cross-section. Input signal power = -30 dBm, $N_t = 2.26\times10^{26}$ m^{-3}, total length = 1 cm, and input pump power = 50 mW, $\lambda_s = 1534$ nm, $\lambda_p = 980$ nm.

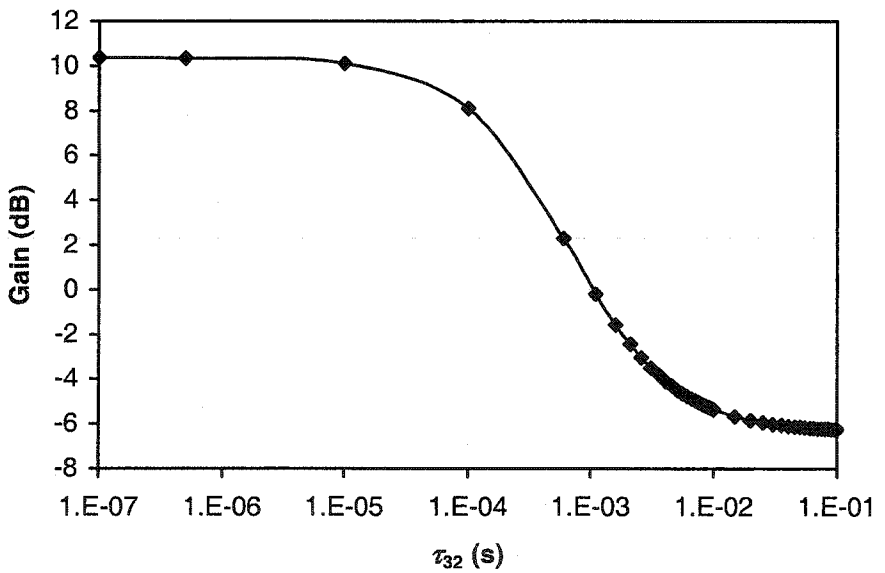

Figure 4.8: Gain as a function of $\tau_{32} = 1/A_{32}$. Input signal power = -30 dBm, $N_t = 2.26\times10^{26}$ m^{-3}, total length = 1 cm, input pump power = 50 mW, $\lambda_s = 1534$ nm, $\lambda_p = 980$ nm.

The results show that there is both an upper and lower limit to the gain produced for the different values of σ_{31} and $\tau_{32} = 1/A_{32}$. A_{32} is clearly the more influential of the two parameters, with gain of approximately 10.3 dB predicted for low values of τ_{32}. Also, in a simulation with σ_{31} and A_{32} set to values of 1×10^{-27} m^2 and 1×10^{6} s^{-1}, respectively, a gain of approximately 10.3 dB is still obtained, indicating that although σ_{31} does influence the gain, its effect is negligible compared to that of A_{32}. Clearly, the low maximum phonon energy in chalcogenide glass, which was expected to help amplifier performance by limiting the amount of useful energy lost to non-radiative transitions, is too low for 980-nm pumping of chalcogenide EDWAs to be feasible. For comparison, the maximum phonon energy in SiO_2 is in the range of 1000 cm^{-1} or 0.12 eV, while in chalcogenide it is in the range of 425 cm^{-1} or 0.05 eV [13]. Given that the difference in energies of the third and second energy states is approximately 0.47 eV, approximately 4 phonons (at the maximum allowed energy) are needed to bridge this gap in SiO_2, compared to 9 in chalcogenide.

4.7. 1480-nm pump simulations

The glass and erbium parameters used in the 980-nm simulations were also used for the 1480-nm simulations. As with the 980-nm model, an initial simulation with all adverse effects set to near-zero values was performed to determine if the amplifier could produce gain near the theoretical limit of 15.5 dB in the best-case scenario. Using an input signal power of 1 μW = -30 dBm, total erbium concentration of 2.26×10^{26} m^{-3}, and length of 1 cm, the gain and pump depletion versus pump power plots depicted in Figure 4.9 were obtained. Unlike the 980-nm model, 1480-nm pumping results in positive gains for pump powers above approximately 25 mW, although the limit of the gain is nowhere near 15.5 dB. Most likely the greatest factor causing this decrease in performance is the values for the pump absorption and emission cross-sections. 1480-nm amplifiers are typically less efficient than 980-nm pumping schemes due to the two cross-sections having values in the same order of magnitude [19]. The close cross-sections cause ions excited by absorption to return to ground state quickly by stimulated emission, greatly reducing the pumping efficiency of the amplifer. The low values of the absorption and emission cross-sections at 1480 nm for this glass system no doubt also contribute to the low gain obtained.

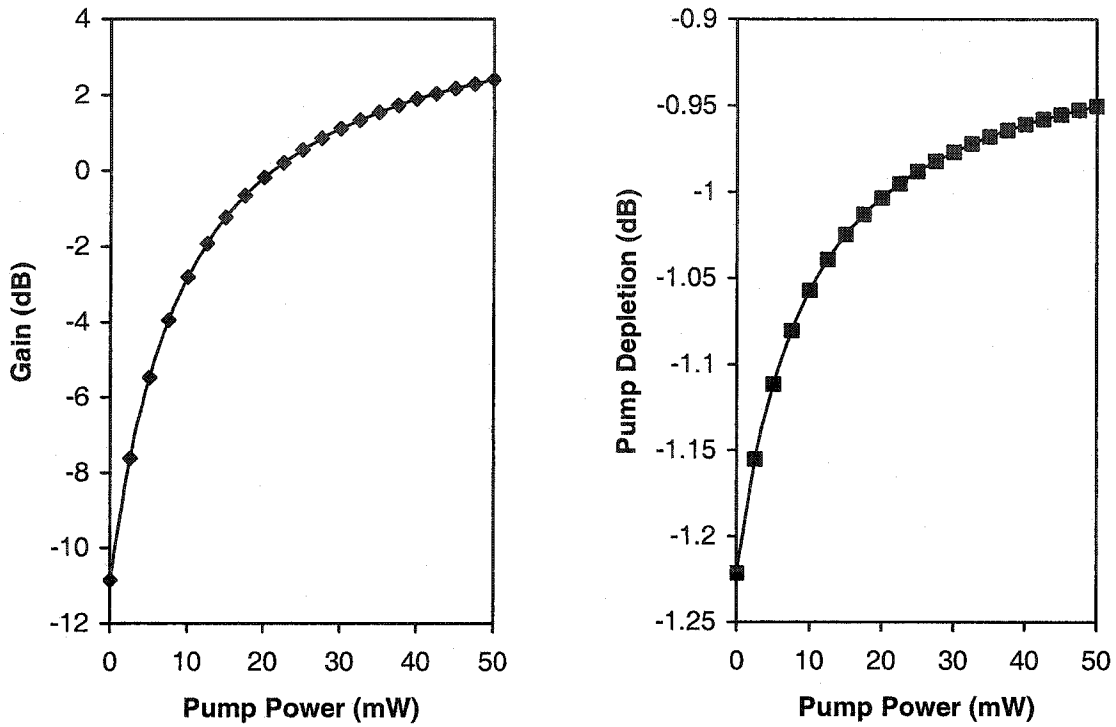

Figure 4.9: Gain and pump depletion behaviour for 1480-nm pumping in chalcogenide EDWA with no adverse effects. Input signal power = -30 dBm, N_t = 2.26×10^{26} m^{-3}, total length = 1 cm, λ_s = 1534 nm, λ_p = 1480 nm.

To see if it is possible to improve the gain, the pump wavelength was varied, which in turn changed the corresponding cross-section values. The results for gain are plotted in Figure 4.10, along with the values of absorption and emission cross-section for reference. The gain reaches a peak value at about 1490 nm and then begins to fall for increasing wavelengths. The scattering of points below 1490 nm is due to noise in the absorption spectrum (since the absorption is so low at the lower wavelengths, host glass absorption and detector noise begins to affect the measured data, which in turn affects the calculated cross-section values). The gain having a peak is surprising, considering that the cross-sections and the difference between them increase in the higher wavelengths.

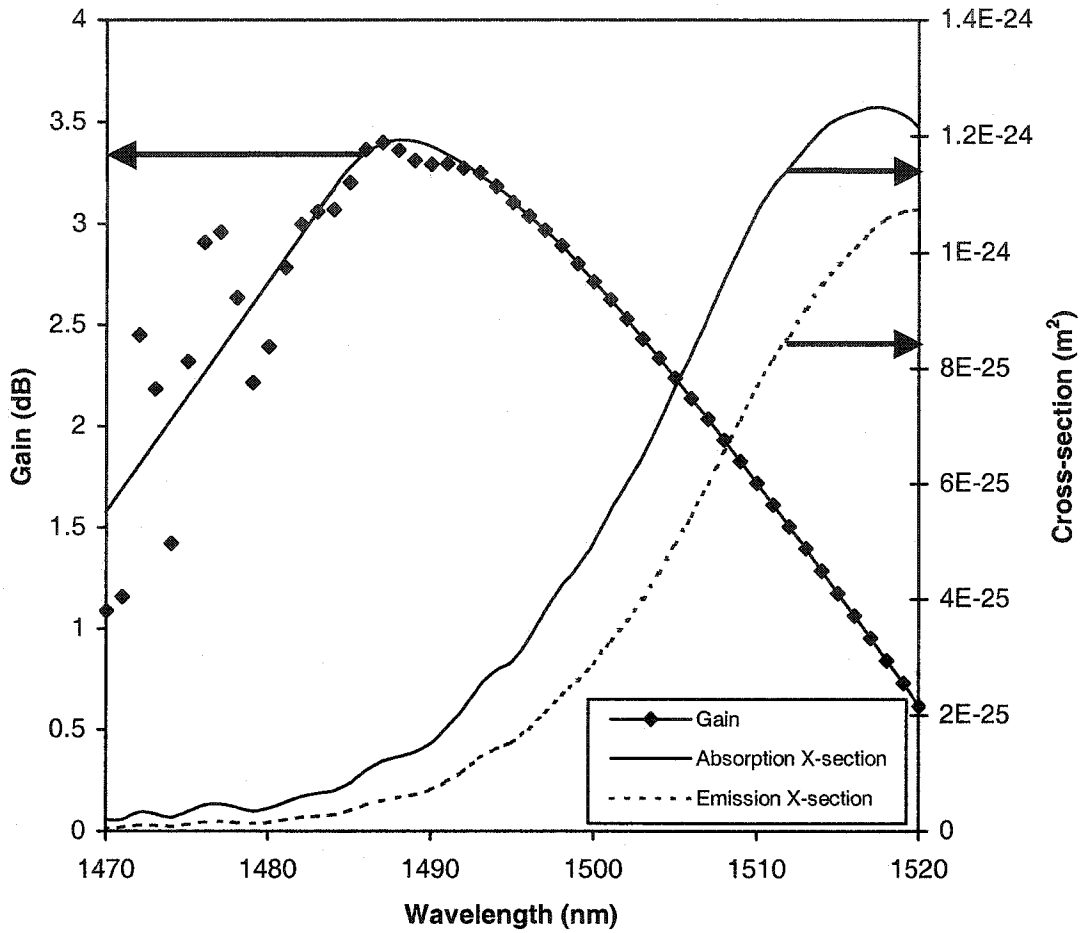

Figure 4.10: Gain and absorption and emission cross-sections versus pumping wavelength. Input signal power = -30 dBm, input pump power = 17 dBm, N_t = 2.26×10^{26} m^{-3}, total length = 1 cm, λ_s = 1534 nm.

In order to get a better idea of what is happening, the effect of absorption and stimulated emission on the pump and signal were monitored at a position halfway through the waveguide. These parameters will be referred to as signal and pump enhancement and absorption, and are defined by:

$$Signal\ enhancement = \Gamma_s \left(N_2 \sigma_{21s} + N_4 \sigma_{42s} \right) \tag{4.37}$$

$$Signal\ absorption = \Gamma_s \left(N_1 \sigma_{12s} + N_2 \sigma_{24s} + N_4 \sigma_{45s} \right) \tag{4.38}$$

$$Pump\ enhancement = \Gamma_p \left(N_2 \sigma_{21p} + N_4 \sigma_{42p} \right) \tag{4.39}$$

$$Pump\ absorption = \Gamma_p \left(N_1 \sigma_{12p} + N_2 \sigma_{24p} + N_4 \sigma_{45p} \right) \tag{4.40}$$

These four equations are essentially Equations (4.30) and (4.31) separated into their gain (transitions that add photons) and absorption (transitions that absorb photons) components, allowing each of them to be studied. In this case, since the ESA cross-sections are set to be near zero, these numbers are directly proportional to N_1 and N_2, the populations of the $^4I_{15/2}$ and $^4I_{13/2}$ states. The results are plotted in Figure 4.11.

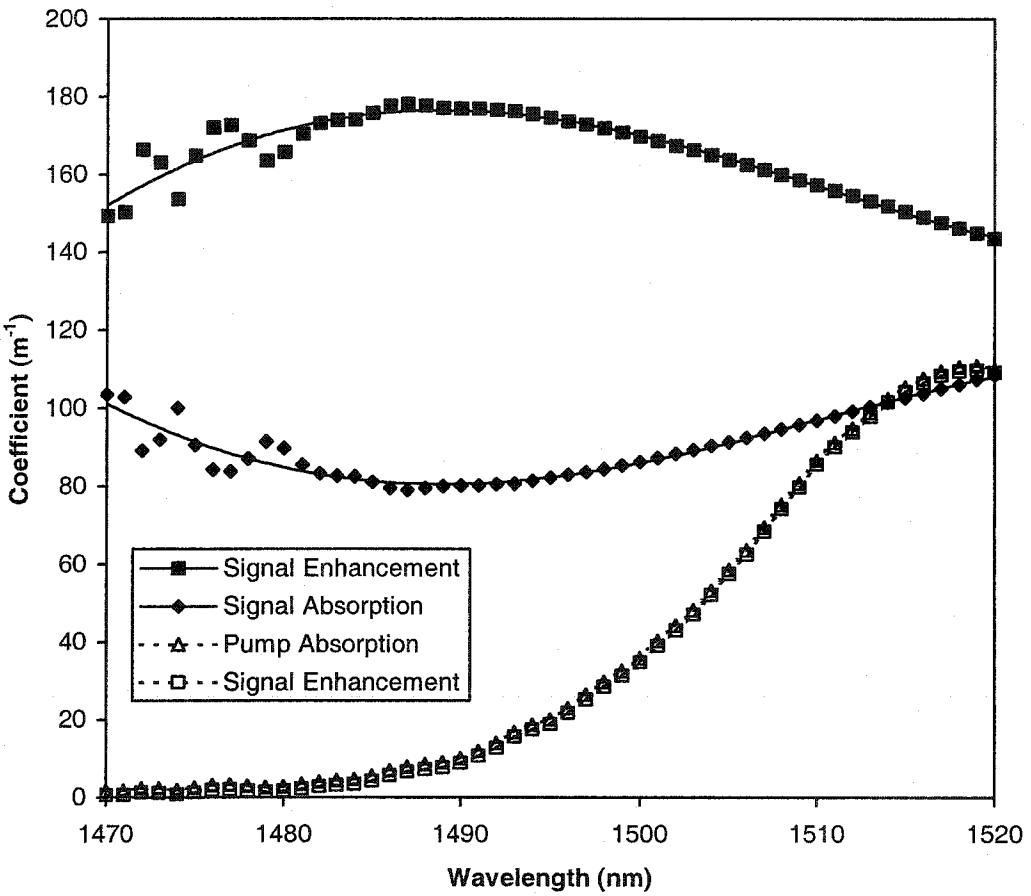

Figure 4.11: Enhancement and absorption values for different pumping wavelengths, monitored at the waveguide halfway point (0.5 cm). Input signal power = -30 dBm, input pump power = 17 dBm, $N_t = 2.26 \times 10^{26}$ m^{-3}, total length = 1 cm, $\lambda_s = 1534$ nm.

The signal enhancement reaches a peak and the signal absorption reaches a minimum where the signal gain is at its maximum. This behaviour is as expected, since the signal enhancement and absorption are roughly proportional to the population

inversion, $N_2 - N_1$, and therefore the larger the difference between the two, the greater the gain. The pump enhancement and gain seem to follow the cross-section plots, but they do not seem to show any behaviour that would indicate why pumping at 1490 nm produces more gain. However, the two plots are very close together, and there may be an issue with scale. Plotting the differences between the absorption and enhancement values for the signal and pump (giving signal and pump absorption coefficients, Equations (4.30) and (4.31)) shows the effect of pumping wavelength more clearly:

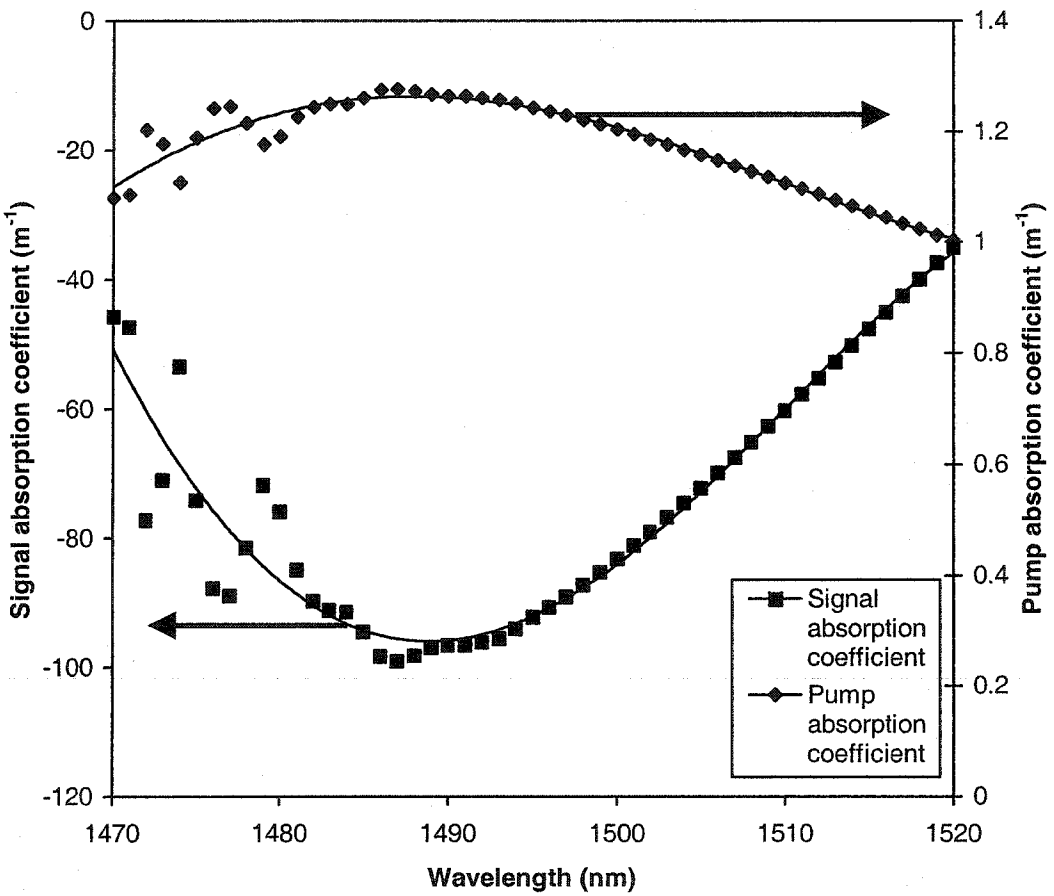

Figure 4.12: Signal and pump absorption coefficients as functions of pumping wavelength. Signal power = -30 dBm, Pump power = 17 dBm, $N_t = 2.26\times10^{26}$ m^{-3}, Total length = 1 cm, $\lambda_s = 1534$ nm.

As expected, the signal absorption coefficient is approximately proportional to the gain. The pump absorption coefficient shows that the pump reaches a peak of absorption where the gain reaches its peak. This indicates an optimal pumping wavelength where

the pump absorption ($N_1\sigma_{12p}$) pulls the farthest away from stimulated emission ($N_2\sigma_{21p}$), and subsequently has the greatest population inversion available for signal amplification. Unfortunately, adjusting the pumping wavelength to optimize the gain is not as easy as it seems from this simple analysis. The actual position of the peak gain will shift if the pump power changes, and also will shift when the adverse effects such as cooperative upconversion are added in. The effect of changing pump powers (without adverse effects) is plotted in Figure 4.13.

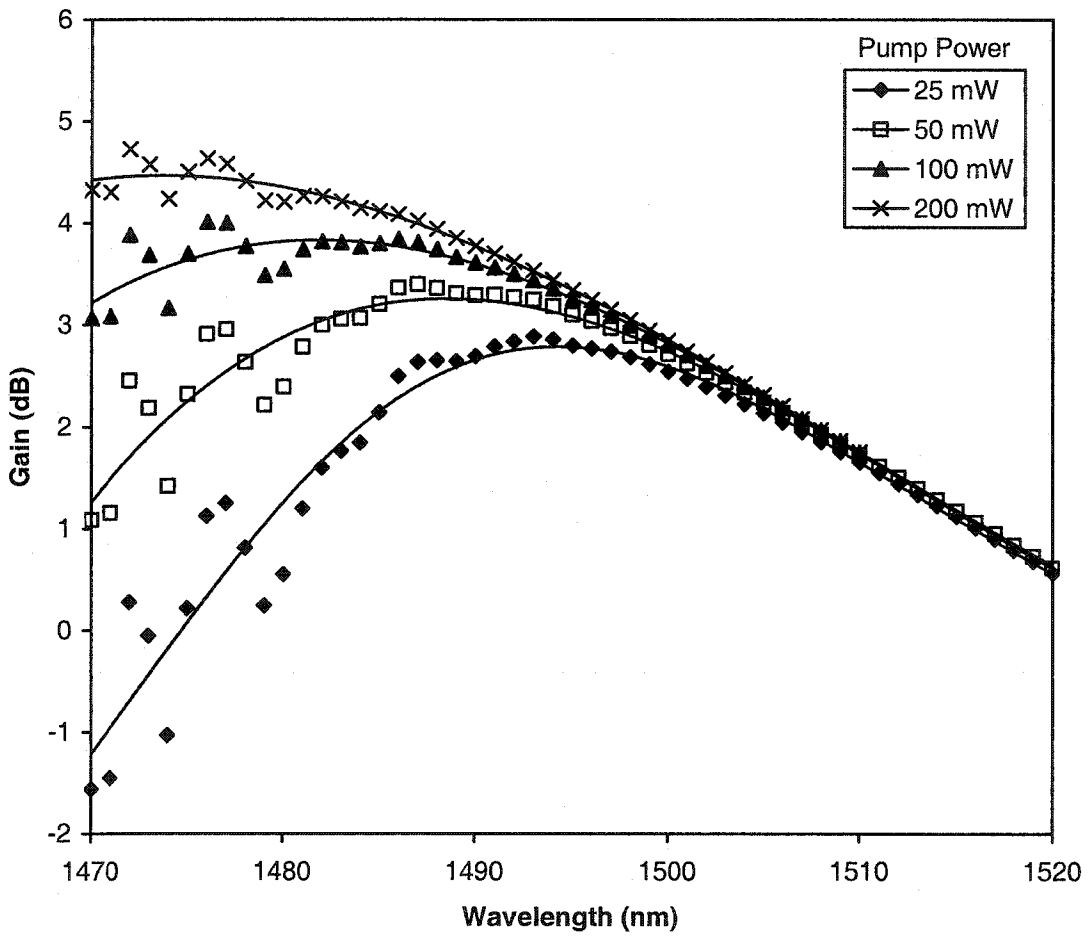

Figure 4.13: Gain versus pumping wavelength for different pump powers. Signal power = -30 dBm, $N_t = 2.26\times10^{26}$ m^{-3}, Total length = 1 cm, λ_s = 1534 nm.

As the pump power increases, the peak of the gain increases and undergoes a blue shift. Lower wavelengths see an increase in gain as the higher pump powers compensate for the low absorption cross-section values (~10^{-26} m^2). The gain limit seen in the higher wavelengths is set by the large emission cross-sections in relation to the absorption cross-

sections. Since the pump emission cross-section is large, a large portion of the excited ions will return to ground through stimulated emission induced by the pump rather than the signal. To illustrate this point, the values of the pump stimulated emission cross-section were scaled down by factors of 10 and 100. Although the results obtained from these simulations are purely artificial, they serve to demonstrate the effect that the size of the emission cross-section relative to the absorption cross-section has on the gain. Figure 4.14 shows the results.

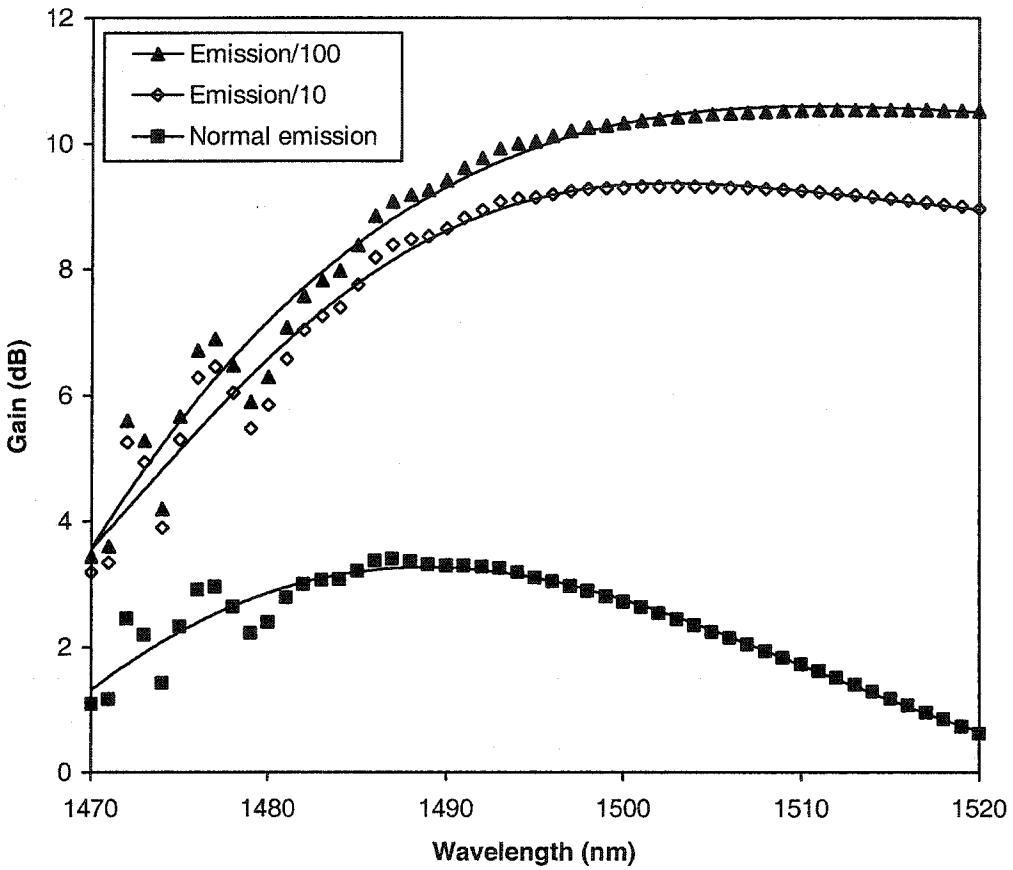

Figure 4.14: Gain as a function of pumping wavelength for differently scaled emission cross-section values. Signal power = -30 dBm, Pump power = 17 dBm, N_t = 2.26×10^{26} m^{-3}, Total length = 1 cm, λ_s = 1534 nm.

The gain shows a marked improvement for both of the scaled emission cross-section simulations. Also, the slope of the straight-line portions of the plots is decreasing, becoming a nearly horizontal line at about 10.8 dB, which is the value of gain that was previously determined to be the limit of the 980-nm pumped model's

performance. Once again, we see that at least in this alloy of chalcogenide glass, problems arise that prevent the glass from realizing its full potential as an amplifying medium.

Although the simulated EDWAs with 1480-nm pumping did not show their maximum potential, they still showed a positive gain for pump power values over 20 mW (see Figure 4.9), albeit for simulations where all parameters for adverse effects were set to near-zero values. To see if positive gain numbers were obtainable for 1480-nm pumping under normal conditions, the adverse effects were added in, and the gain and pump depletion were observed as the pump power was varied. The results are shown in Figure 4.15.

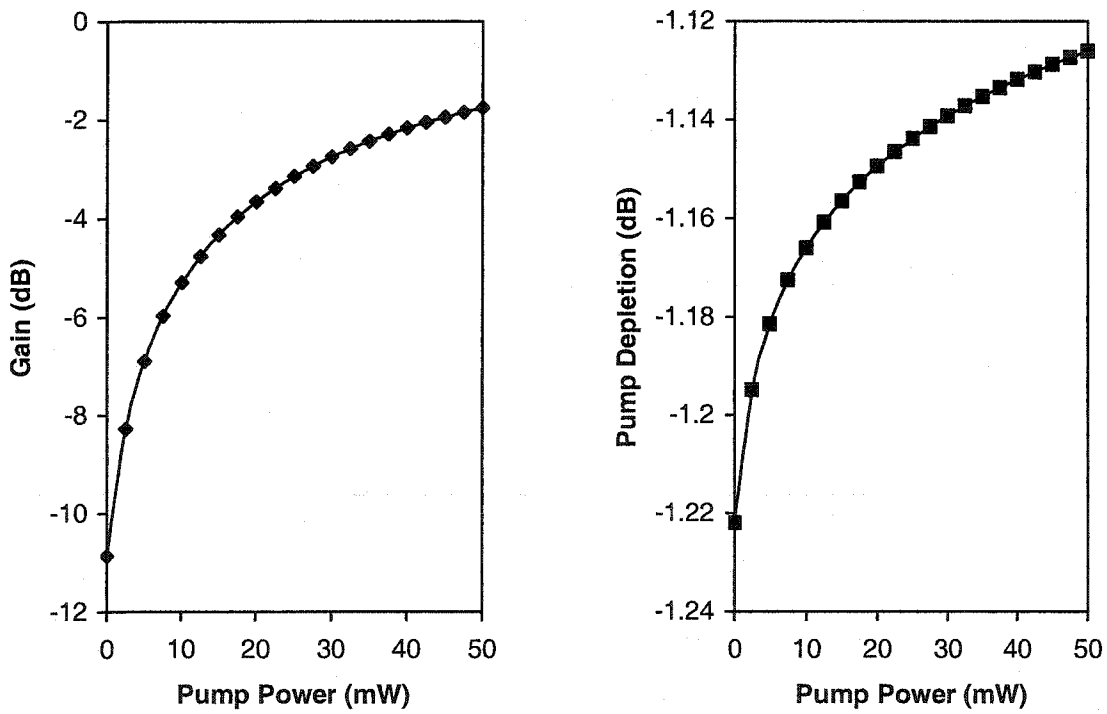

Figure 4.15: Gain and pump depletion behaviour for 1480-nm pumping in chalcogenide EDWA with adverse effects added. Signal power = -30 dBm, N_t = 2.26×10^{26} m^{-3}, Length = 1 cm, λ_s = 1534 nm, λ_p = 1480 nm.

The addition of cooperative upconversion, ESA and cross-relaxation causes the gain to fall below 0 dB. To see which factor contributes most to the reduction in gain, each was added to the ideal model separately, and the gain versus pump power simulation was performed. It was found that all the transitions involving an ion in the 4^{th} ($^4I_{9/2}$) state

had no effect on their own, which is no surprise considering there is no mechanism to populate that state while the other transitions are not present. On the other hand, the transitions originating from the second ($^4I_{13/2}$) state have a much greater effect, as can be seen in Figure 4.16.

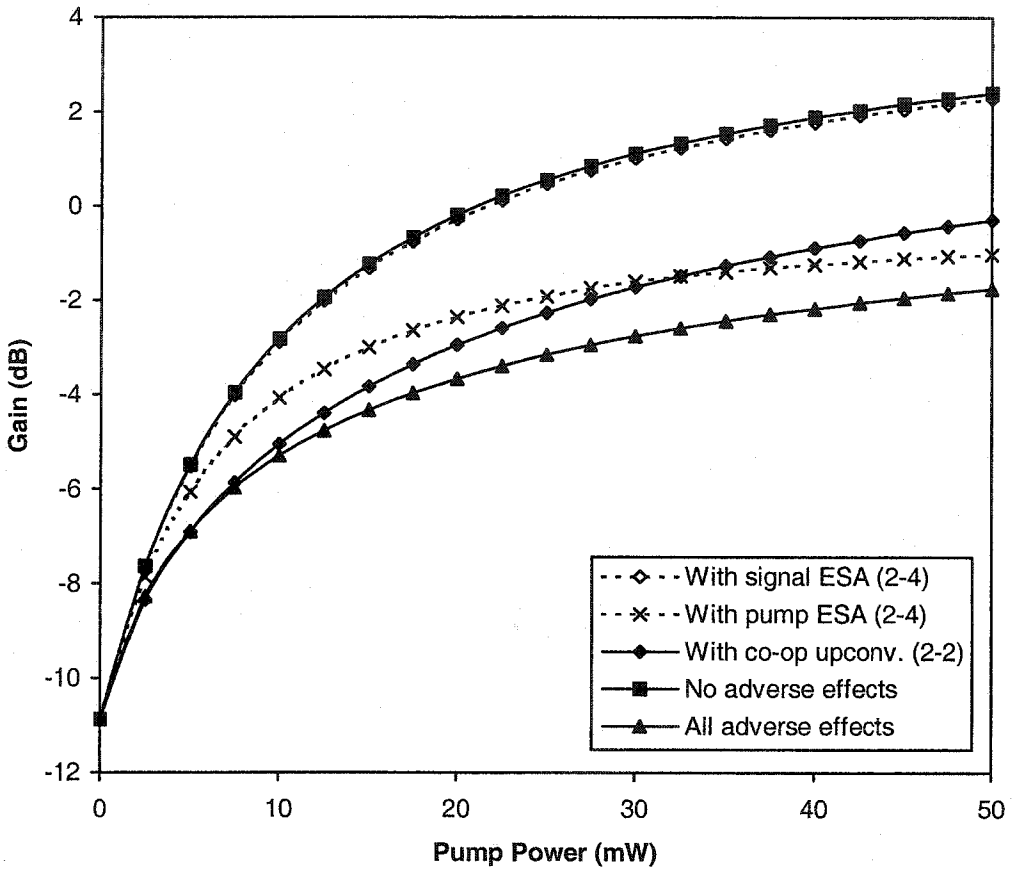

Figure 4.16: Gain versus pump power with different adverse effects active. Signal power = -30 dBm, $N_t = 2.26\times10^{26}$ m^{-3}, Length = 1 cm, λ_s = 1534 nm, λ_p = 1480 nm.

The top and bottom plots represent the model without and with adverse effects, respectively, illustrating the best and worst-case scenarios. Excited state absorption caused by the signal does not cause a significant problem, which is reasonable considering how low the signal power is (1 μW) in relation to the pump power. Cooperative upconversion from state 2 and ESA initiated by the pump beam have a much greater effect, bringing the gain to negative values. Also, the effect of the pump ESA is

more pronounced at higher pump powers, because the extra pump intensity is fed into more ESA, causing the gain to saturate more quickly than normal.

The effect of the transitions originating in state 4 were examined by setting the 2nd level transitions to their default values and then adding in each 4th level transition and observing their effect. The results are plotted in Figure 4.17.

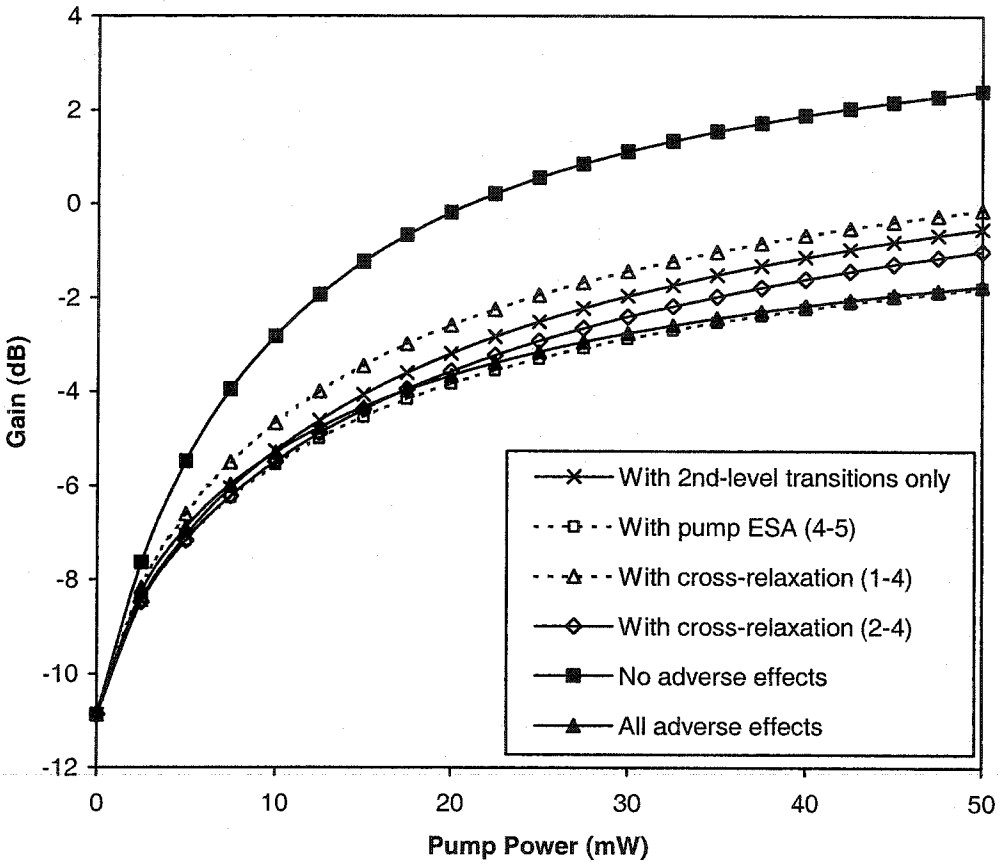

Figure 4.17: Gain versus pump power with different 4th-level adverse effects active. Signal power = -30 dBm, $N_t = 2.26\times10^{26}$ m^{-3}, Length = 1 cm, λ_s = 1534 nm, λ_p = 1480 nm.

The line whose points are represented by crosses denotes the simulation results with all the transitions from the 2nd level active, along with the stimulated emission transitions from state 4 to state 2, to give a base level for comparison. The stimulated emission adds some improvement to the gain as it repopulates level 2, although the gain still remains negative. Also improving the gain is the cross-relaxation between ions in states 1 and 4, which repopulates state 2. The signal ESA and cooperative upconversion

from state 4 to 5 had minimal negative effects on the base level, and are not shown on the graph. The transitions involving the 4th state that have the most effect are the pump ESA and the cross-relaxation between states 2 and 4. It should be noted that the simulation with pump ESA produces lower gain than the simulation with all the parameters because it is missing the cross-relaxation from state 1 to 4 which helps to repopulate the pump level. With these simulations, it can be seen that the excited state absorption of the pump has the greatest effect on amplifier performance.

Although this amplifier model produces negative gain with all the transitions taken into account, there is still potential for improvement by changing the pump wavelength to take advantage of the better cross-sections. A simulation similar to the one in Figure 4.10 was performed, and the results are plotted in Figure 4.18:

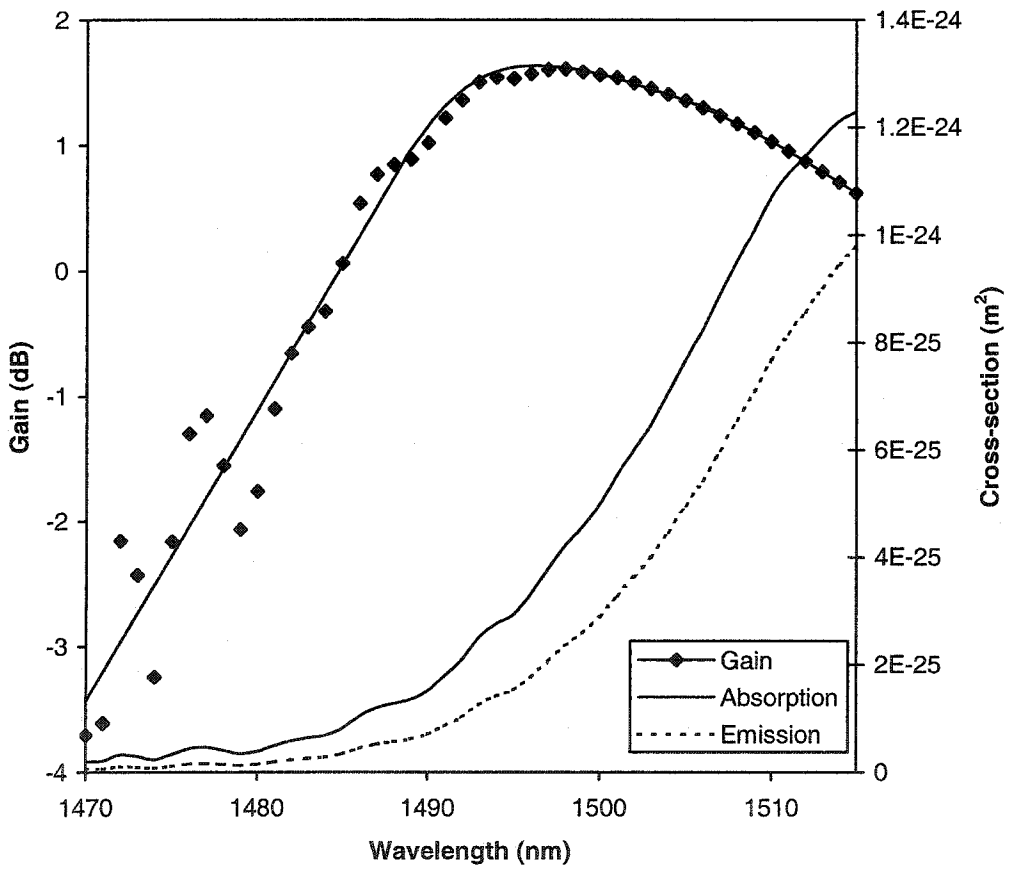

Figure 4.18: Gain and absorption and emission cross-sections versus pumping wavelength for model with adverse effects. Signal power = -30 dBm, Pump power = 17 dBm, $N_t = 2.26\times10^{26}$ m^{-3}, Total length = 1 cm, λ_s = 1534 nm.

The gain reaches a peak of about 1.5 dB in the 1490 to 1500-nm range, and as such, the cross-sections at 1500 nm were for the pump. The gain and pump depletion versus pump power behaviour obtained with these new cross-sections is plotted in Figure 4.19:

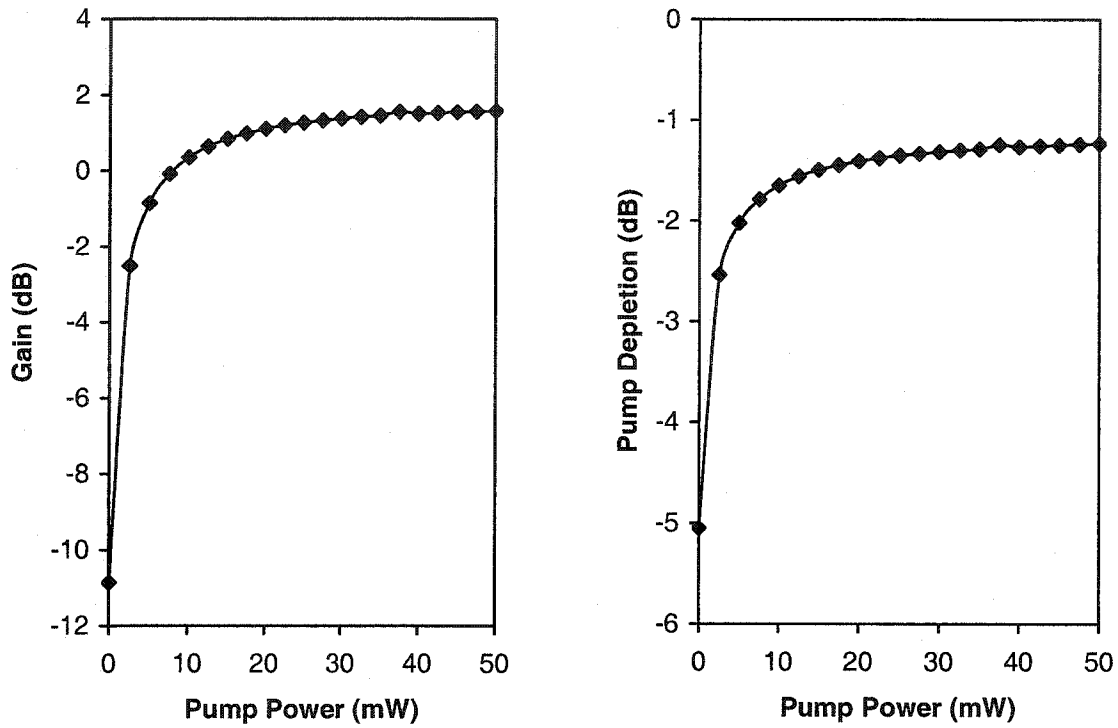

Figure 4.19: Gain and pump depletion behaviour for 1500-nm pumping in chalcogenide EDWA with adverse effects added. Signal power = -30 dBm, N_t = 2.26×10^{26} m^{-3}, Length = 1 cm, λ_s = 1534 nm, λ_p = 1500 nm.

Changing the cross-sections of the pump beam improves the gain, as expected, to a maximum of about 1.5 dB. However, the gain does saturate quickly, indicating that adverse effects are limiting the amount of pump power available for amplification. It should be noted again that changing the pumping wavelength to suit the performance of the amplifier is not a simple task, since the optimum range changes depending on pump power and the parameters of the glass, and high-power pump lasers are not readily available at all wavelengths.

Regardless of this difficulty, further simulations were performed on the amplifier with 1500-nm cross-section values. First, the gain was examined as a function of

waveguide length for different pump power values, to determine the gain saturation behaviour of the amplifiers along with the maximum gain per cm attainable with these waveguides. The results are plotted in Figure 4.20.

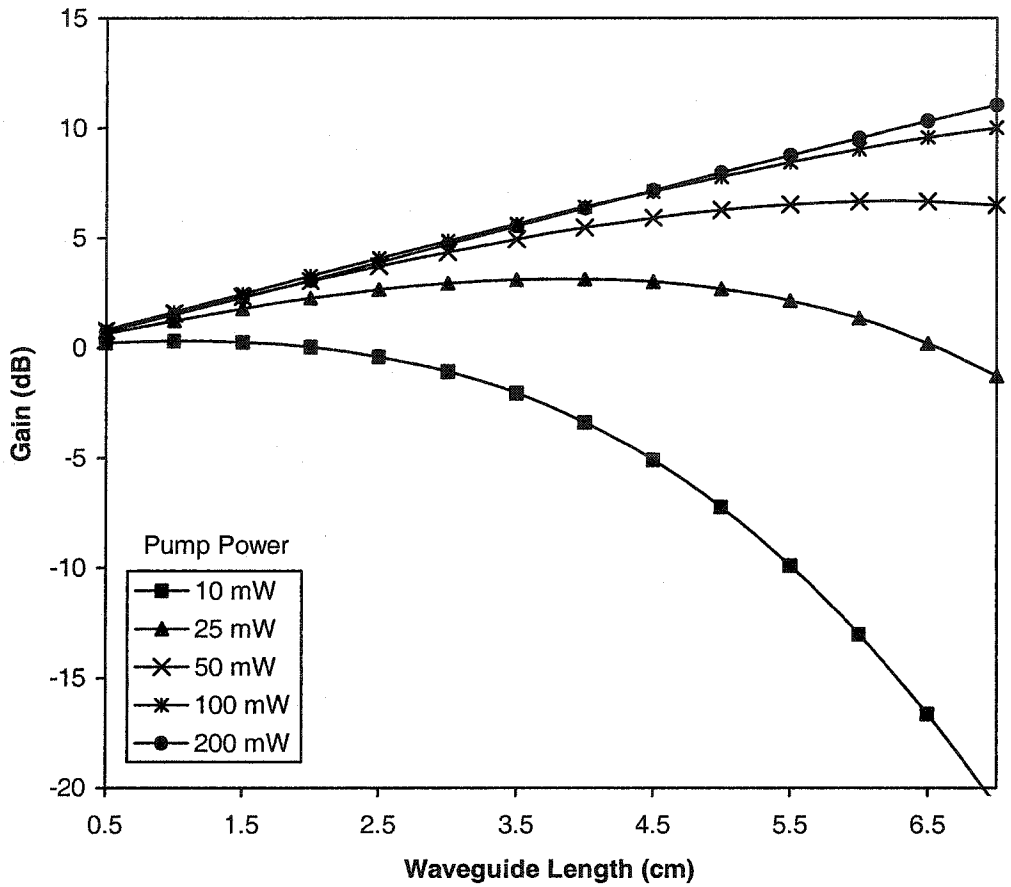

Figure 4.20: Gain as a function of total waveguide length for various values of pump power. Signal power = -30 dBm, $N_t = 2.26\times10^{26}$ m^{-3}, $\lambda_s = 1534$ nm, $\lambda_p = 1500$ nm.

From the plot, it can be seen that lower pump powers produce unacceptable results since they are not strong enough to create a sufficient population inversion. For higher pump powers, there is an optimal length beyond which gain declines as the pump becomes too depleted. The slope of the 200 mW pump also gives a good measure of the maximum possible gain efficiency for this particular amplifier, at 1.64 dB/cm, much lower than the 15.5 dB/cm predicted by Equation (4.36).

The next measure of the amplifier's performance was obtained by simulating how it behaved as the concentration of erbium atoms in the guide was varied. Increasing the number of ions can improve the gain, but it can also lead to increased signal absorption as the pump is depleted by the extra ions. The results of the simulation are plotted in Figure 4.21.

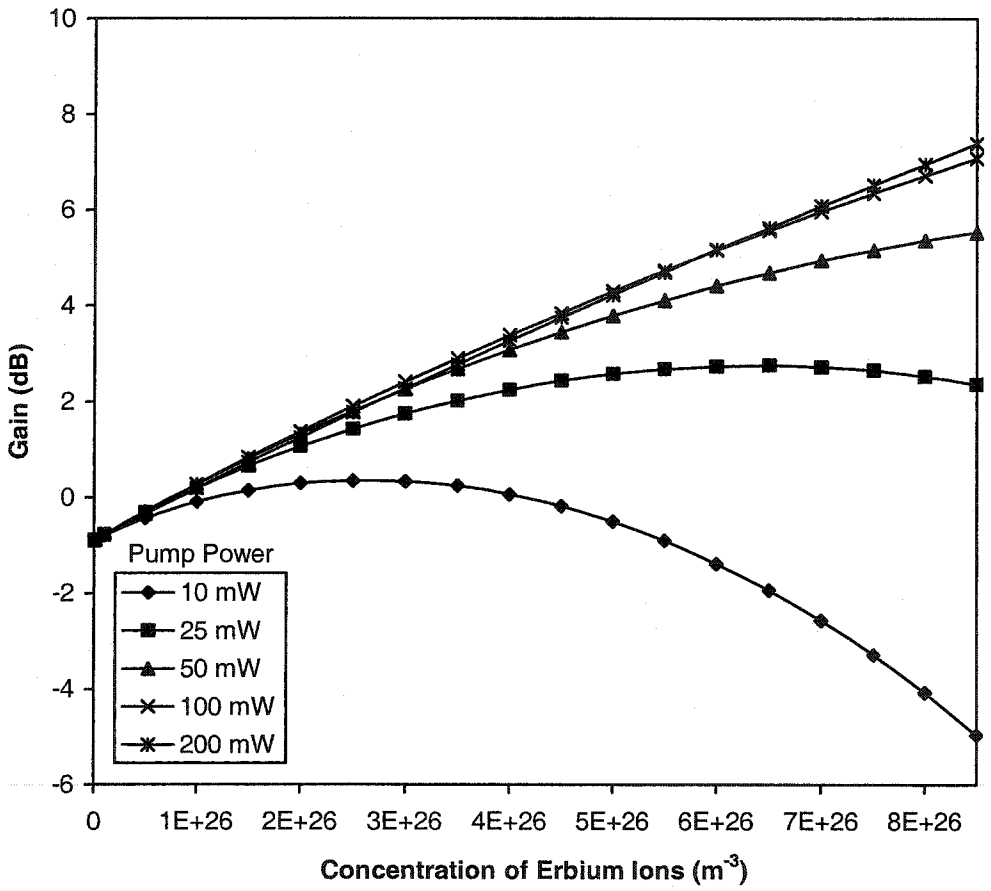

Figure 4.21: Gain versus erbium concentration for various values of pump power. Signal power = -30 dBm, Length = 1 cm, λ_s = 1534 nm, λ_p = 1500 nm.

As expected, adding in erbium ions improves the gain until the pump depletion becomes too large. The 200 mW pump profile shows the best possible improvement obtainable by increasing erbium concentration is approximately 1 dB per 1×10^{26} ions/m^{-3} added.

5. Conclusions

5.1. Summary

5.1.1. Experimental

We measured the PL lifetimes of several chalcogenide glass alloys fabricated with $ErCl_3$ and Er_2S_3 doping sources. The presence of Cl in the glass was determined to be severely detrimental to the photoluminescence lifetime, at the very least reducing it to a length indistinguishable from the error of the experimental apparatus. The lifetime of GaGeAsSe was the shortest of the samples doped with Er_2S_3, although all samples exhibited lifetimes in the range of 1-3 ms. In the GaGeSe and GaGeS samples, it was also observed that lifetime stayed constant up to a certain doping concentration, beyond which clustering effects became a significant factor. This behaviour suggests an optimal concentration of approximately 1 at. % for these glasses. Based on the observed results, we can infer that GaGeSe and GaGeS are promising materials for use in waveguide amplifiers. An optimal concentration of Er^{3+} of approximately 1 at. % was observed in both glasses. For doping concentrations higher than approximately 1 at. %, the luminescence efficiency begins to decrease. We attribute this to deleterious clustering effects.

5.1.2. Simulations

In this thesis, the first detailed simulations of erbium-doped waveguide amplifiers were performed to determine if chalcogenide glass is a good host for such applications. Simulations predict that 980-nm pumping is unworkable in chalcogenide EDWAs. The 980-nm pumping scheme requires a fast transition rate of ions from the $^4I_{11/2}$ to $^4I_{13/2}$ state in order to create a population inversion for signal amplification. Since this transition is primarily non-radiative (phonon-assisted), its probability is significantly reduced by the low maximum phonon energy of chalcogenide glass. This low rate leads to a build-up of ions in the $^4I_{11/2}$ level, which is depopulated through other means such as spontaneous emission, pump stimulated emission or excited state absorption. The $^4I_{13/2}$ level remains sparsely populated and the signal is absorbed as it travels through the waveguide. This problem is not limited to the specific glass alloy studied in this thesis, as other groups

[13,22,31,42,43] have reported similar numbers for the probability of this transition (A_{32}) in other low phonon energy chalcogenide glasses.

1480-nm pumping is also predicted to give a negative gain, though the results are slightly better than for 980-nm pumping. The low gain in this pumping scheme is mainly due to the low values of the absorption cross-section of the 1480-nm pump beam. Since the chalcogenide alloy studied experimentally in Chapter 3 (and assumed in simulations) has a relatively narrow absorption spectrum around 1550 nm, the absorption cross-section at the pumping wavelength of 1480-nm is too low to sustain a sufficient population inversion. Also, the absorption and emission cross-sections are very close at 1480 nm, which causes many of the ions excited by the pump to return to ground by stimulated emission. These two factors coupled together make 1480-nm pumping unusable for this glass. It was also noted that changing the pumping wavelength in the 1550-nm band could improve the gain to positive values. Optimal pumping is reached where the absorption and emission coefficients of the pump beam have a maximum difference between them. However, several problems exist with this solution. High-power lasers at wavelengths other than 1480 nm and 980 nm are not as common, moving the pump closer to the signal wavelength increases the chances of interference between them, and the peak of the gain versus pumping wavelength behaviour will change depending on temperature and pump power. Alternate solutions will need to be found if 1480-nm pumping is to be used in the future.

5.2. Future work

5.2.1. 980-nm pumping

Several areas of future work may improve the performance of these chalcogenide EDWAs. In regards to 980-nm pumping, the solution may lie in adding a codopant that can accept the energy released in the $^4I_{11/2}$ to $^4I_{13/2}$ transition. Other research groups have attempted this procedure with elements such as cerium [43] and have demonstrated some positive results. The ion in the $^4I_{11/2}$ state transfers its energy non-radiatively to the Ce^{3+} ion, facilitating the desired $^4I_{11/2}$ to $^4I_{13/2}$ transition without interfering with other erbium transitions. It should be noted however, that this energy transfer process is still phonon-assisted, and as such, the maximum phonon energy of the glass is still a large factor.

5.2.2. 1480-nm pumping

In the case of 1480-nm pumping, changing the composition of the glass may change the absorption and emission cross-sections to values that are more desirable. Absorption cross-sections for other chalcogenide glass alloys have shown values in the range of 1×10^{25} m^2, with a more significant gap between the absorption and emission values [33]. More research would have to be done to determine if there is an alloy suitable for this pumping scheme.

5.2.3. Broadband excitation

One other alternative that merits investigation is the use of the broadband excitation ability of chalcogenide glass as a pumping source, as detailed in Section 2.3. This technique enables the use of a broadband pumping source and is thought to directly populate the $^4I_{13/2}$ level. This may reduce the impact of problematic upconversion and ESA processes, and avoids the low phonon energy and low cross-sections that hinder 980-nm and 1480-nm pumping. Broadband excitation also has the potential of employing alternate excitation sources such as LEDs, which are more cost-efficient and easier to use than traditional laser pumps.

5.3. Concluding remarks

An experimental and theoretical study of erbium-doped chalcogenide amplifiers was performed, encompassing spectral measurements of erbium-doped chalcogenide glasses and the first known simulations of chalcogenide EDWAs. Simulations showed that traditional optical amplifier pumping methods are not viable for this material system, contrary to the popular belief that chalcogenide glasses will make excellent EDWA hosts. More research must be done to determine if the problems made evident in this research can be overcome, or if we must switch to a different material or rare-earth ion to fully realize efficient, high-gain integrated waveguide amplifiers.

6. References

[1] S. E. Miller, "Integrated optics: an introduction," *Bell System Tech. Journal*, vol. 48, pp. 2059-2069, 1969.

[2] A. M. Andriesh, V. V. Ponomar, V. L. Smirnov, and A. V. Mironos, "Applications of chalcogenide glasses in integrated and fiber optics (review)," *Sov. J. Quantum Electron.*, vol. 16, pp. 721-736, 1986.

[3] A. Polman, "Erbium implanted thin film photonic materials," *J. Appl. Phys.*, vol. 82, pp. 1-39, 1997.

[4] R. Shankar, "Erbium/Ytterbium Planar Waveguide Amplifiers: Modeling and Fabrication," M.Sc. Thesis, *University of Alberta*, Edmonton, Alberta, Canada, 2001.

[5] C. Strohhofer, A. Polman, "Relationship between gain and Yb^{3+} concentration in Er^{3+}-Yb^{3+} doped waveguide amplifiers," *J. Appl. Phys.*, vol. 90, pp. 4314-4320, 2001.

[6] T. Ohtsuki, N. Peyghambarian, "Gain characteristics of a high concentration Er^{3+}-doped phosphate glass waveguide," *J. Appl. Phys.*, vol. 78, pp. 3617-3621, 1995.

[7] M. Krishnaswamy, "Modeling and Fabrication of Rare-Earth-Doped Integrated Optical Waveguide Amplifiers," M.Sc. Thesis, *University of Alberta*, Edmonton, Alberta, Canada, 1998.

[8] S. Jiang, T. Luo, B. Hwang, G. Nunzi-Conti, M. Myers, D. Rhonehouse, S. Honkanen, N. Peyghambarian, "New Er^{3+}-doped phosphate glass for ion-exchanged waveguide amplifiers," *Opt. Eng.*, vol. 37, pp. 3282-3286, 1998.

[9] A. Shooshtari, P. Meshkinfam, T. Touam, M. P. Andrews, S. I. Najafi, "Ion-exchanged Er/Yb phosphate glass waveguide amplifiers and lasers," *Opt. Eng.*, vol. 37, pp. 1188-1192, 1998.

[10] H. Han, S. Seo, J. H. Shin, N. Park, "Coefficient determination related to optical gain in erbium-doped silicon-rich oxide waveguide amplifier," *App. Phys. Letters*, vol. 81, pp. 3720-3722, 2002.

[11] D.A. Turnbull, B.G. Aitken, S.G. Bishop, "Broad-band excitation mechanism for photoluminescence in Er- doped $Ge_{25}Ga_{1.7}As_{8.3}S_{65}$ glasses," *J. Non-Cryst. Solids*, vol. 244, pp. 260-266, 1999.

[12] D.A. Turnbull, S.G. Bishop, "Rare earth dopants as probes of localized states in chalcogenide glasses," *J. Non-Cryst. Solids*, vol. 223, pp. 105-113, 1998.

[13] T. Yu. Ivanova, A. A. Man'shina, A. V. Kurochkin, Yu. S. Tver'yanovich, V. B. Smirnov, "Er^{3+} to glass matrix energy transfer in Ga-Ge-S:Er^{3+} system," *J. Non-Crys. Solids*, vol. 298, pp. 7-14, 2002.

[14] C. J. Haugen, D. T. Tonchev, R. G. DeCorby, J. N. McMullin, T. Allen, K. Maeda, T. Ikari, and S. O. Kasap, "Photoluminescence and thermal properties of Er-doped As-Se-Ga-Ge based glasses," *Nonlinear Optics*, vol. 29, pp. 549-555, 2002.

[15] B. G. Aitken, C. W. Ponader, R. S. Quimby, "Clustering of rare earths in GeAs sulfide glass," *C. R. Chimie*, vol. 5, pp. 865-872, 2002.

[16] Z. G. Ivanova, V. S. Vassilev, E. Cernoskova, Z. Cernosek, "Physiochemical, structural and fluorescence properties of Er-doped Ge-S-Ga glasses," *J. Phys. Chem. Solids*, vol. 64, pp. 107-110, 2003.

[17] S. Q. Gu, S. Ramachandran, E. E. Reuter, D. A. Turnbull, J. T. Verdeyen, S.G. Bishop, "Photoluminescence and excitation spectroscopy of Er-doped As_2S_3 glass: novel broad band excitation mechanism," *J. Appl. Phys.*, vol. 77, pp. 3365-3371, 1995.

[18] S. O. Kasap, *Optoelectronics and Photonics: Principles and Practices*. Upper Saddle River, NJ: Prentice Hall, 2001.

[19] W. J. Miniscalco, "Erbium-doped glasses for fiber amplifiers at 1500 nm," *J. Lightwave Tech.*, vol. 9, pp. 234-250, 1991.

[20] J. T. Verdeyen, *Laser Electronics, Third Edition*. Upper Saddle River, NJ: Prentice Hall, 1995.

[21] E. Desurvire, *Erbium-Doped Fiber Amplifiers: Principles and Applications*, Hoboken, NJ: John Wiley and Sons, Inc., 2002.

[22] J. S. Wang, E. M. Vogel, E. Snitzer, "Tellurite glass: a new candidate for fiber devices," *Optical Materials*, vol. 3, pp. 187-203, 1994.

[23] J. Heo, J. M. Yoon, S. Ryou, "Raman spectroscopic analysis on the solubility mechanism of La^{3+} in GeS_2-Ga_2S_3 glasses," *J. Non-Crys. Solids*, vol. 238, pp. 115-123, 1998.

[24] P. Němec, M. Frumar, "Synthesis and properties of Pr^{3+}-doped Ge-Ga-Se glasses," *J. Non-Crys. Solids*, vol. 299-302, pp. 1018-1022, 2002.

[25] W. J. Miniscalco, R. S. Quimby, "General procedure for the analysis of Er^{3+} cross sections," *Optics Letters*, vol. 16, pp. 258-260, 1991.

[26] Maohe Li, Yan Lin, Hefang Hu, "Evaluation of cross sections of rare-earth ions in glass," *Proc. of SPIE*, vol. 3942, pp. 261-266, 2000.

[27] Alexander A. Kaminskii, *Laser Crystals: Their Physics and Properties, Second Edition*. New York: Springer-Verlag, 1990.

[28] Y. Ohishi, "Rare-earth ions in glasses and transitions for optical amplifiers," in *Optical Fiber Amplifiers: Materials, Devices and Applications*, S. Sudo, Ed. Boston: Artech House, Inc., 1997, pp. 149-189.

[29] M. J. Weber, "Probabilities for radiative and nonradiative decay of Er^{3+} in LaF_3," *Phys. Review*, vol. 157, pp. 262-272, 1967.

[30] D. Tonchev, S. O. Kasap, "Influence of Cl doping on the thermal properties of amorphous Se," *Phys. Chem. Glasses*, vol. 43, pp. 66-71, 2002.

[31] H. Higuchi, M. Takahashi, Y. Kawamoto, "Optical transitions and frequency upconversion emission of Er^{3+} ions in Ga_2S_3-GeS_2-La_2S_3 glasses," *J. Appl. Phys.*, vol. 83, pp. 19-27, 1998.

[32] M. Munzar, C. Koughia, D. Tonchev, K. Maeda, T. Ikari, C. Haugen, R. DeCorby, J. C. McMullin, S. O. Kasap, "Optical properties of Er-doped Ge-Ga-Se glasses," *J. Non-Cryst. Solids*, to be published.

[33] C. C. Ye, D. W. Hewak, M. Hempstead, B. N. Samson, D. N. Payne, "Spectral properties of Er^{3+}-doped gallium lanthanum sulphide glass," *J. Non-Cryst. Solids*, vol. 208, pp. 56-63, 1996.

[34] M. V. D. Vermelho, U. Peschel, J. S. Aitchison, "Simple and accurate procedure for modeling erbium-doped waveguide amplifiers with high concentration," *J. Lightwave Tech.*, vol. 18, pp. 401-408, 2000.

[35] R. G. DeCorby, private communication.

[36] M. A. Muriel, "Field distributions inside fiber gratings," *J. Quantum Electron.*, vol. 35, pp. 548-557, 1999.

[37] P. Yeh, *Optical Waves in Layered Media*. New York: Wiley, 1988.

[38] C. R. Giles and E. Desurvire, "Modeling Erbium-Doped Fiber Amplifiers," *J. Lightwave Tech.*, vol. 9, pp. 271-283, 1991.

[39] Y. C. Yan, A. J. Faber, H. de Waal, P. G. Kik, A. Polman, "Erbium-doped phosphate glass waveguide on silicon with 4.1 dB/cm gain at 1.535 μm," *Appl. Phys. Lett.*, vol. 71, pp. 2922-2924, 1997.

[40] P. G. Kik and A. Polman, "Cooperative upconversion as the gain-limiting factor in Er doped miniature Al_2O_3 waveguide amplifiers," *J. Appl. Phys.*, vol. 93, pp. 5008-5012, 2003.

[41] Y. Hu, S. Jiang, G. Sorbello, T. Luo, Y. Ding, B. Hwang, J. Kim, H. Seo, N. Peyghambarian, "Numerical analyses of the population dynamics and determination of the upconversion coefficients in a new high erbium-doped tellurite glass," *J. Opt. Soc. Am. B*, vol. 18, pp. 1928-1934, 2001.

[42] D. J. Coleman, P. Golding, T. A. King, "Spectroscopic and energy-transfer parameters for Er^{3+}-doped and Er^{3+}, Pr^{3+}-codoped GeGaS glasses," *J. Opt. Soc. Am. B*, vol. 19, pp. 1982-1989, 2002.

[43] Y. G. Choi, K. H. Kim, S. H. Park, J. Heo, "Comparative study of energy transfers from Er3+ to Ce3+ in tellurite and sulfide glasses under 980 nm excitation," *J. Appl. Phys.*, vol. 88, pp. 3832-3839, 2000.

[44] J. H. Mathews, *Numerical Methods for Computer Science, Engineering and Mathematics*. Englewood Cliffs, NJ: Prentice-Hall, Inc., 1987.

[45] T. W. Allen, M. M. Hawkeye, C. J. Haugen, R. G. DeCorby, J. N. McMullin, D. Tonchev, K. Koughia, S. O. Kasap, "Photoluminescence measurements of Er-doped chalcogenide glasses," *J. Vacuum Sci. Tech.*, to be published.

Appendix A: Reduced matrix elements

Table A.1: Calculated values of the squares of the reduced matrix elements $\left(\left\langle f^N \gamma SLJ \left| U^{(t)} \right| f^N \gamma S'L'J' \right\rangle\right)^2$ for Er^{3+} for transitions from the ground state *SLJ* [27].

$S'L'J'$	$\left\|U^{(2)}\right\|^2$	$\left\|U^{(4)}\right\|^2$	$\left\|U^{(6)}\right\|^2$
$^4I_{13/2}$	0.0195	0.1173	1.4316
$^4I_{11/2}$	0.0282	0.0003	0.3953
$^4I_{9/2}$	0.0	0.1733	0.0099
$^4F_{9/2}$	0.0	0.5354	0.4618
$^4S_{3/2}$	0.0	0.0	0.2211
$^2H_{11/2}$	0.7125	0.4125	0.0925
$^4F_{7/2}$	0.0	0.1469	0.6266
$^4F_{5/2}$	0.0	0.0	0.2232
$^4F_{3/2}$	0.0	0.0	0.1272
$^2G_{9/2}$	0.0	0.0189	0.2256
$^4G_{11/2}$	0.9183	0.5262	0.1172
$^4G_{9/2}$	0.0	0.2416	0.1235
$^2K_{15/2}$	0.0219	0.0041	0.0758
$^2G_{7/2}$	0.0	0.0174	0.1163

Table A.2: Calculated values of the squares of the reduced matrix elements $\left(\left\langle f^N \gamma SLJ \left| U^{(t)} \right| f^N \gamma S'L'J' \right\rangle\right)^2$ for Er^{3+} for transitions from the excited state *SLJ* [29].

SLJ	$S'L'J'$	$\left\|U^{(2)}\right\|^2$	$\left\|U^{(4)}\right\|^2$	$\left\|U^{(6)}\right\|^2$
$^4I_{13/2}$	$^4I_{15/2}$	0.0188	0.1176	1.4617
$^4I_{11/2}$	$^4I_{13/2}$	0.021	0.11	1.04
	$^4I_{15/2}$	0.0259	0.0001	0.3994
$^4F_{9/2}$	$^4I_{9/2}$	0.096	0.0061	0.012
	$^4I_{11/2}$	0.0671	0.0088	1.2611
	$^4I_{13/2}$	0.0096	0.1576	0.0870
	$^4I_{15/2}$	0.0	0.5655	0.4651
$^4S_{3/2}$	$^4I_{9/2}$	0.0	0.0729	0.2560
	$^4I_{11/2}$	0.0	0.0037	0.0789
	$^4I_{13/2}$	0.0	0.0	0.3481
	$^4I_{15/2}$	0.0	0.0	0.2285
$^2H_{9/2}$	$^4F_{9/2}$	0.010	0.030	0.059
	$^4I_{9/2}$	0.0076	0.0050	0.0028
	$^4I_{11/2}$	0.077	0.11	0.096
	$^4I_{13/2}$	0.073	0.12	0.41
	$^4I_{15/2}$	0.0	0.078	0.17

Appendix B: Lifetime measurements summary

The lifetime measurements performed on the various chalcogenide alloys in the course of this thesis are summarized in the following tables. The results are sorted by the date of measurements.

May 29, 2002

Sample series	Sample	Lifetime (ms)
GaGeSe Er_2S_3-doped	#1 – 1.0% Er	2.4
	#2 - 0.1% Er	1.42
	#3 - 0.3% Er	3.11
GaGeSe	A – 1.0% Ga	negligible
	B – 3.0% Ga	negligible
	C – 6.0% Ga	negligible
GaGeAsSe 1% Er ($ErCl_3$-doped)	#1 – 3.0% Ge, 5.0% Ga	negligible
	#2 – 3.0% Ge, 2.5% Ga	negligible
	#3 – 3.0% Ge, 1.8% Ga	negligible
GaGeAsSe 1% Er ($ErCl_3$-doped)	#0 – 9.0% Ga	negligible
	#1 - 7.5% Ga	negligible
	#2 – 5.0% Ga	negligible
	#4 – 3.0% Ga	negligible
	#5 - 1.5% Ga	negligible
	#8 - 0.8% Ga	negligible

July 3, 2002

Sample Series	Sample	Lifetime (ms)
GaGeAsSe 0.5% Er (Er_2S_3-doped)	#1 - 10% Ge	negligible
	#2 - 20% Ge	negligible
	#4 – 5.0% Ge	<7
	#5 – 3.0% Ge	negligible
GaGeSe Er_2S_3-doped	#1 – 0.0% Er	negligible
	#2 - 0.1% Er	<6
	#3 - 0.3% Er	3.8
	#4 – 1.0% Er	3.9
	#5 – 3.0% Er	$\sim<4.5$

August 22, 2002

Sample Series	Sample	Lifetime (ms)
GaAsSe Ga dependence Er_2S_3-doped	#2	1.65
	#3	1.10
	#4	2.47
	#5	1.32
GaGeAsSe Er dependence 1 - 10% Er (Er_2S_3-doped)	#1	0.25
	#2	0.49
	#3	0.85
	#5	1.16
	#6	0.17
GaGeSe(S) Er_2S_3-doped Ge - 27% and Se(S) - 61-65%	#1. – 3.0% Er (9.0%Ga)	2.77
	#2. – 1.0% Er (6.0% Ga)	3.81
	#3. - 0.3% Er (6.0%Ga)	3.06
GaGeSe(S) 1% Er (Er_2S_3-doped) Ga – 6.0%	#4. - excess Ge (37.2%)	0.10
	#5. - excess Se (72.9%)	1.68

October 17, 2002

Sample series	Sample	Lifetime (ms)
GaGeSe Er_2S_3-doped	#1 – 1.0% Er	2.48
	#2 - 0.8% Er	2.76
GaGeAsSe	#1 – 1.0% Er (Er_2S_3)	0.25
	#2 – 2.0% Er (Er_2S_3)	1.27
	#3 – 2.0% Er ($ErCl_3$)	0.25

January 31, 2003

Sample series	Sample	Lifetime (ms)
GaGeAsSe(S) Er_2S_3-doped	#5 – 2.0% Er	1.37
	#7 - 2.5% Er	1.35
	#8 – 3.0% Er	negligible
	#9 - 0.5% Er	negligible
	#10 – 5.0% Er	1.32

January 23, February 5, 2003 *Results shown in Section 3.2.3

Sample Series	Sample	Lifetime (ms)
GaGeS Er_2S_3 doped	#1 - 0.3% Er	2.76
	#2 - 0.6% Er	2.77
	#3 - 0.9% Er	2.87
	#4 - 1.8% Er	2.25
	#5 - 2.1% Er	1.61
	#6 - 2.4% Er	1.55
GaGeSe Er_2S_3-doped	#1 - 0.3% Er	2.35
	#2 – 1.0% Er	2.85
	#3 – 3.0% Er	2.75

Appendix C: Newton-Raphson method

The Newton-Raphson method is a commonly used tool for solving systems of nonlinear equations like the ones used in the simulation models in this thesis [44]. Given a system of equations

$$\begin{aligned} 0 &= f_1(x_1, x_2, x_3 \ldots, x_n) \\ 0 &= f_2(x_1, x_2, x_3 \ldots, x_n) \\ 0 &= f_3(x_1, x_2, x_3 \ldots, x_n) \\ &\vdots \\ 0 &= f_n(x_1, x_2, x_3 \ldots, x_n) \end{aligned} \tag{C.1}$$

and an initial estimate for a solution point $\mathbf{P}_k = (x_{k1}, x_{k2}, x_{k3} \ldots, x_{kn})$, a function $\mathbf{F}(\mathbf{P}_k)$ defining the evaluation of these equations at $\mathbf{P}_k$ is created:

$$\mathbf{F}(\mathbf{P}_k) = \begin{bmatrix} f_1(\mathbf{P}_k) \\ f_2(\mathbf{P}_k) \\ f_3(\mathbf{P}_k) \\ \vdots \\ f_n(\mathbf{P}_k) \end{bmatrix} \tag{C.2}$$

Next, the Jacobian matrix is formulated:

$$\mathbf{J}(\mathbf{P}_k) = \begin{bmatrix} \frac{\partial}{\partial x_1} f_1(\mathbf{P}_k) & \frac{\partial}{\partial x_2} f_1(\mathbf{P}_k) & \frac{\partial}{\partial x_3} f_1(\mathbf{P}_k) & \cdots & \frac{\partial}{\partial x_n} f_1(\mathbf{P}_k) \\ \frac{\partial}{\partial x_1} f_2(\mathbf{P}_k) & \ddots & & & \vdots \\ \frac{\partial}{\partial x_1} f_3(\mathbf{P}_k) & & \ddots & & \vdots \\ \vdots & & & \ddots & \vdots \\ \frac{\partial}{\partial x_1} f_n(\mathbf{P}_k) & \cdots\cdots\cdots & \cdots\cdots\cdots & \cdots & \frac{\partial}{\partial x_n} f_n(\mathbf{P}_k) \end{bmatrix} \tag{C.3}$$

The following linear system is then solved for $\Delta\mathbf{P}$:

$$\mathbf{J}(\mathbf{P}_k)\Delta\mathbf{P} = -\mathbf{F}(\mathbf{P}_k) \tag{C.4}$$

$\Delta\mathbf{P}$ is then used to increment the initial guess:

$$\mathbf{P}_{k+1} = \mathbf{P}_k + \Delta\mathbf{P} \tag{C.5}$$

and the procedure is repeated until the new point produces **F** values less than a given convergence tolerance.

The rate equations given by Equations (4.15) to (4.20) and (4.21) to (4.26) were set equal to zero (i.e., $dN/dt = 0$, the steady state condition) and then put into the following forms using simple algebra:

980-nm equations:

$$f_1 = \frac{\left(\begin{array}{c}(W_{12}+R_{13})N_1-(W_{21}+A_{21})N_2-(R_{31}+A_{31})N_3\\ -A_{51}N_5-Cup_2N_2^{\,2}-Cup_3N_3^{\,2}\end{array}\right)}{A_{41}-C_{14}N_1+C_{24}N_2} - N_4 \tag{C.6}$$

$$f_2 = \frac{\left(\begin{array}{c}-W_{12}N_1+(W_{21}+W_{24}+A_{21})N_2-(W_{42}+A_{42})N_4\\ -2C_{14}N_1N_4+C_{24}N_2N_4+2Cup_2N_2^{\,2}-Cup_4N_4^{\,2}\end{array}\right)}{A_{32}} - N_3 \tag{C.7}$$

$$f_3 = \frac{(R_{31}+R_{35}+A_{31}+A_{32})N_3-A_{43}N_4+2Cup_3N_3^{\,2}}{R_{13}} - N_1 \tag{C.8}$$

$$f_4 = \frac{\left(\begin{array}{c}W_{24}N_2-(W_{45}+W_{42}+A_{41}+A_{42}+A_{43})N_4-C_{24}N_2N_4\\ +Cup_2N_2^{\,2}-2Cup_4N_4^{\,2}\end{array}\right)}{C_{14}N_4} - N_1 \tag{C.9}$$

$$f_5 = \frac{R_{35}N_3+W_{45}N_4+C_{24}N_2N_4+Cup_3N_3^{\,2}+Cup_4N_4^{\,2}}{A_{51}} - N_5 \tag{C.10}$$

$$f_6 = N_t - N_1 - N_2 - N_3 - N_4 - N_5 \tag{C.11}$$

1480-nm equations:

$$f_1 = \frac{\left(\begin{array}{c}(R_{12}+W_{12})N_1-(W_{21}+R_{21}+A_{21})N_2-A_{31}N_3-A_{51}N_5\\ -Cup_2N_2^{\,2}\end{array}\right)}{A_{41}-C_{14}N_1+C_{24}N_2} - N_4 \tag{C.12}$$

$$f_2 = \frac{\begin{pmatrix} -(R_{12}+W_{12})N_1 + (W_{21}+R_{21}+A_{21}+R_{24}+W_{24})N_2 \\ -(R_{42}+W_{42}+A_{42})N_4 + C_{24}N_2N_4 \\ +2Cup_2N_2^{\,2} - 2C_{14}N_1N_4 - Cup_4N_4^{\,2} \end{pmatrix}}{A_{32}} - N_3 \qquad \text{(C.13)}$$

$$f_3 = \frac{A_{43}N_4}{A_{31}+A_{32}} - N_3 \qquad \text{(C.14)}$$

$$f_4 = \frac{\begin{pmatrix} (R_{24}+W_{24})N_2 \\ -(R_{42}+W_{42}+R_{45}+W_{45}+A_{43}+A_{42}+A_{41})N_4 \\ -C_{24}N_2N_4 + Cup_2N_2^{\,2} - 2Cup_4N_4^{\,2} \end{pmatrix}}{C_{14}N_4} - N_1 \qquad \text{(C.15)}$$

$$f_5 = \frac{(R_{45}+W_{45})N_4 + C_{24}N_2N_4 + Cup_4N_4^{\,2}}{A_{51}} - N_5 \qquad \text{(C.16)}$$

$$f_6 = N_t - N_1 - N_2 - N_3 - N_4 - N_5 \qquad \text{(C.17)}$$

Putting the equations in this form aided in the method's ability to converge to a solution. The partial derivatives for use in the Jacobian matrix were then derived:

980-nm equations:

$$\frac{\partial f_1}{\partial N_4} = \frac{\partial f_2}{\partial N_3} = \frac{\partial f_3}{\partial N_1} = \frac{\partial f_4}{\partial N_1} = \frac{\partial f_5}{\partial N_5} = \frac{\partial f_6}{\partial N_1} = \frac{\partial f_6}{\partial N_2} = \frac{\partial f_6}{\partial N_3} = \frac{\partial f_6}{\partial N_4} = \frac{\partial f_6}{\partial N_5} = -1$$

$$\frac{\partial f_2}{\partial N_5} = \frac{\partial f_3}{\partial N_2} = \frac{\partial f_3}{\partial N_5} = \frac{\partial f_4}{\partial N_3} = \frac{\partial f_4}{\partial N_5} = \frac{\partial f_5}{\partial N_1} = 0$$

$$\frac{\partial f_1}{\partial N_1} = \frac{W_{12}+R_{13}}{A_{41}-C_{14}N_1+C_{24}N_2} + \left(\frac{\begin{pmatrix} (W_{12}+R_{13})N_1 - (W_{21}+A_{21})N_2 - (R_{31}+A_{31})N_3 - A_{51}N_5 \\ -Cup_2N_2^{\,2} - Cup_3N_3^{\,2} \end{pmatrix}}{(A_{41}-C_{14}N_1+C_{24}N_2)^2} \right) C_{14}$$

$$\frac{\partial f_1}{\partial N_2} = \frac{-W_{21} - A_{21} - 2Cup_2 N_2}{A_{41} - C_{14}N_1 + C_{24}N_2} - \left(\frac{\begin{array}{c}(W_{12} + R_{13})N_1 - (W_{21} + A_{21})N_2 - (R_{31} + A_{31})N_3 \\ -A_{51}N_5 - Cup_2 N_2{}^2 - Cup_3 N_3{}^2\end{array}}{(A_{41} - C_{14}N_1 + C_{24}N_2)^2} \right) C_{24}$$

$$\frac{\partial f_1}{\partial N_3} = \frac{-R_{31} - A_{31} - 2Cup_3 N_3}{A_{41} - C_{14}N_1 + C_{24}N_2}$$

$$\frac{\partial f_1}{\partial N_5} = \frac{-A_{51}}{A_{41} - C_{14}N_1 + C_{24}N_2}$$

$$\frac{\partial f_2}{\partial N_1} = \frac{-W_{12} - 2C_{14}N_4}{A_{32}}$$

$$\frac{\partial f_2}{\partial N_2} = \frac{W_{21} + W_{24} + A_{21} + C_{24}N_4 + 4Cup_2 N_2}{A_{32}}$$

$$\frac{\partial f_2}{\partial N_4} = \frac{-W_{42} - A_{42} - 2C_{14}N_1 + C_{24}N_2 - 2Cup_4 N_4}{A_{32}}$$

$$\frac{\partial f_3}{\partial N_3} = \frac{R_{31} + R_{35} + A_{31} + A_{32} + 4Cup_3 N_3}{R_{13}}$$

$$\frac{\partial f_3}{\partial N_4} = \frac{-A_{43}}{R_{13}}$$

$$\frac{\partial f_4}{\partial N_2} = \frac{W_{24} - C_{24}N_4 + 2Cup_2 N_2}{C_{14}N_4}$$

$$\frac{\partial f_4}{\partial N_4} = \frac{-W_{45} - W_{42} - A_{41} - A_{42} - A_{43} - C_{24}N_2 - 4Cup_4 N_4}{C_{14}N_4} - \left(\frac{\begin{array}{c}W_{24}N_2 - (W_{45} + W_{42} + A_{41} + A_{42} + A_{43})N_4 - C_{24}N_2 N_4 \\ +Cup_2 N_2{}^2 - 2Cup_4 N_4{}^2\end{array}}{C_{14}N_4{}^2} \right)$$

$$\frac{\partial f_5}{\partial N_2} = \frac{C_{24} N_4}{A_{51}}$$

$$\frac{\partial f_5}{\partial N_3} = \frac{R_{35} + 2Cup_3 N_3}{A_{51}}$$

$$\frac{\partial f_5}{\partial N_4} = \frac{W_{45} + C_{24} N_2 + 2Cup_4 N_4}{A_{51}}$$

1480-nm equations:

$$\frac{\partial f_1}{\partial N_4} = \frac{\partial f_2}{\partial N_3} = \frac{\partial f_3}{\partial N_3} = \frac{\partial f_4}{\partial N_1} = \frac{\partial f_5}{\partial N_5} = \frac{\partial f_6}{\partial N_1} = \frac{\partial f_6}{\partial N_2} = \frac{\partial f_6}{\partial N_3} = \frac{\partial f_6}{\partial N_4} = \frac{\partial f_6}{\partial N_5} = -1$$

$$\frac{\partial f_2}{\partial N_5} = \frac{\partial f_3}{\partial N_1} = \frac{\partial f_3}{\partial N_2} = \frac{\partial f_3}{\partial N_5} = \frac{\partial f_4}{\partial N_3} = \frac{\partial f_4}{\partial N_5} = \frac{\partial f_5}{\partial N_1} = \frac{\partial f_5}{\partial N_3} = 0$$

$$\frac{\partial f_1}{\partial N_1} = \frac{R_{12} + W_{12}}{A_{41} - C_{14} N_1 + C_{24} N_2} + \left(\frac{\left(R_{12} + W_{12}\right) N_1 - \left(W_{21} + R_{21} + A_{21}\right) N_2 - A_{31} N_3 - A_{51} N_5}{\left(A_{41} - C_{14} N_1 + C_{24} N_2\right)^2} \right) C_{14}$$

$$\frac{\partial f_1}{\partial N_2} = \frac{-W_{21} - R_{21} - A_{21} - 2Cup_2 N_2}{A_{41} - C_{14} N_1 + C_{24} N_2} - \left(\frac{\left(R_{12} + W_{12}\right) N_1 - \left(W_{21} + R_{21} + A_{21}\right) N_2 - A_{31} N_3 - A_{51} N_5}{\left(A_{41} - C_{14} N_1 + C_{24} N_2\right)^2} \right) C_{24}$$

$$\frac{\partial f_1}{\partial N_3} = \frac{A_{31}}{A_{41} - C_{14} N_1 + C_{24} N_2}$$

$$\frac{\partial f_1}{\partial N_5} = \frac{A_{51}}{A_{41} - C_{14} N_1 + C_{24} N_2}$$

$$\frac{\partial f_2}{\partial N_1} = \frac{-R_{12} - W_{12} - 2C_{14} N_4}{A_{32}}$$

$$\frac{\partial f_2}{\partial N_2} = \frac{W_{21} + R_{21} + A_{21} + R_{24} + W_{24} + C_{24}N_4 + 4Cup_2N_2}{A_{32}}$$

$$\frac{\partial f_2}{\partial N_4} = \frac{-R_{42} - W_{42} - A_{42} + C_{24}N_2 - 2C_{14}N_1 - 2Cup_4N_4}{A_{32}}$$

$$\frac{\partial f_3}{\partial N_4} = \frac{A_{43}}{A_{31} + A_{32}}$$

$$\frac{\partial f_4}{\partial N_2} = \frac{R_{24} + W_{24} - C_{24}N_4 + 2Cup_2N_2}{C_{14}N_1}$$

$$\frac{\partial f_4}{\partial N_4} = \frac{-R_{42} - W_{42} - R_{45} - W_{45} - A_{43} - A_{42} - A_{41} - C_{24}N_2 - 4Cup_4N_4}{C_{14}N_4} - \frac{\left(\begin{array}{c}\left(R_{24} + W_{24}\right)N_2 - \left(R_{42} + W_{42} + R_{45} + W_{45} + A_{43} + A_{42} + A_{41}\right)N_4 \\ -C_{24}N_2N_4 + Cup_2N_2^{\,2} - 2Cup_4N_4^{\,2}\end{array}\right)}{C_{14}N_4^{\,2}}$$

$$\frac{\partial f_5}{\partial N_2} = \frac{C_{24}N_4}{A_{51}}$$

$$\frac{\partial f_5}{\partial N_4} = \frac{R_{45} + W_{45} + C_{24}N_2 + 2Cup_4N_4}{A_{51}}$$

Since there are six equations with five unknown variables, one equation, f_4 ((C.9) for 980 nm and (C.15) for 1480 nm) was dropped off. If the simulation proceeded to get stuck at a local minimum that produced an unacceptable solution, f_4 was added back in and f_3 ((C.8) for 980 nm and (C.14) for 1480 nm) was dropped. The set of equations with f_3 tended to produce results much faster, while the set with f_4 took longer, but could generally handle sets of simulation parameters that caused the f_3 set to fail.

To ensure that the Newton-Raphson method was converging properly, the simulator was run with different sets of initial solution estimates and it always produced the same results.